



MORGAN & CLAYPOOL PUBLISHERS

Accurate Computation of Mathieu Functions

Malcolm M. Bibby
Andrew F. Peterson

*SYNTHESIS LECTURES ON
COMPUTATIONAL ELECTROMAGNETICS*

Constantine A. Balanis, *Series Editor*

Accurate Computation of Mathieu Functions

Synthesis Lectures on Computational Electromagnetics

Editor

Constatine A. Balanis, Arizona State University

Synthesis Lectures on Computational Electromagnetics will publish 50- to 100-page publications on topics that include advanced and state-of-the-art methods for modeling complex and practical electromagnetic boundary value problems. Each lecture develops, in a unified manner, the method based on Maxwell's equations along with the boundary conditions and other auxiliary relations, extends underlying concepts needed for sequential material, and progresses to more advanced techniques and modeling. Computer software, when appropriate and available, is included for computation, visualization and design. The authors selected to write the lectures are leading experts on the subject that have extensive background in the theory, numerical techniques, modeling, computations and software development.

The series is designed to:

- Develop computational methods to solve complex and practical electromagnetic boundary-value problems of the 21st century.
- Meet the demands of a new era in information delivery for engineers, scientists, technologists and engineering managers in the fields of wireless communication, radiation, propagation, communication, navigation, radar, RF systems, remote sensing, and biotechnology who require a better understanding and application of the analytical, numerical and computational methods for electromagnetics.

[Accurate Computation of Mathieu Functions](#)

Malcolm M. Bibby and Andrew F. Peterson
2013

[Selected Asymptotic Methods with Applications to Electromagnetics and Antennas](#)

George Fikioris, Ioannis Tatsoglou, and Odysseas N. Bakas
2013

[Double-Grid Finite-Difference Frequency-Domain \(DG-FDFD\) Method for Scattering from Chiral Objects](#)

Erdogan Alkan, Veysel Demir, Atef Elsherbeni, and Ercument Arvas
2013

Multiresolution Frequency Domain Technique for Electromagnetics

Mesut Gokten, Atef Elsherbeni, and Ercument Arvas

2012

Scattering Analysis of Periodic Structures Using Finite-Difference Time-Domain Method

Khaled ElMahgoub, Fan Yang, and Atef Elsherbeni

2012

Introduction to the Finite-Difference Time-Domain (FDTD) Method for Electromagnetics

Stephen D. Gedney

2011

Analysis and Design of Substrate Integrated Waveguide Using Efficient 2D Hybrid Method

Xuan Hui Wu and Ahmed A. Kishk

2010

An Introduction to the Locally-Corrected Nyström Method

Andrew F. Peterson and Malcolm M. Bibby

2009

Transient Signals on Transmission Lines: An Introduction to Non-Ideal Effects and Signal Integrity Issues in Electrical Systems

Andrew F. Peterson and Gregory D. Durgin

2008

Reduction of a Ship's Magnetic Field Signatures

John J. Holmes

2008

Integral Equation Methods for Electromagnetic and Elastic Waves

Weng Cho Chew, Mei Song Tong, and Bin Hu

2008

Modern EMC Analysis Techniques Volume II: Models and Applications

Nikolaos V. Kantartzis and Theodoros D. Tsiboukis

2008

Modern EMC Analysis Techniques Volume I: Time-Domain Computational Schemes

Nikolaos V. Kantartzis and Theodoros D. Tsiboukis

2008

Particle Swarm Optimization: A Physics-Based Approach

Said M. Mikki and Ahmed A. Kishk

2008

- Three-Dimensional Integration and Modeling: A Revolution in RF and Wireless Packaging**
Jong-Hoon Lee and Manos M. Tentzeris
2007
- Electromagnetic Scattering Using the Iterative Multiregion Technique**
Mohamed H. Al Sharkawy, Veysel Demir, and Atef Z. Elsherbeni
2007
- Electromagnetics and Antenna Optimization Using Taguchi's Method**
Wei-Chung Weng, Fan Yang, and Atef Elsherbeni
2007
- Fundamentals of Electromagnetics 1: Internal Behavior of Lumped Elements**
David Voltmer
2007
- Fundamentals of Electromagnetics 2: Quasistatics and Waves**
David Voltmer
2007
- Modeling a Ship's Ferromagnetic Signatures**
John J. Holmes
2007
- Mellin-Transform Method for Integral Evaluation: Introduction and Applications to Electromagnetics**
George Fikioris
2007
- Perfectly Matched Layer (PML) for Computational Electromagnetics**
Jean-Pierre Bérenger
2007
- Adaptive Mesh Refinement for Time-Domain Numerical Electromagnetics**
Costas D. Sarris
2006
- Frequency Domain Hybrid Finite Element Methods for Electromagnetics**
John L. Volakis, Kubilay Sertel, and Brian C. Usner
2006
- Exploitation of A Ship's Magnetic Field Signatures**
John J. Holmes
2006
- Support Vector Machines for Antenna Array Processing and Electromagnetics**
Manel Martínez-Ramón and Christos Christodoulou
2006

[**The Transmission-Line Modeling \(TLM\) Method in Electromagnetics**](#)

Christos Christopoulos

2006

[**Computational Electronics**](#)

Dragica Vasileska and Stephen M. Goodnick

2006

[**Higher Order FDTD Schemes for Waveguide and Antenna Structures**](#)

Nikolaos V. Kantartzis and Theodoros D. Tsiboukis

2006

[**Introduction to the Finite Element Method in Electromagnetics**](#)

Anastasis C. Polycarpou

2006

[**MRTD\(Multi Resolution Time Domain\) Method in Electromagnetics**](#)

Nathan Bushyager and Manos M. Tentzeris

2006

[**Mapped Vector Basis Functions for Electromagnetic Integral Equations**](#)

Andrew F. Peterson

2006

Copyright © 2014 by Morgan & Claypool

All rights reserved. No part of this publication may be reproduced, stored in a retrieval system, or transmitted in any form or by any means—electronic, mechanical, photocopy, recording, or any other except for brief quotations in printed reviews, without the prior permission of the publisher.

Accurate Computation of Mathieu Functions

Malcolm M. Bibby and Andrew F. Peterson

www.morganclaypool.com

ISBN: 9781627050852 paperback

ISBN: 9781627050869 ebook

DOI 10.2200/S00526ED1V01Y201307CEM032

A Publication in the Morgan & Claypool Publishers series

SYNTHESIS LECTURES ON COMPUTATIONAL ELECTROMAGNETICS

Lecture #32

Series Editor: Constantine A. Balanis, *Arizona State University*

Series ISSN

Synthesis Lectures on Computational Electromagnetics

Print 1932-1252 Electronic 1932-1716

Accurate Computation of Mathieu Functions

Malcolm M. Bibby and Andrew F. Peterson
Georgia Institute of Technology

SYNTHESIS LECTURES ON COMPUTATIONAL ELECTROMAGNETICS
#32



MORGAN & CLAYPOOL PUBLISHERS

ABSTRACT

This lecture presents a modern approach for the computation of Mathieu functions. These functions find application in boundary value analysis such as electromagnetic scattering from elliptic cylinders and flat strips, as well as the analogous acoustic and optical problems, and many other applications in science and engineering. The authors review the traditional approach used for these functions, show its limitations, and provide an alternative “tuned” approach enabling improved accuracy and convergence. The performance of this approach is investigated for a wide range of parameters and machine precision. Examples from electromagnetic scattering are provided for illustration and to show the convergence of the typical series that employ Mathieu functions for boundary value analysis.

KEYWORDS

elliptic cylinder, electromagnetic scattering, boundary value problems

Contents

1	Introduction	1
2	Mathieu Functions	3
2.1	The Mathieu Equations	3
2.2	Angular Functions	5
2.2.1	Relations Satisfied by the Expansion Functions $\{A\}$ and $\{B\}$	6
2.3	Radial Functions	9
2.4	Computational Steps	12
2.5	Summary	14
3	Observed Accuracy Using Traditional and Tuned Methods	15
3.1	Angular Functions	16
3.1.1	Subtraction Error	17
3.1.2	Back Substitution	21
3.2	Radial Functions	26
3.3	Example: Computing a Hankel Function in Terms of a Summation of Mathieu Functions	33
3.4	Summary	34
4	Recommended Algorithm for Mathieu Function Computation	37
4.1	The Tuned Algorithm	37
4.2	Example: Calculation of a Uniform Plane Wave	38
4.3	Adaptive Error Estimation Based on the Plane Wave	40
4.4	Summary	40
5	Electromagnetic Scattering from Conducting Elliptic Cylinders	43
5.1	The TM_z Case	43
5.2	The TE_z Case	46
5.3	Examples	49
5.4	The Size, N , of the Eigenmatrix for the Computations to Follow	51
5.5	Current Density and Scattering Cross Section for TM_z Excitation	52

5.6	Current Density and Scattering Cross Section for TE_z Excitation	65
5.7	Summary	78
6	Electromagnetic Scattering from an Infinite Conducting Strip	79
6.1	The TM_z Case	79
6.2	The TE_z Case	82
6.3	Results	83
6.4	Summary	94
A	Converting Between Two Common Mathieu Function Conventions	95
B	Tables of Select Eigenvalues and Eigenvectors	97
C	Tables of Select Angular Mathieu Functions	103
D	Tables of Select Radial Mathieu Functions	109
	References	119
	Authors' Biographies	123

CHAPTER 1

Introduction

Mathieu functions, first described in 1868 in connection with the vibrations of an elliptic drum [1], are the natural wave functions associated with elliptic-cylinder coordinates. They find application in the solution of boundary-value problems involving structures with elliptic boundaries. The properties of these functions were elaborated in [2]. As a representative sample of the literature, references [3–13] provide basic background information on these functions as well as some examples of their use for the classical boundary value analysis of a number of physical problems. Modern applications of the Mathieu equation include oscillations of a pendulum, the physics of a capacitor microphone, and several types of particle traps [10].

For electromagnetic field analysis, such problems include scattering from perfectly conducting cylinders whose cross section has the shape of an ellipse [14–17], scattering from conducting strips [9] (which are a degenerate case of an ellipse) scattering from coated strips [18], scattering from dielectric elliptic cylinders [17, 19], and propagation within elliptic waveguides [20]. In addition, the problem of elliptic cylinders with loss has been expressed in terms of Mathieu functions of complex argument [21].

Other more complicated structures that may be analyzed in terms of Mathieu expansions include suspended strips in a circular waveguide [22], semi-elliptic channels or troughs in ground planes [23, 24], and a blade protruding from a ground plane [25]. Within the usual assumptions of perfect materials and shapes, these geometries permit an exact analysis in terms of a summation of Mathieu functions. Such an analysis is only useful if it leads to an expression that can be computed.

The computation of Mathieu functions is far from trivial. Built in functions and/or library routines for Mathieu functions are not widespread. Articles on the computation of Mathieu functions are scattered throughout the literature and include, as a representative sample, references [7, 11–13, 26–34]. Available sources of software for computing Mathieu functions may be found as companions to [12, 28, 29, 32–34]; some specific websites are [35, 36]. However, there appears to be no single repository where information about the computation of Mathieu functions and reliable software may be found.

Initial attempts by the authors to use the software of [28] led to the conclusion that, while the codes produced results with single-precision accuracy (7 decimal places), it was not possible to easily extend them to obtain double-precision accuracy (15 decimal places). Others also report slow convergence, or the lack of convergence, of some of the expressions for Mathieu functions [37]. This led the authors on an investigation, the result of which is this lecture.

2 1. INTRODUCTION

Chapter 2 reviews the definition of Mathieu functions and the conventional algorithm for their numerical evaluation. Chapter 3 explores some of the numerical difficulties associated with their computation. Chapter 4 summarizes a more robust algorithm than some of those found in the literature, the “tuned” method. Chapters 5 and 6 illustrate the application to electromagnetic scattering from perfectly conducting elliptical cylinders and the perfectly conducting strip, respectively. Some appendices provide numerical values that can be used for benchmarking to assist reader’s interested in generating their own Mathieu functions.

It is necessary to say a few words about notation. There are at least five different conventions for expressing Mathieu functions, as delineated in [11], and some of these affect the normalization of the functions as well as their labels. The differences mostly impact the various types of radial Mathieu functions. In the present lecture, we employ the Goldstein-Ince notation, and, where necessary, freely convert expressions from cited works into that notation. Appendix A discusses two common notations.

CHAPTER 2

Mathieu Functions

2.1 THE MATHIEU EQUATIONS

Mathieu functions are defined in the framework of the elliptical cylinder coordinates (u, v, z) [8, p. 17]; [38, p. 202]. These are related to Cartesian coordinates (x, y, z) by:

$$\begin{aligned} x &= F \cosh u \cos v & y &= F \sinh u \sin v & z &= z \\ \cosh u &= \sqrt{\frac{x^2 + y^2 + F^2 + \sqrt{(x^2 + y^2)^2 + F^4 - 2F^2(x^2 - y^2)}}{2F^2}} & \cos v &= \frac{x}{F \cosh u}, \end{aligned} \quad (2.1)$$

where F is the semi-focal length of the specific elliptic system, and the other parameters range over $0 \leq u < \infty$, $0 \leq v \leq 2\pi$ and $-\infty < z < \infty$. An elliptical coordinate system is illustrated in Figure 2.1. A particular ellipse is defined by F and u .

Classical boundary value problems are often solved using the separation-of-variables procedure. Consider the Helmholtz equation, in which k is the wave number:

$$\nabla^2 \Psi + k^2 \Psi = 0. \quad (2.2)$$

Separation-of-variables involves seeking a solution of the form [8, p.19],

$$\Psi = U(u) V(v) Z(z). \quad (2.3)$$

After (2.3) is substituted in (2.2), like variables are grouped together, and the resulting functions of u , v and z must each be equal to a constant. The equations may be expressed as

$$\begin{aligned} \frac{d^2 V}{d v^2} + (\alpha^2 - k^2 F^2 \cos^2 v) V &= \frac{d^2 V}{d v^2} + \left(\alpha^2 - k^2 F^2 \left(\frac{\cos 2v + 1}{2} \right) \right) V \\ &= \frac{d^2 V}{d v^2} + ((\alpha^2 - 2q) - 2q \cos 2v) V = 0, \end{aligned} \quad (2.4)$$

$$\begin{aligned} \frac{d^2 U}{d u^2} - (\alpha^2 - k^2 F^2 \cosh^2 u) U &= \frac{d^2 U}{d u^2} - \left(\alpha^2 - k^2 F^2 \left(\frac{\cosh 2u + 1}{2} \right) \right) U \\ &= \frac{d^2 U}{d u^2} - ((\alpha^2 - 2q) - 2q \cosh 2u) U = 0, \end{aligned} \quad (2.5)$$

4 2. MATHIEU FUNCTIONS

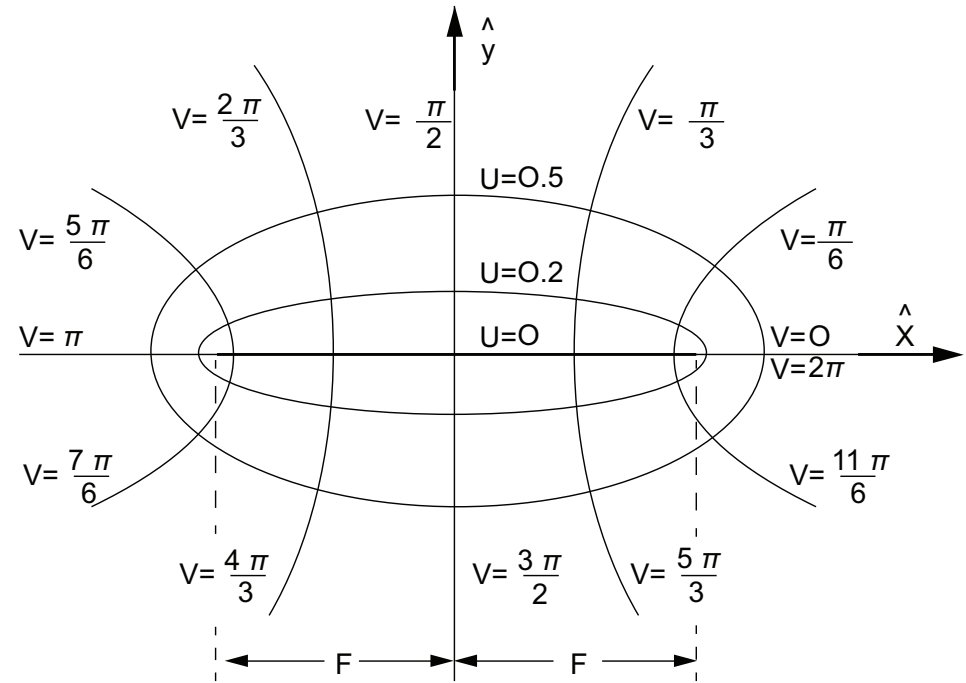


Figure 2.1: Elliptic cylinder coordinates.

$$\frac{d^2Z}{dz^2} + \left(k^2 + \frac{4q}{k^2} \right) Z = 0 . \quad (2.6)$$

Restricting the discussion to two dimensions by ignoring the z dependence, Eqs. (2.2) and (2.4) can be restated as:

$$\frac{d^2V}{dv^2} + (\lambda - 2q \cos 2v) V = 0 , \quad (2.7)$$

$$\frac{d^2U}{du^2} - (\lambda - 2q \cosh 2u) U = 0 , \quad (2.8)$$

where $q = k^2 F^2 / 4 = (kF/2)^2$, $\lambda = \alpha^2 - k^2 F^2 / 2$ and where α is a separation constant. For reference, q and F are related as shown in Table 2.1. Note that F has units of length (wavelength in this work) while q is dimensionless. An ellipse with an inter-focal distance of $2F = 1.0$ has a q value of 2.4674. An ellipse with an inter-focal distance of $2F = 10.0$ has a q value of 246.74.

Equation (2.7) is known as the *canonical Mathieu equation* and its solutions are known as the angular functions. Equation (2.8) is known as the *modified Mathieu equation* and results in the so-called radial functions. Both equations are second order and each can be expected to deliver two independent solutions.

Table 2.1: Relation between parameters q and F

q	F
1	0.3183
10	1.0066
100	3.1831
1000	10.066
10000	31.831

2.2 ANGULAR FUNCTIONS

Of the two independent solutions of Eq. (2.7), one is periodic and the second is not. As stated by Stratton [5, p. 376], “the electromagnetic field is a single-valued function of position and hence, if the properties of the medium are homogeneous with respect to the variable, v , it is necessary that $V(v)$ be a periodic function of the angle, v .” In other words, for problems such as electromagnetic scattering from an elliptic target, where v represents the angle around the target, the field outside the target is obviously periodic in v . Blanch [7, p. 722] states “the function must be periodic, of period π or 2π . It can be shown that there exists a countably infinite set of characteristic values, $a_r(q)$, which yield even periodic solutions” of (2.7); “there is another countably infinite sequence of characteristic values, $b_r(q)$ which yield odd periodic solutions” of (2.7). In the following, all angular Mathieu functions are associated with solutions of periods π and 2π .

Given that the angular function is periodic, one can expand $V(v)$ as a Fourier Series

$$V(v) = \sum_{m=0}^{\infty} (A_m \cos(mv) + B_m \sin(mv)) . \quad (2.9)$$

When this expansion is substituted into (2.7), one obtains the constraining equations

$$\begin{aligned} & \sum_{m=0}^{\infty} ((\lambda - m^2) A_m - q [A_{m-2} + A_{m+2}]) \cos(mv) \\ & + \sum_{m=1}^{\infty} ((\lambda - m^2) B_m - q [B_{m-2} + B_{m+2}]) \sin(mv) = 0 \\ & A_{-m}, B_{-m} = 0 \quad m > 0 . \end{aligned} \quad (2.10)$$

Equation (2.10) can be reduced to four simpler types where A_m and B_m are expansion coefficients yet to be determined.

6 2. MATHIEU FUNCTIONS

The four angular functions are defined, and computed, for a parameter range $0 \leq r \leq \infty$ using:

$$ce_{2r}(v, q) = \sum_{k=0}^{\infty} A_{2k}^{2r}(q) \cos(2kv), \quad (2.11)$$

$$ce_{2r+1}(v, q) = \sum_{k=0}^{\infty} A_{2k+1}^{2r+1}(q) \cos((2k+1)v), \quad (2.12)$$

$$se_{2r+1}(v, q) = \sum_{k=0}^{\infty} B_{2k+1}^{2r+1}(q) \sin((2k+1)v), \quad (2.13)$$

$$se_{2r+2}(v, q) = \sum_{k=0}^{\infty} B_{2k+2}^{2r+2}(q) \sin((2k+2)v), \quad (2.14)$$

where $r = 0, 1, 2, \dots$ and $k = 0, 1, 2, \dots$. The angular Mathieu functions of even order have a period of π , and those of an odd order have a period of 2π . The symbols used to represent the angular functions are ce and se which are abbreviated forms of “cosine elliptic” and “sine elliptic.” Note that $se_0 = 0$. In order to evaluate these functions, we need to know the values of the expansion coefficients $\{A\}$ and $\{B\}$ defined in (2.10).

2.2.1 RELATIONS SATISFIED BY THE EXPANSION FUNCTIONS $\{A\}$ AND $\{B\}$

The expansion coefficients satisfy a set of recurrence relations that define the ratios of the coefficients *and* a normalization of those coefficients. The recurrence relationships, together with their (arbitrary) normalization relationships, are summarized as follows. The functions $\{A\}$ and $\{B\}$ are determined as follows.

1. For $ce_{2r}(v, q)$

Recurrence relationship:

$$\begin{aligned} \lambda A_0^{2r} - q A_2^{2r} &= 0, \\ (\lambda - 4) A_2^{2r} - q (2A_0^{2r} + A_4^{2r}) &= 0, \\ (\lambda - (2k)^2) A_{2k}^{2r} - q (A_{2k-2}^{2r} + A_{2k+2}^{2r}) &= 0, \quad (k \geq 2). \end{aligned} \quad (2.15a)$$

Normalization relationship:

$$2(A_0^{2r})^2 + \sum_{k=1}^{\infty} (A_{2k}^{2r})^2 = 1. \quad (2.15b)$$

2. For $ce_{2r+1}(v, q)$

Recurrence relationship:

$$\begin{aligned} (\lambda - 1 - q) A_1^{2r+1} - q A_3^{2r+1} &= 0, \\ (\lambda - (2k+1)^2) A_{2k+1}^{2r+1} + A_{2k+3}^{2r+1} &= 0, \quad (k \geq 1). \end{aligned} \quad (2.15c)$$

Normalization relationship:

$$\sum_{k=0}^{\infty} (A_{2k+1}^{2r+1})^2 = 1. \quad (2.15d)$$

3. For $se_{2r+1}(v, q)$

Recurrence relationship:

$$\begin{aligned} (\lambda - 1 + q) B_1^{2r+1} - q B_3^{2r+1} &= 0, \\ (\lambda - (2k+1)^2) B_{2k+1}^{2r+1} - q (B_{2k-1}^{2r+1} + B_{2k+1}^{2r+1}) &= 0, \quad (k \geq 1). \end{aligned} \quad (2.15e)$$

Normalization relationship:

$$\sum_{k=0}^{\infty} (B_{2k+1}^{2r+1})^2 = 1. \quad (2.15f)$$

4. For $se_{2r+2}(v, q)$

Recurrence relationship:

$$\begin{aligned} (\lambda - 4) B_2^{2r+2} - q B_4^{2r+2} &= 0, \\ (\lambda - (2k+2)^2) B_{2k+2}^{2r+2} - q (B_{2k}^{2r+2} + B_{2k+4}^{2r+2}) &= 0, \quad (k \geq 1) \end{aligned} \quad (2.15g)$$

Normalization relationship:

$$\sum_{k=0}^{\infty} (B_{2k+2}^{2r+2})^2 = 1. \quad (2.15h)$$

Historically, the values of $\{A\}$ and $\{B\}$ have been computed through the use of continued fractions. An alternative, used in the present approach, is to express the preceding equations as matrix equations and solve them using matrix eigenvalue routines [12, 21, 26, 27, 31, 34]. The availability of reliable, fast and accurate matrix diagonalization programs allows the evaluation

8 2. MATHIEU FUNCTIONS

of N characteristic numbers and their respective N eigenvectors in a single pass for an N by N matrix. Equations (2.15a)–(2.15h) may be recast as:

$$\begin{bmatrix} 0 & \sqrt{2}q & 0 & 0 \\ \sqrt{2}q & 4 & q & \\ 0 & q & 16 & q \\ & & & \ddots \\ & & & & \ddots \\ & & & & & q & (2k)^2 & q \\ & & & & & & & \ddots \end{bmatrix} \begin{bmatrix} \sqrt{2}A_0^{2r} \\ A_2^{2r} \\ A_4^{2r} \\ & \ddots \\ & & A_{2k}^{2r} \\ & & & \ddots \end{bmatrix} = \lambda_{2k} \begin{bmatrix} \sqrt{2}A_0^{2r} \\ A_2^{2r} \\ A_4^{2r} \\ & \ddots \\ & & A_{2k}^{2r} \\ & & & \ddots \end{bmatrix}, \quad (2.16a)$$

$$\begin{bmatrix} 1+q & q & 0 & 0 \\ q & 9 & q & \\ 0 & q & 25 & q \\ & & & \ddots \\ & & & & \ddots \\ & & & & & q & (2k+1)^2 & q \\ & & & & & & & \ddots \end{bmatrix} \begin{bmatrix} A_1^{2r+1} \\ A_3^{2r+1} \\ A_5^{2r+1} \\ & \ddots \\ & & A_{2k+1}^{2r+1} \\ & & & \ddots \end{bmatrix} = \lambda_{2k+1} \begin{bmatrix} A_1^{2r+1} \\ A_3^{2r+1} \\ A_5^{2r+1} \\ & \ddots \\ & & A_{2k+1}^{2r+1} \\ & & & \ddots \end{bmatrix}, \quad (2.16b)$$

$$\begin{bmatrix} 4 & q & 0 & 0 \\ q & 16 & q & \\ 0 & q & 36 & q \\ & & & \ddots \\ & & & & \ddots \\ & & & & & q & (2k)^2 & q \\ & & & & & & & \ddots \end{bmatrix} \begin{bmatrix} B_2^{2r+2} \\ B_4^{2r+2} \\ B_6^{2r+2} \\ & \ddots \\ & & B_{2k}^{2r+2} \\ & & & \ddots \end{bmatrix} = \lambda_{2k} \begin{bmatrix} B_2^{2r+2} \\ B_4^{2r+2} \\ B_6^{2r+2} \\ & \ddots \\ & & B_{2k}^{2r+2} \\ & & & \ddots \end{bmatrix}, \quad (2.16c)$$

$$\begin{bmatrix} 1-q & q & 0 & 0 \\ q & 9 & q & \\ 0 & q & 25 & q \\ & & \ddots & \\ & & & \ddots \\ & & & q & (2k+1)^2 & q \\ & & & & \ddots & \end{bmatrix} \begin{bmatrix} B_1^{2r+1} \\ B_3^{2r+1} \\ B_5^{2r+1} \\ \vdots \\ B_{2k+1}^{2r+1} \\ \vdots \end{bmatrix} = \lambda_{2k+1} \begin{bmatrix} B_1^{2r+1} \\ B_3^{2r+1} \\ B_5^{2r+1} \\ \vdots \\ B_{2k+1}^{2r+1} \\ \vdots \end{bmatrix}. \quad (2.16d)$$

Assuming the dimension of any one of the preceding matrix eigenvalue equations is truncated to N , it yields N different eigenvalues $\{\lambda\}$, each corresponding to a different eigenvector of coefficients $\{A\}$ and $\{B\}$. In the computation of Mathieu functions, each eigenresult will be assigned a unique index ($2r$, $2r + 1$ or $2r + 2$, as shown in the equations), which will correspond to a different Mathieu function “order.” As an example, consider (2.16a). The N eigenvalues obtained from solving (2.16a) must be ordered from smallest to largest, and appropriate indices assigned to the eigenvectors according to $r = \{0, 1, 2, \dots, N - 1\}$, or, equivalently, $2r = \{0, 2, 4, \dots, 2(N - 1)\}$. Each eigenvector therefore contains coefficients that contribute to Mathieu functions of one order, as defined in the following sections.

The symmetry in (2.16b)–(2.16d) arises naturally from the defining equations of (2.15c), (2.15e), and (2.15g), respectively. The defining equation of (2.15a) does not lead immediately to a symmetrical matrix, but can be manipulated to do so, as shown by [26, 27, 31]. Each of the Eqs. (2.15a)–(2.15d) thus involves a symmetrical tri-diagonal matrix. Several matrix solution packages [39–41] are available that can be used to solve these equations. As already stated, the final results need to be arranged with the eigenvalues ranked in ascending order so that the associated eigenvectors can be readily used in evaluating the terms in Eqs. (2.11)–(2.14). The convergence of these summations is discussed in Chapter 3.

2.3 RADIAL FUNCTIONS

The two linearly independent solutions for the radial functions will be denoted $Mc_i^{(j)}$ and $Ms_i^{(j)}$ where $j = 1, 2, 3, 4$ signifies the kind of the function (in a manner similar to those used in Hankel function definitions) and $i = 2r, 2r + 1$ or $2r + 2$ with $0 \leq r < \infty$. The general expressions used hereafter are given by [7] in terms of products of Bessel functions and are reproduced as follows together with their derivatives.

10 2. MATHIEU FUNCTIONS

The first type of radial function is defined by

$$Mc_{2r}^{(j)} = \frac{1}{\varepsilon_s A_{2s}^{2r}(q)} \sum_{k=0}^{\infty} (-1)^{k+r} A_{2k}^{2r}(q) \left[J_{k-s}(u_1) Z_{k+s}^{(j)}(u_2) + J_{k+s}(u_1) Z_{k-s}^{(j)}(u_2) \right], \quad (2.17)$$

where $\varepsilon_s = 2$ when $s = 0$ and $\varepsilon_s = 1$ when $s = 1, 2, 3, \dots$. In this expression,

$$\begin{aligned} Z_p^{(1)}(u) &= J_p(u); & Z_p^{(2)}(u) &= Y_p(u); & Z_p^{(3)}(u) &= H_p^{(1)}(u); & Z_p^{(4)}(u) &= H_p^{(2)}(u) \\ u_1 &= \sqrt{q}e^{-u} & \frac{du_1}{dz} &= -\sqrt{q}e^{-u} & u_2 &= \sqrt{q}e^u & \frac{du_2}{dz} &= \sqrt{q}e^u. \end{aligned} \quad (2.18)$$

The coefficients in (2.17) are the same as those used in the angular Mathieu function in (2.13). The first derivative of (2.17) is

$$\begin{aligned} \frac{d}{du} Mc_{2r}^{(j)} &= \frac{1}{\varepsilon_s A_{2s}^{2r}(q)} \sum_{k=0}^{\infty} (-1)^{k+r} A_{2k}^{2r}(q) \\ &\quad \left[\frac{d}{du} \left(J_{k-s}(u_1) Z_{k+s}^{(j)}(u_2) \right) + \frac{d}{du} \left(J_{k+s}(u_1) Z_{k-s}^{(j)}(u_2) \right) \right] \\ &= \frac{\sqrt{q}}{\varepsilon_s A_{2s}^{2r}(q)} \sum_{k=0}^{\infty} (-1)^{k+r} A_{2k}^{2r}(q) \\ &\quad \left[\begin{array}{l} e^u \left\{ J_{k-s}(u_1) Z_{k+s}^{(j)}(u_2) + J_{k+s}(u_1) Z_{k-s}^{(j)}(u_2) \right\} \\ -e^{-u} \left\{ J'_{k-s}(u_1) Z_{k+s}^{(j)}(u_2) + J'_{k+s}(u_1) Z_{k-s}^{(j)}(u_2) \right\} \end{array} \right]. \end{aligned} \quad (2.19)$$

The function $Mc_{2r+1}^{(j)}$ is defined

$$\begin{aligned} Mc_{2r+1}^{(j)} &= \frac{1}{A_{2s+1}^{2r+1}(q)} \sum_{k=0}^{\infty} (-1)^{k+r} A_{2k+1}^{2r+1}(q) \\ &\quad \left[J_{k-s}(u_1) Z_{k+s+1}^{(j)}(u_2) + J_{k+s+1}(u_1) Z_{k-s}^{(j)}(u_2) \right]. \end{aligned} \quad (2.20)$$

The derivative of (2.20) is

$$\begin{aligned}
\frac{d}{du} Mc_{2r+1}^{(j)} &= \frac{1}{A_{2s+1}^{2r+1}(q)} \sum_{k=0}^{\infty} (-1)^{k+r} A_{2k+1}^{2r+1}(q) \\
&\quad \left[\frac{d}{du} (J_{k-s}(u_1) Z_{k+s+1}^{(j)}(u_2)) + \frac{d}{du} (J_{k+s+1}(u_1) Z_{k-s}^{(j)}(u_2)) \right] \\
&= \frac{\sqrt{q}}{A_{2s+1}^{2r+1}(q)} \sum_{k=0}^{\infty} (-1)^{k+r} A_{2k+1}^{2r+1}(q) \\
&\quad \left[\begin{array}{l} e^u \left\{ J_{k-s}(u_1) Z'_{k+s+1}^{(j)}(u_2) + J_{k+s+1}(u_1) Z'_{k-s}^{(j)}(u_2) \right\} \\ -e^{-u} \left\{ J'_{k-s}(u_1) Z_{k+s+1}^{(j)}(u_2) + J'_{k+s+1}(u_1) Z_{k-s}^{(j)}(u_2) \right\} \end{array} \right]. \tag{2.21}
\end{aligned}$$

For $Ms_{2r+1}^{(j)}$, we have

$$\begin{aligned}
Ms_{2r+1}^{(j)} &= \frac{1}{B_{2s+1}^{2r+1}(q)} \sum_{k=0}^{\infty} (-1)^{k+r} B_{2k+1}^{2r+1}(q) \\
&\quad \left[J_{k-s}(u_1) Z_{k+s+1}^{(j)}(u_2) - J_{k+s+1}(u_1) Z_{k-s}^{(j)}(u_2) \right]. \tag{2.22}
\end{aligned}$$

The derivative of (2.22) is

$$\begin{aligned}
\frac{d}{du} Ms_{2r+1}^{(j)} &= \frac{1}{B_{2s+1}^{2r+1}(q)} \sum_{k=0}^{\infty} (-1)^{k+r} B_{2k+1}^{2r+1}(q) \\
&\quad \left[\frac{d}{du} (J_{k-s}(u_1) Z_{k+s+1}^{(j)}(u_2)) - \frac{d}{du} (J_{k+s+1}(u_1) Z_{k-s}^{(j)}(u_2)) \right] \\
&= \frac{\sqrt{q}}{B_{2s+1}^{2r+1}(q)} \sum_{k=0}^{\infty} (-1)^{k+r} B_{2k+1}^{2r+1}(q) \\
&\quad \left[\begin{array}{l} e^u \left\{ J_{k-s}(u_1) Z'_{k+s+1}^{(j)}(u_2) - J_{k+s+1}(u_1) Z'_{k-s}^{(j)}(u_2) \right\} \\ -e^{-u} \left\{ J'_{k-s}(u_1) Z_{k+s+1}^{(j)}(u_2) - J'_{k+s+1}(u_1) Z_{k-s}^{(j)}(u_2) \right\} \end{array} \right]. \tag{2.23}
\end{aligned}$$

Finally, $Ms_{2r}^{(j)}$ is defined as

$$Ms_{2r}^{(j)} = \frac{1}{B_{2s}^{2r}(q)} \sum_{k=1}^{\infty} (-1)^{k+r} B_{2k}^{2r}(q) \left[J_{k-s}(u_1) Z_{k+s}^{(j)}(u_2) - J_{k+s}(u_1) Z_{k-s}^{(j)}(u_2) \right], \tag{2.24}$$

12 2. MATHIEU FUNCTIONS

where the summation index k starts at 1, and $s \geq 1$. The first derivative of (2.24) is

$$\begin{aligned} \frac{d}{du} Ms_{2r}^{(j)} &= \frac{1}{B_{2s}^{2r}(q)} \sum_{k=1}^{\infty} (-1)^{k+r} B_{2k}^{2r}(q) \\ &\quad \left[\frac{d}{du} (J_{k-s}(u_1) Z_{k+s}^{(j)}(u_2)) - \frac{d}{du} (J_{k+s}(u_1) Z_{k-s}^{(j)}(u_2)) \right] \\ &= \frac{\sqrt{q}}{B_{2s}^{2r}(q)} \sum_{k=1}^{\infty} (-1)^{k+r} B_{2k}^{2r}(q) \\ &\quad \left[\begin{array}{l} e^u \left\{ J_{k-s}(u_1) Z'_{k+s}^{(j)}(u_2) - J_{k+s}(u_1) Z'_{k-s}^{(j)}(u_2) \right\} \\ -e^{-u} \left\{ J'_{k-s}(u_1) Z_{k+s}^{(j)}(u_2) - J'_{k+s}(u_1) Z_{k-s}^{(j)}(u_2) \right\} \end{array} \right]. \end{aligned} \quad (2.25)$$

These specific equations for $Mc_q^{(j)}$ and $Ms_q^{(j)}$ were derived in the early 1900s. A more recent derivation is reported by Van Buren and Boisvert [33], along with references to earlier works.

The preceding equations involve the parameter s in the subscripts of the Bessel functions, which according to Blanch [7] is an “arbitrary” integer. As stated by Van Buren and Boisvert [33], “researchers have traditionally … computed Mathieu radial functions with s set equal to 0 except for $Ms_n^j(u, q)$ with n even where s is set equal to 1. This choice can provide accurate radial function values for some parameter values, especially when n and q are not large.” These choices of s (0 and/or 1) were adopted by Zhang and Jin [28], for example, in their codes, and are used by Cojocaru in his MATLAB toolbox [34, 36]. In the following, we label this choice the “traditional” approach.

Blanch [7] reported that the choice of s affects the convergence rate of the summations, and suggested alternative choices. In addition, Van Buren and Boisvert [33] noted that when n or q are large, using $s = 0$ (or $s = 1$) “can lead to significant subtraction errors” in the computations. In Chapter 3, we explore an alternative choice for selecting s and demonstrate the superiority of algorithms that employ it. We note that many other researchers have also employed alternative choices for the parameter s [12, 15, 18, 26].

2.4 COMPUTATIONAL STEPS

At this point, we have derived all the various terms of the Mathieu equations. It remains to show how they are used. By way of illustration, suppose we want to express a uniform plane wave (normal to the z axis and subtending an angle ϕ^{inc} , to the x axis)

$$E_z^{inc} = E_0 e^{-jk(x \cos \phi^{inc} + y \sin \phi^{inc})}, \quad (2.26)$$

in terms of Mathieu functions. The expression in Mathieu functions in terms of the variables (u, v) that correspond to (x, y) is

$$E_z^{inc} = 2E_0 \sum_{m=0}^{\infty} j^m \begin{bmatrix} Mc_m^{(1)}(kF, u) ce_m(kF, v) ce_m(kF, \phi^{inc}) \\ + Ms_m^{(1)}(kF, u) se_m(kF, v) se_m(kF, \phi^{inc}) \end{bmatrix}. \quad (2.27)$$

Note the summation over m . As m proceeds through even and odd values, the summed terms must include values associated with the angular functions of Eqs. (2.13)–(2.16a)–(2.16d) and those associated with the radial functions of Eqs. (2.17), (2.20), (2.22) and (2.24), in which the superscript is $j = 1$. As we will see in later chapters, calculations arising in various boundary value problems will always include Eqs. (2.13)–(2.16a)–(2.16d) and some of the Eqs. (2.17)–(2.25), although the value of the superscript in the latter equations may vary.

For the present illustration, we will approach the computation of Mathieu functions by computing the complete set of vectors. We will use the traditional approach where s is set equal to 0 except for $Ms_n^j(u, q)$ with n even where s is set equal to 1. Note that an accurate calculation of Bessel function(s) is important.

The necessary steps for computing the various components of any function that is expressed in terms of Mathieu functions may be summarized as follows:

1. Determine the appropriate value of $q = k^2 F^2 / 4$, where F is the semi-focal dimension of the elliptic structure being examined as shown in Figure 2.1. (For the plane wave, any value of F may be used.)
2. Next, decide on the initial size of the matrix, $N \times N$, for computing the eigenvalues and eigenvectors of the matrices of (2.16a)–(2.16d). Many of the examples in this book can be resolved with $N < 50$. However, depending on the value of q , one might need to use a value of $N = 1000$ or higher. (More insight into the choice of N will be provided in Chapters 4 and 5.) In any event, after the first choice of N , the calculation may need to be repeated with a higher value of N to investigate convergence of the final result.
3. Calculate the eigenvalues and eigenvectors of the matrices of (2.16a)–(2.16d), using the values of N and q selected in steps 1 and 2 above.
4. Sort the columns of each matrix so that the left-most column is associated with the smallest eigenvalue and the right-most column is associated with the largest eigenvector. These eigenvectors are a function of q only.
5. Using appropriate values of the angular value, v , and ϕ^{inc} , the angular functions of Eqs. (2.11)–(2.14) can be calculated.
6. The process continues with the calculation of the radial functions using the radial dimension, u . The specific radial functions, which are defined by the parameter, $1 \leq j \leq 4$, and possibly their derivatives, will be those that are required by the problem formulation.

14 2. MATHIEU FUNCTIONS

7. Finally, the summation in (2.27) is undertaken, noting that the maximum value of m is $2(N - 1)$ because the odd and even values of the angular and radial functions each have a matrix size of $(N \times N)$.
8. Terms in the summation (2.27) are examined to see if the result, as a function of m , has converged. If it has, the result is accepted. If it has not, increasing the value of N may help. However, it may be necessary to move away from the traditional approach to that recommended by [7], which is covered in Chapters 3 and 4.

2.5 SUMMARY

Elliptic coordinates and Mathieu functions are defined. Mathieu functions are defined in terms of infinite summations, for which coefficients must be separately computed. These coefficients may be obtained as eigenvectors of tri-diagonal matrices. In the traditional approach for computing radial Mathieu functions, an arbitrary parameter, s , is set equal to 0 except for $M_s^j(u, q)$ with n even where s is set equal to 1. However, the resulting convergence of some of the summations may be slow, and may actually diverge after a few terms, and the possible accuracy obtained from the summations is limited in some cases by subtraction errors. These issues will be explored in the following chapter, where an alternative algorithm to the traditional approach is introduced for the computation of the radial functions.

CHAPTER 3

Observed Accuracy Using Traditional and Tuned Methods

The previous chapter defined Mathieu functions, but intentionally deferred a discussion of the convergence rates of the various summations, an assessment of the accuracy of the calculations of the various functions, the question of how large the coefficient matrices must be to produce results of desired accuracy and the effects of machine precision on the computations. This chapter will attempt to address such issues.

To illustrate the need for accuracy consider the results of Table 3.1, where m is the eigenvector column number and N is the matrix size. Here the error in the value of a plane wave expressed in Mathieu functions, as described in Section 2.4 of Chapter 2, is shown as a function of series truncation (m) and matrix size (N). The table shows the common logarithm of the difference between the exact value and the value produced by (2.27), for location $x = 0, y = 0$. This calculation was done with $q = 10$. Two issues are immediately apparent. First, although the error initially decreases as m is increased, beyond a value of $m = 9$ the error increases and never again reaches the original best level. Second, increasing the value of N does not help above $N = 50$. These results were obtained using the traditional approach described at the end of Chapter 2. Since double precision software was used, one would expect to see an error that converges to -15.0 or better as m and N increase.

In summary, there are two problematic issues. First, as m increases the reduction in the error is not sustained. Second, the error minimum plateaus around $m = 9$ regardless of the value of N .

As the theoretical underpinnings of Mathieu functions are rigorous, there are apparently numerical issues associated with the convergence of the summations in (2.27) that need to be investigated. In this chapter, the computational issues associated with the angular functions are examined first, followed by an examination of the radial functions. In connection with the radial functions, we introduce an alternative approach for the choice of s in the various summations, following the recommendations of Blanch [7]. We name the alternative approach the tuned approach and label the results of this procedure with tuned in various plots. Since this arises only in connection with the radial functions, we defer the discussion of the tuned approach until Section 3.2.

The issue of machine precision, mentioned in the opening paragraph of this chapter, is multi-faceted. When appropriate, multiple precision software [42] is used to establish a key result.

16 3. OBSERVED ACCURACY USING TRADITIONAL AND TUNED METHODS

Table 3.1: Results for $\log_{10}(E_z^{inc} - 1)$, where E_z^{inc} is computed using Eq. (2.27) with M terms and $E_0 = 1$. N denotes the matrix size for the eigenvalue calculation. E_z^{inc} is evaluated at (0,0)

M	N = 10	N = 20	N = 30	N = 40	N = 50	N = 60	N = 70	N = 80
1	-0.36376	-0.36376	-0.36376	-0.36376	-0.36376	-0.36376	-0.36376	-0.36376
2	-0.48641	-0.48641	-0.48641	-0.48641	-0.48641	-0.48641	-0.48641	-0.48641
3	-1.15471	-1.15471	-1.15471	-1.15471	-1.15471	-1.15471	-1.15471	-1.15471
4	-2.46268	-2.46268	-2.46268	-2.46268	-2.46268	-2.46268	-2.46268	-2.46268
5	-4.00107	-4.00107	-4.00107	-4.00107	-4.00107	-4.00107	-4.00107	-4.00107
6	-5.71370	-5.71370	-5.71370	-5.71370	-5.71370	-5.71370	-5.71370	-5.71370
7	-7.04549	-7.56974	-7.56974	-7.56973	-7.56973	-7.56972	-7.56972	-7.56973
8	-4.34725	-9.55112	-9.54864	-9.54923	-9.54982	-9.54756	-9.55361	-9.54994
9	-1.44704	-10.6733	-10.7076	-11.6193	-11.6941	-11.1133	-10.6416	-11.0338
10	1.28246	-9.96849	-9.71621	-10.0762	-10.0743	-11.1133	-9.55015	-10.1132
11		-9.03065	-8.84505	-8.87929	-8.87916	-9.37688	-8.71435	-9.12651
12		-8.47863	-8.84505	-8.87929	-8.21463	-8.70553	-8.04095	-9.12651
13		-8.47863	-7.46205	-7.81757	-7.25396	-7.50707	-8.04095	-7.47071
14		-6.56422	-6.5172	-6.92264	-6.58871	-6.78033	-6.84218	-6.51817
15		-6.22794	-6.5172	-6.12075	-5.66332	-6.78033	-5.84791	-6.2061
:								
20		6.03197	-1.82669	-2.21914	-2.23922	-1.76002	-1.82237	-2.76339
:								
25			1.22896	1.3723	1.79459	1.42046	1.04569	1.43009
:								
30			11.29127	5.42657	5.4971	5.37856	4.69763	4.48562

If and when it is used in this work, it is explicitly so stated. Much of the work reported in the literature uses double precision Fortran. This was found to be adequate for small values of q . However, for large values of q and particularly for low values of u , underflow/overflow occurred in the calculation of the Bessel functions necessary in the calculation of the radial functions. Consequently, the radial functions were all calculated in quad precision Fortran. Since all of the target functions, such as Hankel functions, the plane wave, currents on a 2D strip, etc., involve both angular and radial functions, the angular functions were also calculated in quad precision. However, all associated results are reported to double precision accuracy only.

3.1 ANGULAR FUNCTIONS

The angular Mathieu functions are defined in Eqs. (2.11)–(2.14). These are functions of the elliptic angle, v , the parameter q and the number of terms, N , used in the summations. There are no

known analytical solutions to these functions to use as a reference, so the question of how to assess the accuracy of the summations remains. Two approaches to answering this question are considered next.

3.1.1 SUBTRACTION ERROR

It was observed by Van Buren and Boisvert [33] that a major source of potential error in these summations is subtraction error, which occurs when two numbers of similar magnitudes, but different signs, are added together. When summing a series of numbers in finite precision arithmetic, the most robust approach is to separately sum negative and positive terms. Using this approach, negative values are temporarily stored in one array as absolute values, while positive values are stored in a separate array. The values of each array are sorted in order of ascending values and then summed starting with the smallest value. Let us define Sum_+ as the sum of the positive terms, while Sum_- is the sum of the absolute values of all the negative terms. As the final step, Sum_- is subtracted from Sum_+ to arrive at the ultimate answer. This procedure guards against 1) loss of accuracy that can arise if one subtracts two numbers that are large with respect to their difference and 2) by adding the smallest numbers first, one is assured that a large value is not added directly to a much smaller number, albeit of the same sign, which could result in the information in the smaller number being lost.

Subtraction error may be defined [33] as

$$\text{Subtraction Error} = \log_{10} \left| \frac{Sum_+}{Sum_+ - Sum_-} \right|. \quad (3.1)$$

The subtraction error is the number of digits lost during the calculation, even when following the robust process explained above. The number of digits of accuracy in a result is the number of digits of the precision of the code in use minus the subtraction error. For example, when using double precision Fortran code, the inherent precision is approximately 16 digits. So, if a particular calculation has a subtraction error of 10 digits, the final result can be, at best, good to only 6 digits.

The magnitude of the subtraction error is shown in Figure 3.1 for one set of parameters—the same as those used in Figure 1 of [33]. They use a parameter c which is related to q by $q = c^2/4$ [43]. The results of Figures 3.1 and 3.2 were calculated using two different levels of precision. One approach used the multiple precision package mpfun90 [42] using 500 decimal digits, and the other approach used the quad-double, QD, package of [44] which uses 64 decimal digits. Both produced the same results. In Figure 3.1 the worst case subtraction error is 43 digits—calculated with both mpfun90 and QD. The agreement with Figure 1 of [33], which was calculated in double precision, is excellent, providing independent validation of the two codes.

The results shown in Figures 3.3–3.6 were calculated with the aforementioned multiple precision software. Figure 3.3 illustrates the effect of the elliptic angle, v , on subtraction error for the angular functions. These results use only the eigenvectors associated with the two smallest eigenvalues. As can be seen, the error is worst at the extremes of the range ($v = 0, \pm\pi$) and for

18 3. OBSERVED ACCURACY USING TRADITIONAL AND TUNED METHODS

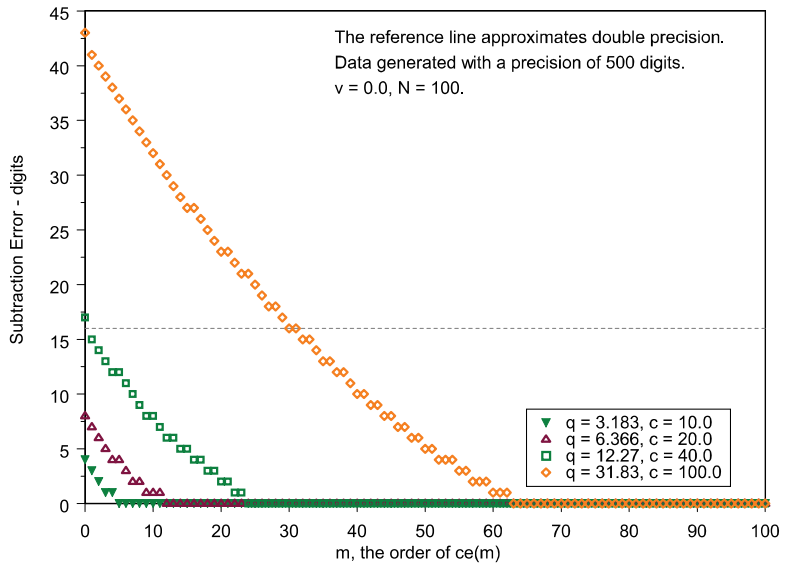


Figure 3.1: Plot of the Subtraction Error for ce_m as a function of m . Although the matrix size is only 100, the even and odd functions, when combined, produce a total of 200 values. Only the first 100 are shown.

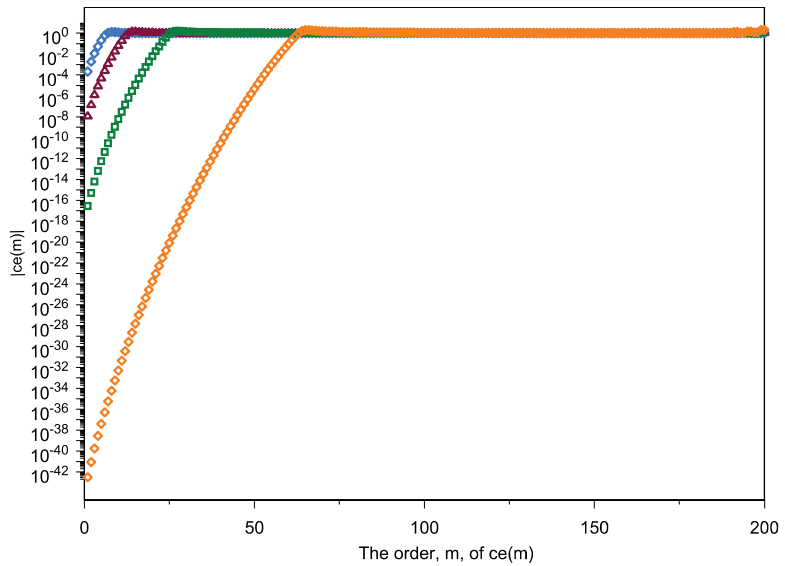


Figure 3.2: Plot of the magnitude of ce_m as a function of m for $v = 0$. Although the matrix size is only 100, the even and odd functions, when combined, produce a total of 200 values.

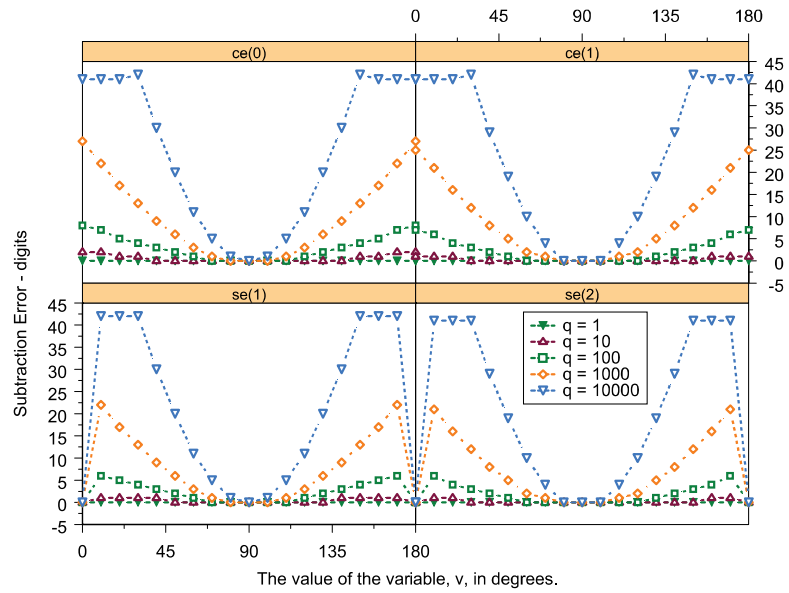


Figure 3.3: Plots of the Subtraction Error encountered in the first two ce and se functions versus the value of the angular function for $N = 100$.

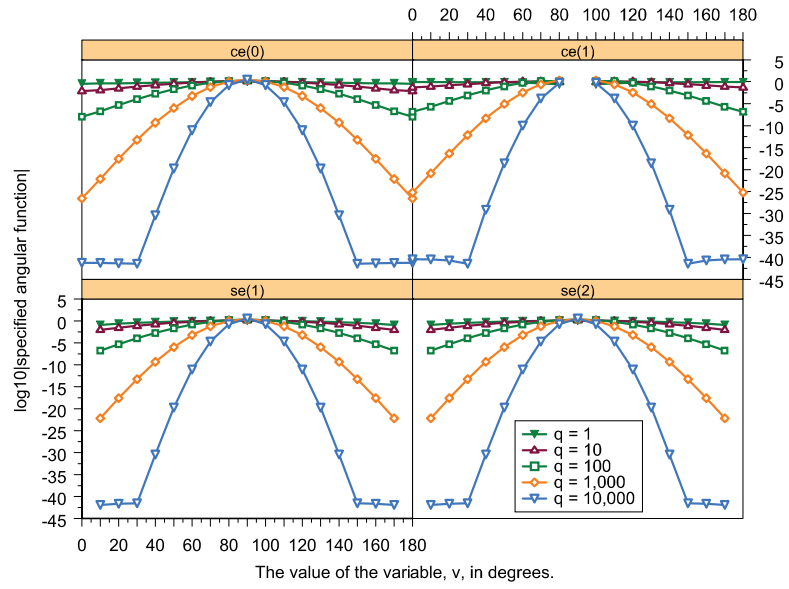


Figure 3.4: Plots of the magnitude of the first and second values of the angular functions ce and se , for $N = 100$.

20 3. OBSERVED ACCURACY USING TRADITIONAL AND TUNED METHODS

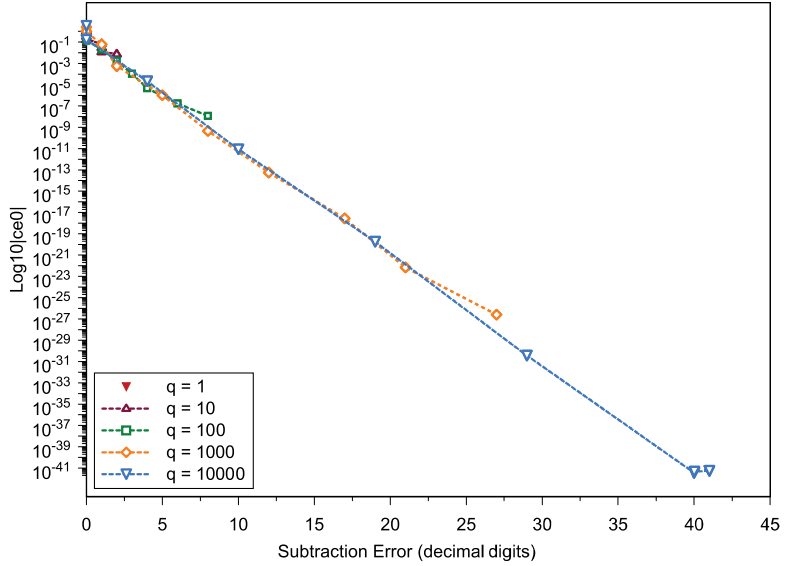


Figure 3.5: Plot of the magnitude of the Mathieu function, ce_0 versus the Subtraction Error evaluated at various values of v in 10-degree increments between 0 and 180 degrees, for various values of q .

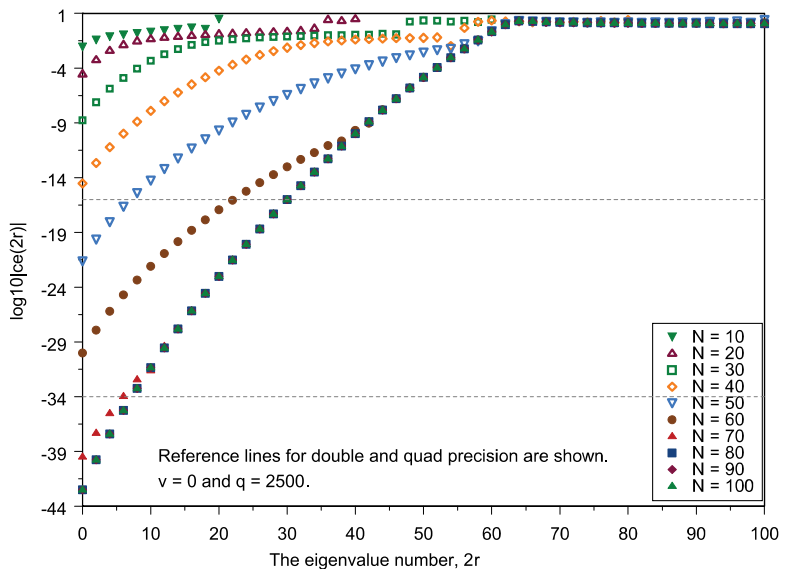


Figure 3.6: Plot of the even order angular function ce_{2r} versus the eigenvalue number $2r$, $r = 0, 1, 2, \dots$ for various values of N .

large values of q . It should be noted that the data in Figure 3.1 were calculated with $v = 0$ which, as we now see, is the worst case.

The effect of q on the subtraction error is also illustrated in Figure 3.3, where we see that high values of subtraction error are correlated with high values of q . The large values of subtraction error shown in Figure 3.3 would normally be of considerable concern. However, they need not be in this case, since the terms with the highest subtraction errors are also associated with values of ce_m and se_m that have the smallest magnitudes as seen in Figure 3.4.

The favorable relationship between the magnitude of the angular functions and their associated subtraction error is illustrated somewhat differently in Figure 3.5, where it can be seen that the values of $\log_{10} |ce_{2r}|$ are inversely proportional to the order of the eigenvalue, $2r$, up to a value of $2r \simeq 64$, which is in agreement with the findings of [33]. Also as reported in Figure 3.5, it is observed that a strong relationship exists between the magnitude of $\log_{10} |ce_{2r}|$ and the associated subtraction error which is independent of both q and v , although it is not known at this time how to exploit this relationship.

Figure 3.6 illustrates the effect of varying N on the value of $\log_{10} |ce_{2r}|$. For the parameters used, a value of $N = 100$ suffices. As this is for a value of $v = 0$, smaller values of N may be suitable. To date no deterministic method for *a priori* deciding on the necessary minimum value of N is known. We will return to this issue in Section 3.3.

Many applications may never use values close to the extremes of Figure 3.3, in which case the subtraction errors may become insignificant. However, as pointed out by Van Buren and Boisvert [33], “the angular functions and their derivatives at $v = 0$ and $v = \pi/2$ do appear in some traditional expressions for the radial functions in series of Bessel functions. Since some of these special values involve significant subtraction errors during computation, their appearance often determines which expressions to use to compute a given function.”

Finally, it should be understood that there is no way to avoid subtraction error. However, knowledge of its existence means that special attention should be paid to the summations involved so that the consequences are minimized. If subtraction error is determined to be a problem, it can be overcome with the use of higher precision.

3.1.2 BACK SUBSTITUTION

Another form of error analysis/detection was used by Van den Berg and Van Schaik [15] in which they substituted the computed eigenvalue and the associated eigenvector into the Mathieu equation in (2.7) to estimate the error. Specifically, where the subscripts k and r are the same as those used in (2.11)–(2.14):

$$\begin{aligned} Error_{ce2r} &= \frac{\partial^2}{\partial v^2} (ce_{2r}(v, q)) + (\lambda_{2k} - 2q \cos(2kv)) ce_{2r}(v, q) \\ &= \sum_{k=0}^{\infty} A_{2k}^{2r}(q) \cos(2kv) \left[(\lambda_{2k} - 2q \cos(2kv)) - (2k)^2 \right], \end{aligned} \tag{3.2a}$$

22 3. OBSERVED ACCURACY USING TRADITIONAL AND TUNED METHODS

$$\begin{aligned} Error_{ce_{2r+1}} &= \frac{\partial^2}{\partial v^2} (ce_{2r+1}(v, q)) + (\lambda_{2k+1} - 2q \cos((2k+1)v)) ce_{2r+1}(v, q) \\ &= \sum_{k=0}^{\infty} A_{2k+1}^{2r+1}(q) \cos((2k+1)v) \\ &\quad \left[(\lambda_{2k+1} - 2q \cos((2k+1)v)) - (2k+1)^2 \right], \end{aligned} \quad (3.2b)$$

$$\begin{aligned} Error_{se_{2r+1}} &= \frac{\partial^2}{\partial v^2} (se_{2r+1}(v, q)) + (\lambda_{2k+1} - 2q \cos((2k+1)v)) se_{2r+1}(v, q) \\ &= \sum_{k=0}^{\infty} B_{2k+1}^{2r+1}(q) \sin((2k+1)v) \\ &\quad \left[(\lambda_{2k+1} - 2q \cos((2k+1)v)) - (2k+1)^2 \right], \end{aligned} \quad (3.2c)$$

$$\begin{aligned} Error_{se_{2r+2}} &= \frac{\partial^2}{\partial v^2} (se_{2r+2}(v, q)) + (\lambda_{2k+2} - 2q \sin((2k+2)v)) se_{2r+2}(v, q) \\ &= \sum_{k=0}^{\infty} B_{2k+2}^{2r+2}(q) \sin((2k+2)v) \\ &\quad \left[(\lambda_{2k+2} - 2q \sin((2k+2)v)) - (2k+2)^2 \right]. \end{aligned} \quad (3.2d)$$

When either term was less than a certain threshold, in their case 10^{-10} , Van den Berg and Van Schaik [15] terminated the summation for that specific eigenvector.

A somewhat different approach is adopted here. Before describing this approach, we need to examine the data in Figures 3.7–3.12. The difference between each of these graphs is the size, $N \times N$, of the eigenvalue/vector matrix. The values of v were selected simply to avoid sub-multiples of 90 and 180 degrees. The data were calculated in quad precision before converting to double precision.

The following conclusions can be drawn from Figures 3.7–3.12:

1. As the value of q increases, so does the need for a larger value of N to obtain stability in the measure of the error value.
2. The sharp change in slope of the error curve, the break-point—if there is one—can be observed easily.
3. Over the range considered, the error values associated with the highest order, i.e., the largest eigenvalue, cannot be avoided by simply increasing N .

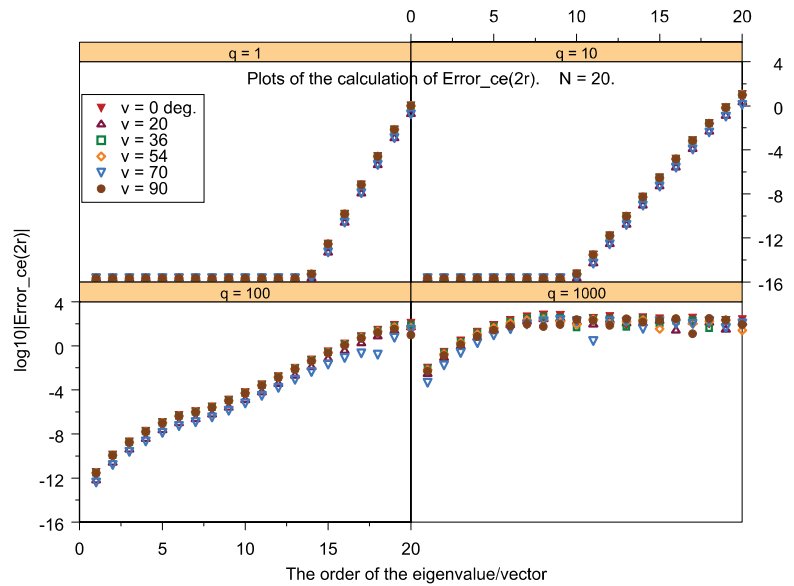


Figure 3.7: Plots of the error in ce_{2r} , Eq. (3.2a), as a function of the order of the eigenvector for $N = 20$.

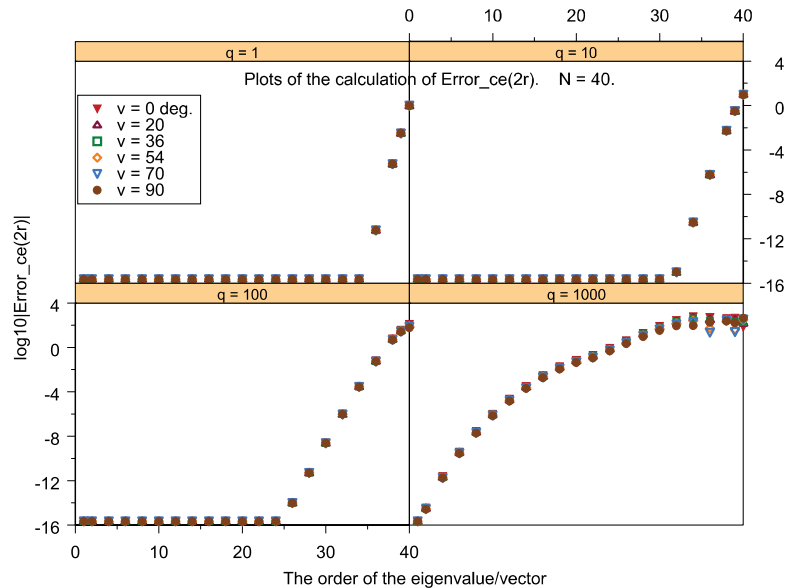


Figure 3.8: Plots of the error in ce_{2r} , Eq. (3.2a), as a function of the order of the eigenvector for $N = 40$.

24 3. OBSERVED ACCURACY USING TRADITIONAL AND TUNED METHODS

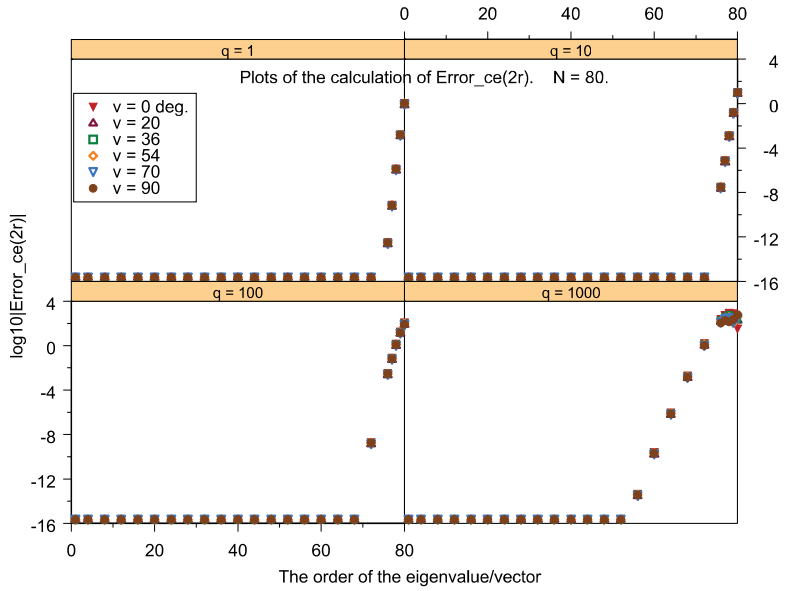


Figure 3.9: Plots of the error in ce_{2r} , Eq. (3.2a), as a function of the order of the eigenvector for $N = 80$.

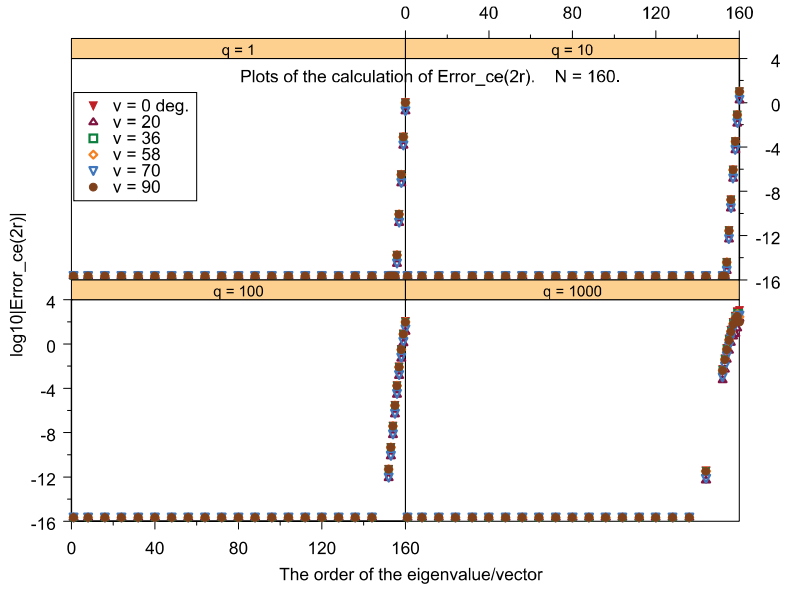


Figure 3.10: Plots of the error in ce_{2r} , Eq. (3.2a), as a function of the order of the eigenvector for $N = 160$.

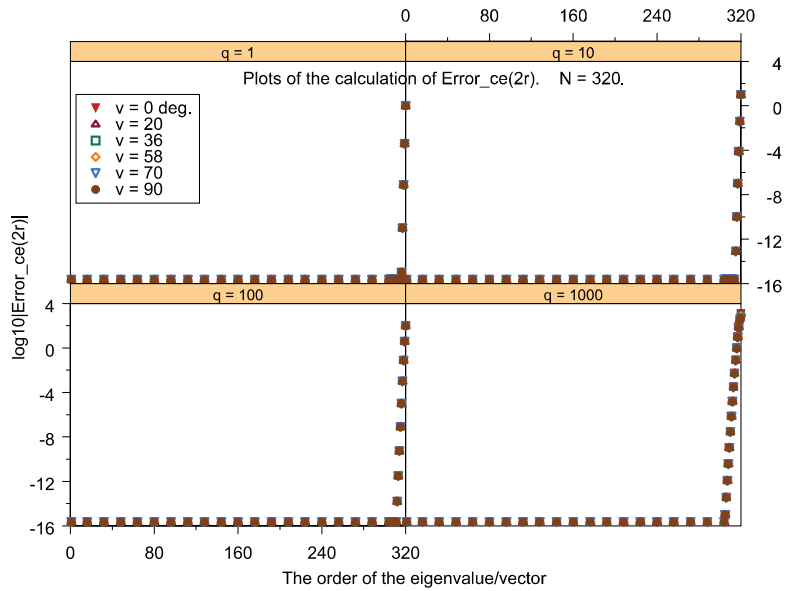


Figure 3.11: Plots of the error in ce_{2r} , Eq. (3.2a), as a function of the order of the eigenvector for $N = 320$.

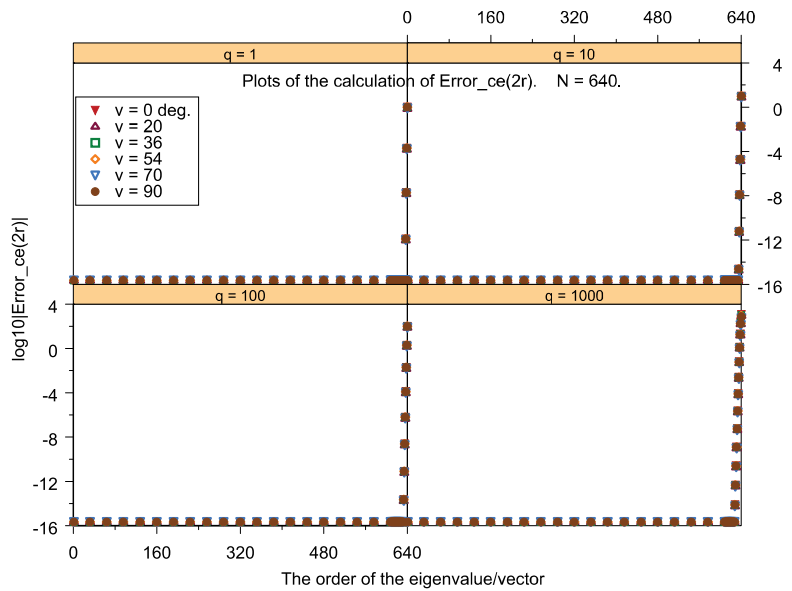


Figure 3.12: Plots of the error in ce_{2r} , Eq. (3.2a), as a function of the order of the eigenvector for $N = 640$.

26 3. OBSERVED ACCURACY USING TRADITIONAL AND TUNED METHODS

Unfortunately, there is no obvious simple relationship evident in Figures 3.7–3.12 that can be used to choose an appropriate value for N .

In the above, the break-point defines the maximum value of the summation in (2.11) in order to avoid introducing avoidable, large, or significant errors. The value of the order of the break-point must be remembered for later use, as it indicates the maximum number of terms that should be used in any summation that uses this function; for example, the summation described later in Section 3.3. Similarly, the order of the break-point for each of the terms in (2.12)–(2.14) must be remembered and the smallest value of all four break-points must be used in further summations involving these functions.

Instead of using a fixed threshold value to determine the break-point, as done by [15], an alternative approach was used. In this approach, a running mean and standard deviation of the ordinate values was calculated. The break-point was determined to occur when an ordinate value exceeding the mean by ten (arbitrary) standard deviations. This approach has the advantage of being dictated by the data at hand rather than a fixed arbitrary threshold.

To summarize, the errors encountered in the calculations of the angular functions have been explored as functions of the three key variables v , q and N . Values of v that approach 0 or 180 degrees can produce large amounts of subtraction error, which are ameliorated by the low magnitude of those Mathieu functions. These subtraction errors increase as the value of q increases. When the errors in any term are examined by back-substitution into the original Mathieu equations, we find that N must be increased as q is increased. As N is increased, the error in the angular function decreases, except when the order of the angular function approaches N when the error rises sharply. This sharp rise in error cannot be avoided by increasing the value of N .

3.2 RADIAL FUNCTIONS

The accurate computation of radial Mathieu functions is challenging. There are several available expressions for these functions, as reported by Blanch [7] and Zhang & Jin [28]. As noted in Chapter 2, the traditional approach for computing Mathieu radial functions is with the parameter s in Eqs. (2.17)–(2.19) set equal to 0 while that in (2.20) is set equal to 1, which is the approach adopted by [28]. This was the approach used in Table 3.1 and clearly the summations do not converge. Both Blanch [7] and Van Buren and Boisvert [33] recommended against this choice. Blanch recommended that s be selected so that the value of the coefficient used in the divisor of the equations in (2.17)–(2.25) be the maximum absolute value of the associated set of the eigenvectors. In the following, we implement Blanch's recommendation, which turns out to be a direct and deterministic approach. We refer to this approach (choosing s to maximize the divisor) as the tuned approach. Van Buren and Boisvert [33] proposed a somewhat different procedure for selecting s that attempts to adaptively minimize subtraction errors.

To illustrate the concept raised in the previous paragraph, consider a problem where $q = 1$ is used. Shown in Table 3.2 are the expansion coefficients for a 10×10 matrix (representing the A coefficients corresponding to Eq. (2.17)). Each column of this matrix is an eigenvector obtained

from the associated tri-diagonal matrix in (2.12). The eigenvector in column 1 is associated with the smallest eigenvalue and the eigenvector in column 10 is associated with the largest eigenvalue. The range of the values in any one column is large and the largest absolute value in the columns tends to move from the top left corner of the matrix to the bottom right corner. This can be seen in Table 3.2. Thus, if one sets s equal to the column number, one will be at, or near, the maximum absolute value. It is not essential that the expansion coefficient used in the divisor of the above equations be strictly the maximum absolute value; it is only necessary that the expansion coefficient not be of a small value. Nevertheless, in the tuned approach we always use the position of the maximum absolute value to determine the value of s .

Table 3.2: The eigenvectors associated with a 10×10 matrix and $q = 1.0$

	1	2	3	4	5	6	7	8	9	10
1	6.7E-01	2.2E-01	5.2E-03	4.3E-05	1.9E-07	5.4E-10	1.0E-12	1.4E-15	1.5E-18	1.2E-21
2	-3.1E-01	9.5E-01	8.4E-02	1.6E-03	1.2E-05	5.4E-08	1.5E-10	2.7E-13	3.7E-16	3.9E-19
3	1.9E-02	-8.2E-02	1.0E+00	5.0E-02	7.4E-04	5.2E-06	2.1E-08	5.3E-11	9.4E-14	1.2E-16
4	-5.1E-04	2.6E-03	-5.0E-02	1.0E+00	3.6E-02	4.3E-04	2.6E-06	9.5E-09	2.3E-11	3.8E-14
5	7.9E-06	-4.3E-05	1.0E-03	-3.6E-02	1.0E+00	2.8E-02	2.8E-04	1.5E-06	5.0E-09	1.1E-11
6	-7.9E-08	4.5E-07	-1.2E-05	5.6E-04	-2.8E-02	1.0E+00	2.3E-02	2.0E-04	9.5E-07	2.8E-09
7	5.5E-10	-3.2E-09	9.7E-08	-5.2E-06	3.5E-04	-2.3E-02	1.0E+00	1.9E-02	1.5E-04	6.4E-07
8	-2.8E-12	1.7E-11	-5.4E-10	3.2E-08	-2.6E-06	2.4E-04	-1.9E-02	1.0E+00	1.7E-02	1.1E-04
9	1.1E-14	-6.7E-14	2.2E-12	-1.5E-10	1.4E-08	-1.5E-06	1.7E-04	-1.7E-02	1.0E+00	1.5E-02
10	-3.3E-17	2.1E-16	-7.3E-15	5.1E-13	-5.3E-11	6.8E-09	-9.5E-07	1.3E-04	-1.5E-02	1.0E+00

As the size of the matrix increases, so does the ratio of the maximum to minimum values in each eigenvector. The matrix size needed to produce accurate calculations for specific Mathieu functions is discussed in subsequent chapters.

The ratio of the maximum to minimum absolute values in each eigenvector is a function of q . Table 3.3 is similar to Table 3.2 except that the value of q is now equal to 100.0. It can be seen that the ratio of the maximum to minimum values in each eigenvector is now not so large. However, it was observed that as the size of the matrix increases so does this ratio. (Note that in practice N should be significantly larger than 10 for $q = 100$.)

We now consider the accuracy of the computations for the radial Mathieu functions. In contrast with the angular functions, there is an independent way to assess the accuracy of the summations involved in these functions, although it is an indirect approach to the issue. The analytic solution is the value of the Wronskian of the radial functions, namely $2/\pi$, when using the definitions adopted in this book. The computed values of the Wronskians of the radial functions are a function of (u, q) and the matrix size, N . All three parameters are explored below.

28 3. OBSERVED ACCURACY USING TRADITIONAL AND TUNED METHODS

Table 3.3: The eigenvectors associated with a 10×10 matrix and $q = 100.0$

	1	2	3	4	5	6	7	8	9	10
1	3.6E-01	2.6E-01	2.4E-01	2.3E-01	2.4E-01	2.7E-01	2.5E-01	6.2E-02	3.9E-03	7.7E-05
2	-6.5E-01	-2.7E-01	-7.3E-02	8.4E-02	2.4E-01	4.1E-01	5.0E-01	1.5E-01	1.2E-02	3.2E-04
3	4.7E-01	-2.3E-01	-4.5E-01	-4.3E-01	-2.5E-01	1.0E-01	4.6E-01	2.2E-01	2.9E-02	1.2E-03
4	-2.8E-01	5.5E-01	2.8E-01	-1.7E-01	-4.4E-01	-2.7E-01	3.4E-01	3.4E-01	7.2E-02	4.4E-03
5	1.4E-01	-5.3E-01	2.6E-01	4.3E-01	-3.3E-02	-4.3E-01	8.4E-02	4.7E-01	1.7E-01	1.6E-02
6	-5.6E-02	3.4E-01	-5.3E-01	5.6E-02	4.3E-01	-1.3E-01	-2.2E-01	4.8E-01	3.4E-01	5.1E-02
7	1.9E-02	-1.6E-01	4.4E-01	-4.7E-01	3.1E-02	3.6E-01	-3.0E-01	1.8E-01	5.4E-01	1.5E-01
8	-5.4E-03	6.0E-02	-2.3E-01	4.4E-01	-4.4E-01	1.7E-01	6.2E-02	-3.0E-01	5.5E-01	3.5E-01
9	1.3E-03	-1.8E-02	8.9E-02	-2.4E-01	4.0E-01	-4.3E-01	3.0E-01	-3.1E-01	7.8E-02	6.3E-01
10	-2.6E-04	4.2E-03	-2.5E-02	8.4E-02	-1.8E-01	2.5E-01	-2.4E-01	3.6E-01	-5.1E-01	6.7E-01

The definition of the relevant Wronskian, W , is given by

$$\begin{aligned}
& W \left(Mc_m^{(1)}(u, q), Mc_m^{(2)}(u, q) \right) \\
&= Mc_m^{(1)}(u, q) \frac{d}{du} Mc_m^{(2)}(u, q) - Mc_m^{(2)}(u, q) \frac{d}{du} Mc_m^{(1)}(u, q) = \frac{2}{\pi} \\
& W \left(Ms_m^{(1)}(u, q), Ms_m^{(2)}(u, q) \right) \\
&= Ms_m^{(1)}(u, q) \frac{d}{du} Ms_m^{(2)}(u, q) - Ms_m^{(2)}(u, q) \frac{d}{du} Ms_m^{(1)}(u, q) = \frac{2}{\pi}.
\end{aligned} \tag{3.3}$$

In the figures that follow, the error in the Wronskian value will be used to assess the accuracy of the terms involved in its calculation. The influence of the parameter s of the previous chapter will be investigated. The radial function will be calculated using the traditional approach, namely with s set equal to 0 except for $Ms_n^j(u, q)$ with n even where s is set equal to 1. This will be designated as the traditional method. The radial function will also be calculated using the method outlined earlier in this chapter, designated tuned, by setting s equal to the position (row number) of the maximum value in each associated eigenvector.

As already mentioned, for the range of parameter values considered when generating the data in the following figures, it was found that the use of double precision software was not adequate over the whole range. This was due to high values of the order and/or the argument encountered in the calculation of the Bessel functions, particularly in the functions of the second kind. In order to overcome this shortcoming, the routine necessary to calculate the Wronskian was written in quad precision code. This required that all the radial functions be calculated in quad precision.

Figure 3.13 shows plots of the error in the Wronskian, for $u = 0$ and $q = 10$. The abscissa is the order of the radial functions evaluated using eight different $N \times N$ matrices, with sizes of

10, 20, . . . 80. The ordinate is the error dimension. Each curve illustrates the effect of increasing the value of r starting at 0 and terminating at $N - 1$, whose value may be discerned by noting where each tuned curve stops. These results were generated using the multiple precision software package *mpf90* [42] with 500 decimal digits of precision. The specific radial function used for this figure was Mc_{2r} $r = 0, 1, 2, \dots$ and its derivative. The data when using the Mc_{2r+1} , Ms_{2r+1} and Ms_{2r+2} functions, although not identical, are similar. Some data points for the traditional method are not shown because of their large magnitudes.

For the tuned method, one can clearly see from Figure 3.13 that as the order, m , of the terms in the Wronskian increase, the value of the error in the Wronskian rises, sometimes after passing through a minimum, but never becomes excessive. In contrast, when using the traditional approach under the same conditions, the value of the error in the Wronskian becomes very large as the order rises. This is true even for small values of N .

In summary, the data in Figure 3.13 clearly show the superiority of the tuned approach for these values of the various parameters.

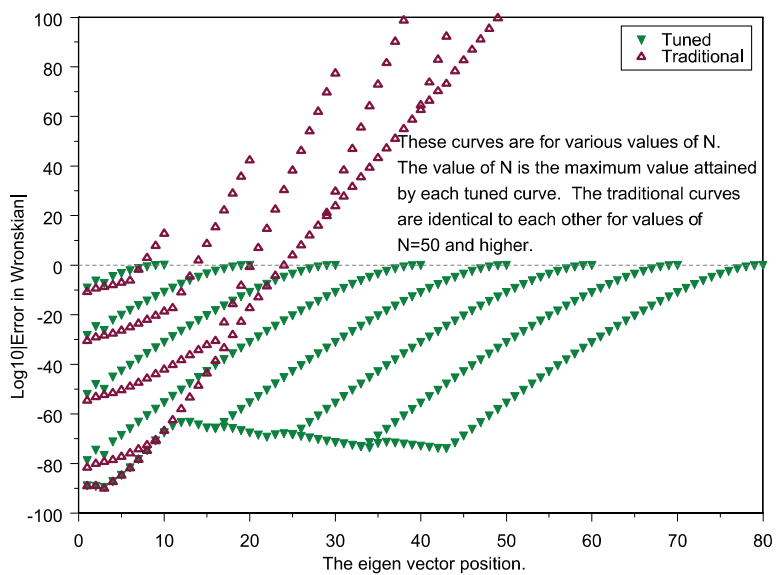


Figure 3.13: Plot of the error in the Wronskian corresponding to ce_{2r} for matrices of different sizes, N , as eigenvectors are included.

Figures 3.14–3.19 report the use of the tuned method to investigate the effects of varying u , q and N on the error in the Wronskian of Eq. (3.3). The data were calculated in quad precision before being converting to double precision. The difference between the graphs is the size $N \times N$ of the eigenvalue/vector matrix. The values of u were selected to represent a large range.

30 3. OBSERVED ACCURACY USING TRADITIONAL AND TUNED METHODS

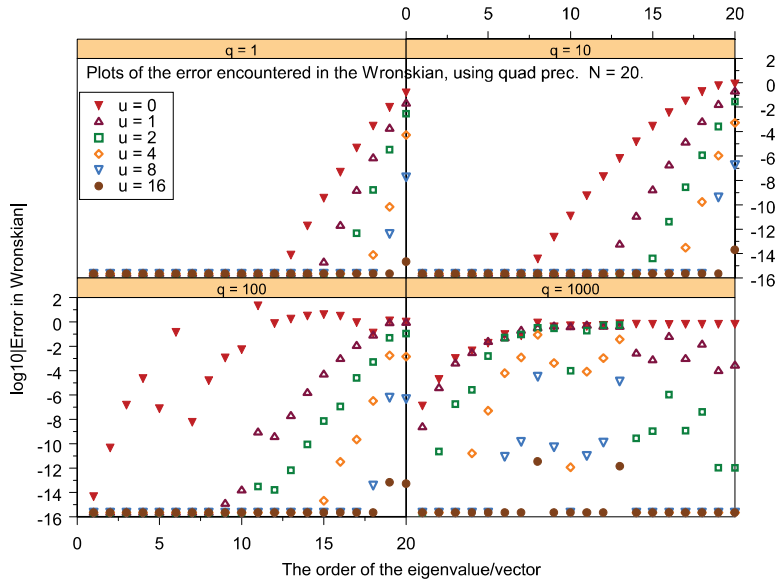


Figure 3.14: Plots of the error in the Wronskian for $N = 20$.

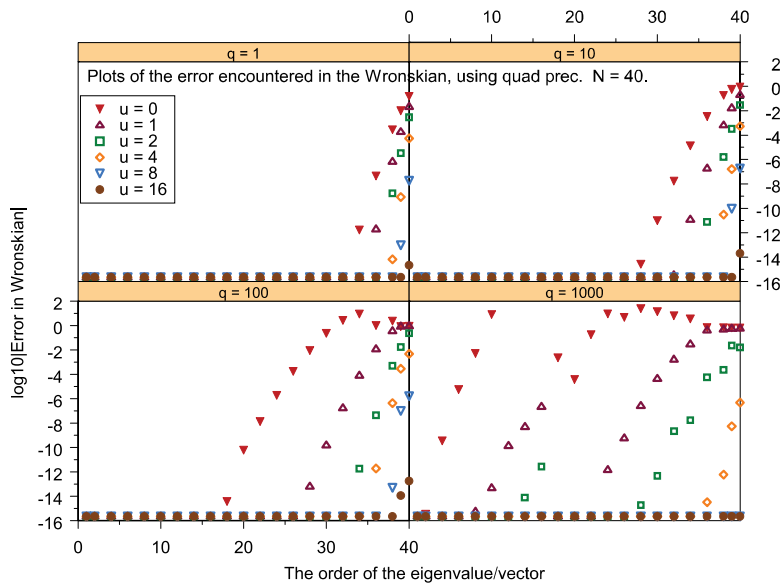


Figure 3.15: Plots of the error in the Wronskian for $N = 40$.

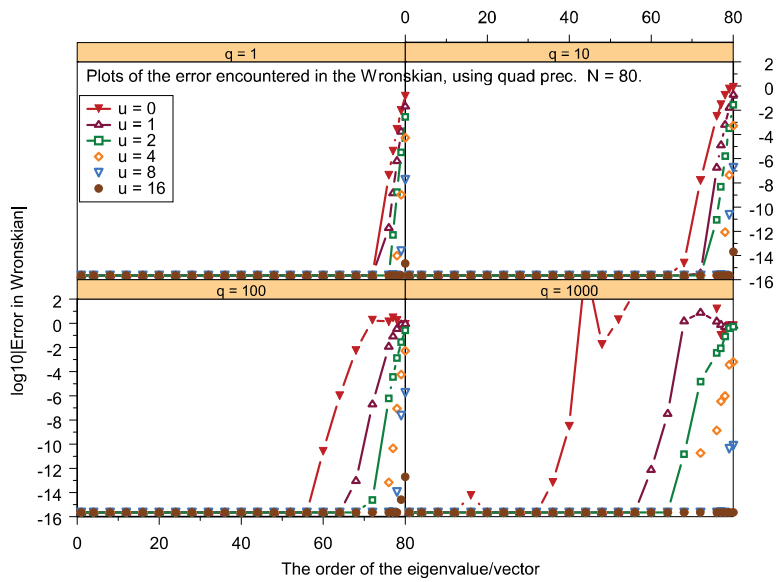


Figure 3.16: Plots of the error in the Wronskian for $N = 80$.

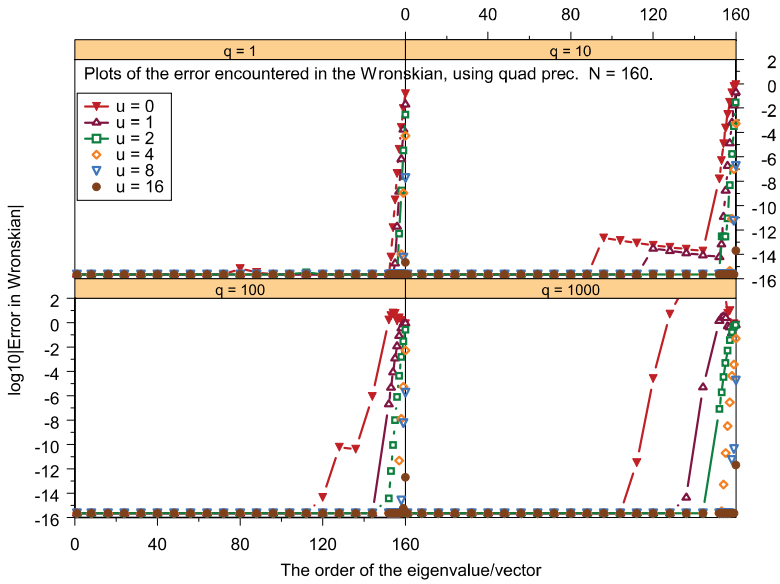


Figure 3.17: Plots of the error in the Wronskian for $N = 160$.

32 3. OBSERVED ACCURACY USING TRADITIONAL AND TUNED METHODS

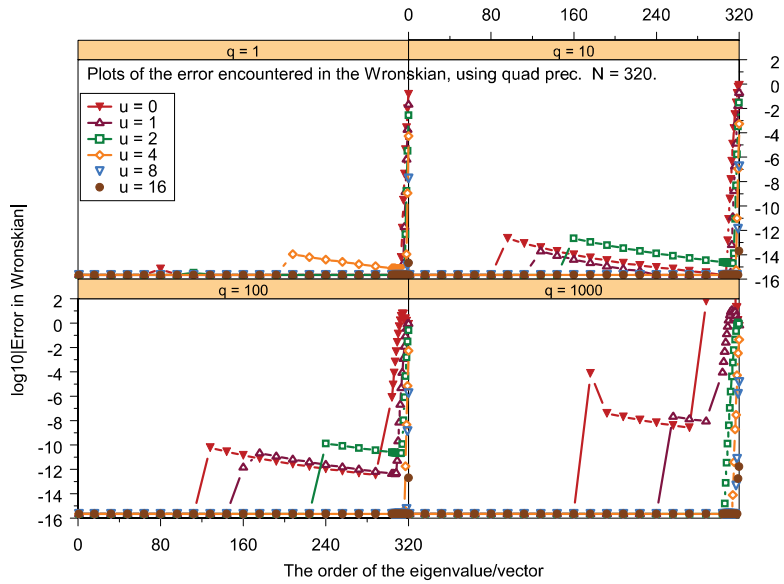


Figure 3.18: Plots of the error in the Wronskian for $N = 320$.

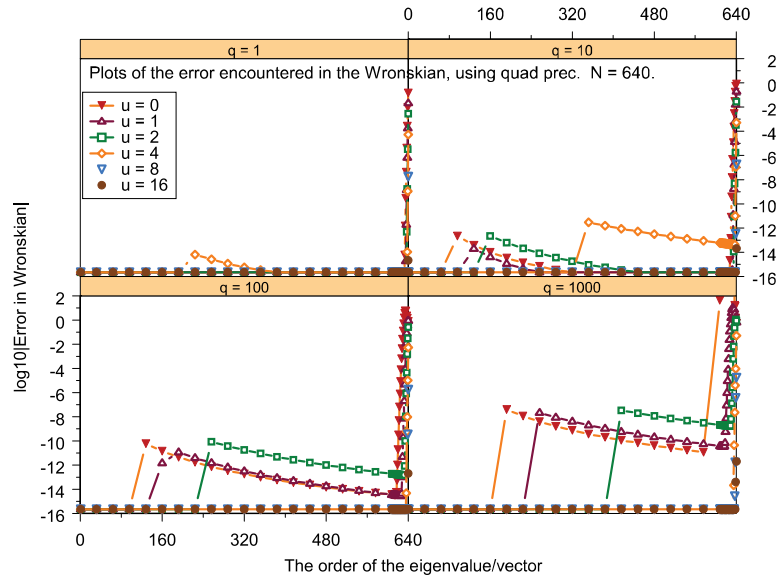


Figure 3.19: Plots of the error in the Wronskian for $N = 640$.

3.3. EXAMPLE: COMPUTING A HANKEL FUNCTION 33

The following observations of the preceding graphs are of interest:

1. As the value of q increases so does the need for a larger value of N to obtain stability in the measure of the error value.
2. Lower values of u incur higher values of error than higher values of u .
3. The sharp change in slope of the error curve, the break-point—if there is one—can be observed easily.
4. Over the range considered, the error values associated with the highest order, i.e., the largest eigenvalue, cannot be avoided by simply increasing N .

So far, we have explored some of the issues associated with evaluating the angular and radial Mathieu functions over a range of variables. In many applications, angular and radial Mathieu functions appear together in expressions for electromagnetic fields. To illustrate the composite evaluation of these functions, we explore the computation of a Hankel function expressed as a sum of Mathieu functions. This problem was suggested by Erricolo [37], who observed serious convergence problems in its evaluation. We will see how this convergence problem is avoided by using the tuned method for evaluating the radial functions.

3.3 EXAMPLE: COMPUTING A HANKEL FUNCTION IN TERMS OF A SUMMATION OF MATHIEU FUNCTIONS

Consider a Hankel function of the second kind, $H_0^{(2)}(kR)$, where $k = 2\pi$ and $R = \sqrt{2.0}$, as defined by the expansion in Mathieu functions [6, p. 1421]:

$$H_0^{(2)}(kR) = 2 \sum_{m=0}^{\infty} \left[\begin{array}{l} Mc_m^{(1)}(kF, u_-) Mc_m^{(4)}(kF, u_+) ce_m(kF, v_0) ce_m(kF, v_1) \\ + Ms_m^{(1)}(kF, u_-) Ms_m^{(4)}(kF, u_+) se_m(kF, v_0) se_m(kF, v_1) \end{array} \right]. \quad (3.4)$$

This summation was studied using the traditional formulation by Erricolo [37], who found that the real part of the calculated value quickly converged. However, the imaginary part of the solution initially converged and then began to diverge, in a manner similar to that illustrated in Table 3.1. His remedy to this undesirable outcome was to apply an adaptation of the Shanks transformation to the imaginary component to accelerate the convergence. In the following, we show that the problem of the divergence of the solution is avoided by applying the tuned formulation.

To cast the calculation in terms of (3.4), we need to select a specific elliptic coordinate system, and starting and ending points for the displacement R . Here we use $F = 1.0$, $q = \pi^2$. Stated in terms of the Cartesian coordinate system (x, y) , R originates at $(0, 0)$ and terminates at $(1, 1)$. The arguments u_- (u_+) are the smaller (larger) value between u_0 and u_1 , obtained from Eq. (2.1). We have adapted the expressions in [37] to the Goldstein-Ince convention used throughout the present lecture.

34 3. OBSERVED ACCURACY USING TRADITIONAL AND TUNED METHODS

For a reference solution, the value of $H_0^{(2)}(k\sqrt{2})$, itself a summation of an infinite series, was calculated using 64-digit arithmetic [44]. That value, expressed in quad precision, is

$$H_{ref} = H_0^{(2)}(k\sqrt{2}) = \begin{pmatrix} -0.196548095270468200040793372087932 \\ -j0.428287398117322672149805575696119 \end{pmatrix}. \quad (3.5)$$

When using (3.4), the calculated value of the real component converged quickly to the reference value and remained stable as more terms were added. Tables 3.4 and 3.5 report the error in the imaginary component only, as $\log 10 |H_{calc} - H_{ref}|$, and were computed with quad-precision arithmetic. The results reported in Table 3.4 were obtained using the traditional formulation. It can be seen that the error in the imaginary component reaches a minimum after summing 11 or 12 terms, and that only about 11 digits of accuracy are possible.

When the tuned formulation was used (Table 3.5), both the real and imaginary components converge to a stable value. An eigenvalue/vector matrix size of $N = 40$ permits series convergence to quad precision accuracy in this case.

The results shown in Tables 3.4 and 3.5 show that the lack of convergence illustrated by Table 3.1, using the traditional algorithm for calculating Mathieu functions, also occurs in practice in the calculation of the Hankel function and can seriously limit the available accuracy. When a tuned formulation is used, the computation behaves in a much more desirable manner. Thus, we recommend the tuned approach for all Mathieu function calculations.

3.4 SUMMARY

Subtraction error calculations were used to evaluate the behavior of the angular functions over a range of parameters. It was found that the subtraction error increases as the values of v approach $v = 0$ or $v = \pi$, but this problem is ameliorated because the value of the angular function is shrinkingly small at these extremes. The accuracy of the calculations of the four angular functions was also examined with the aid of Eqs. (3.2a)–(3.2d), and a procedure for determining the maximum number of terms to be included in the summation of subsequent terms was proposed.

The results reported in this chapter indicate that the numerical evaluation of Mathieu radial functions requires the use of the tuned method when evaluating the radial functions. It also indicates that the precision of the arithmetic software plays an important role. The importance of the tuned method was explored by evaluating the Hankel function with both the traditional approach and the tuned approach. The latter method is unequivocally superior. The following chapter summarizes the algorithm we recommend for computing Mathieu functions, and provides a means of estimating the accuracy of the results.

Table 3.4: Error in the imaginary part of the Hankel function using the traditional approach. The error is reported in terms of $\log 10|H_{\text{calc}} - H_{\text{ref}}|$

N = 10		N = 20		N = 30		N = 40	
1	-1.81611	1	-1.81611	1	-1.81611	1	-1.81611
2	-2.00167	2	-2.00167	2	-2.00167	2	-2.00167
3	-3.51975	3	-3.51975	3	-3.51975	3	-3.51975
4	-4.50516	4	-4.50516	4	-4.50516	4	-4.50516
5	-5.45772	5	-5.45772	5	-5.45772	5	-5.45772
6	-6.97272	6	-6.97272	6	-6.97272	6	-6.97272
7	-7.41698	7	-7.41664	7	-7.41664	7	-7.41664
8	-3.05256	8	-9.10435	8	-9.10435	8	-9.10435
9	3.33779	9	-9.42902	9	-9.42902	9	-9.42902
10	10.70583	10	-10.5593	10	-10.5593	10	-10.5593
		11	-11.5463	11	-11.5514	11	-11.5488
		12	-11.5463	12	-11.5514	12	-10.9404
		13	-7.47944	13	-7.47944	13	-10.9404
		14	-5.50959	14	-5.20624	14	-5.50496
		15	-0.70888	15	-5.20624	15	-1.0099
		16	5.13349	16	2.02425	16	-1.0099
		17	14.2708	17	5.85182	17	5.85176
		18	23.13867	18	5.85182	18	5.85176
		19	31.7143	19	12.54512	19	12.97109
		20	40.75357	20	16.57893	20	16.27765
				30	76.00563	30	54.25355
						40	114.1679

36 3. OBSERVED ACCURACY USING TRADITIONAL AND TUNED METHODS

Table 3.5: Error in the imaginary part of the Hankel function using the tuned approach. The error is reported in terms of $\log 10|H_{\text{calc}} - H_{\text{ref}}|$

N = 10		N = 20		N = 30		N = 40	
1	-1.81611	1	-1.81611	1	-1.81611	1	-1.81611
2	-2.00167	2	-2.00167	2	-2.00167	2	-2.00167
3	-3.51975	3	-3.51975	3	-3.51975	3	-3.51975
4	-4.50516	4	-4.50516	4	-4.50516	4	-4.50516
5	-5.45772	5	-5.45772	5	-5.45772	5	-5.45772
6	-6.97272	6	-6.97272	6	-6.97272	6	-6.97272
7	-7.41664	7	-7.41664	7	-7.41664	7	-7.41664
8	-9.10433	8	-9.10435	8	-9.10435	8	-9.10435
9	-9.42913	9	-9.42902	9	-9.42902	9	-9.42902
10	-10.3441	10	-10.5593	10	-10.5593	10	-10.5593
		15	-15.6808	15	-15.6808	15	-15.6808
		20	-20.5274	20	-21.0489	20	-21.0489
				25	-24.9742	25	-24.9742
				30	-29.5397	30	-29.4362
						35	-33.6185
						40	-33.7154

CHAPTER 4

Recommended Algorithm for Mathieu Function Computation

This chapter describes the detailed steps associated with the recommended approach: the tuned algorithm described in Chapter 3. Throughout, our emphasis is on accurate results. The algorithm is illustrated by the computation of a uniform plane wave formulated in terms of Mathieu functions. This example is possibly the simplest of any such formulations and has a known solution. Consequently, it is also possible to use the computation of a plane wave to assess the accuracy of computed Mathieu functions over a wide range of parameters.

4.1 THE TUNED ALGORITHM

The principal steps associated with the tuned algorithm are as follows:

- Step 1.* Determine the value of F and q for the problem at hand. These define the elliptic system and are directly related to the physical dimension(s) of the target, such as the width of a strip, or the major/minor axes of an ellipse. F and q are related by $q = \left(\frac{kF}{2}\right)^2$.
- Step 2a.* For the value of q obtained in the previous step, evaluate the relevant eigenvalues and associated eigenvectors as defined in equations (2.16a)–(2.16d). The four matrices involved in this step are each tri-diagonal and symmetrical and hence amenable to rapid processing. The initial size N of these square matrices may be estimated from Figure 4.4 and Table 5.3. If the solution converges to some (sensible) limit as the index m approaches N , the value of N may be sufficient. N should be increased in order to see if a similar result is obtained with the larger value of N . The eigenvalues and eigenvectors should be stored for use in calculating the angular and radial functions.
- Step 2b.* Each column of the four eigenvector matrices must be searched for the location (the row number) of the maximum absolute value. The row number and the signed maximum value should be stored. (Each row index corresponds to the variable s required in equations (2.17)–(2.25)). These parameters will be used in the calculation of the radial functions.

38 4. RECOMMENDED ALGORITHM FOR MATHIEU FUNCTION COMPUTATION

- Step 3.* Calculate the angular functions for argument v using the coefficients calculated in *Step 2a*. For each angular function this involves the summation of N real numbers. It is recommended that these numbers be segregated into two groups—one for negative numbers and one for positive numbers. The group of negative numbers is stored as absolute values. Each group is sorted by magnitude and then summed starting with the smallest value first. Finally, the aggregated result of the negative group is subtracted from the aggregated result of the positive group. This process is also used to calculate the first derivative, if needed, along with the calculation of the error of the angular function.
- Step 4.* Calculate the radial functions for argument u according to equations (2.17)–(2.25) and the values determined in *Steps 2a* and *2b*. For the tuned approach, use the value of s determined in *Step 2b* with each summation. It is recommended that the summations be sorted, aggregated and subtracted as done for the angular functions. Since both the radial functions and their derivatives are calculated for both the first and second types, it is appropriate at this point to calculate the associated Wronskian in order to check for accuracy. If accuracy is not sufficient, return to *Step 2a* and repeat with a larger value of N .

4.2 EXAMPLE: CALCULATION OF A UNIFORM PLANE WAVE

As an example, we examine the calculation of the plane wave discussed in Chapter 2, which may be expressed in terms of Mathieu functions as described in [5, p. 385] and [6, p. 1422]. The expression evaluated at elliptic-cylinder variables (u, v) corresponding to Cartesian variables (x, y) is reproduced from Chapter 2 with $E_0 = 1.0$:

$$E_z^{inc} = 2 \sum_{m=0}^{\infty} j^m \left[\begin{array}{l} Mc_m^{(1)}(kF, u) ce_m(kF, v) ce_m(kF, \phi^{inc}) \\ + Ms_m^{(1)}(kF, u) se_m(kF, v) se_m(kF, \phi^{inc}) \end{array} \right] \quad (4.1)$$

Note the summation over m . As m proceeds through even and odd values, the summed terms must include values associated with the angular functions of equations (2.13)–(2.16a)–(2.16d) and those associated with the radial functions of equations (2.17), (2.20), (2.22) and (2.24), in which the superscript is $j = 1$.

The value of q is arbitrary since any elliptic coordinate system may be chosen. Initially, consider $q = 1.0$. Figure 4.1 shows the convergence of the summation over m for various values of N , for $u = v = 0$. In this case, with a value of $q = 1.0$, the error (more precisely, the common logarithm of the error) quickly approaches and reaches the double precision limit of approximately -16.0 with $m = 8$ terms in the summation. To achieve this error level, it is necessary to use matrices of order $N = 9$ or larger.

Figure 4.2 illustrates what happens when a value of $q = 100.0$ is used. The results are similar to those shown in Figure 4.1, except now approximately $m = 19$ terms are required for convergence to the limit of double precision. The matrix order N must approach 30.

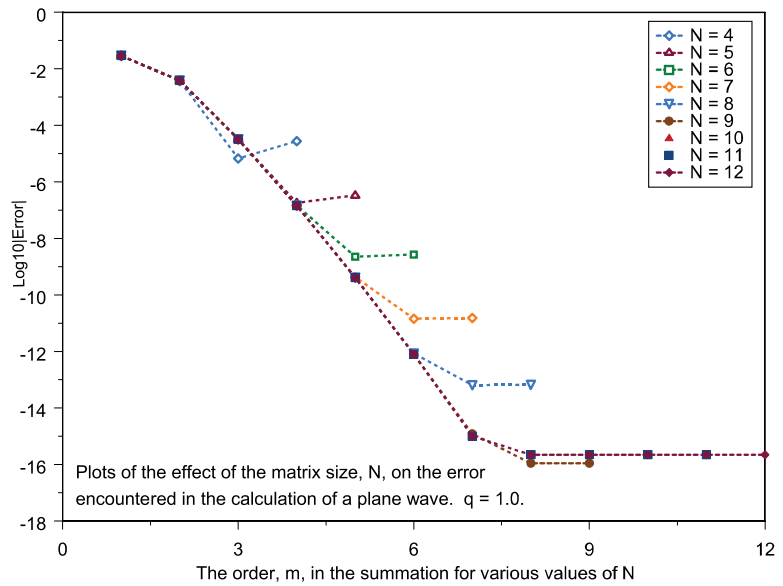


Figure 4.1: The error curves realized in the calculation of a plane wave for $q = 1$ and argument $(0, 0)$.

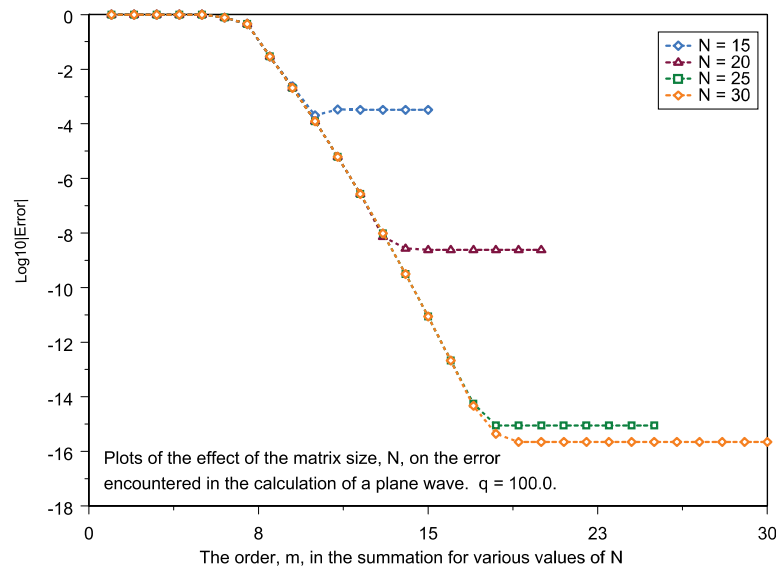


Figure 4.2: The error curves realized in the calculation of a plane wave for $q = 100$ and argument $(0, 0)$.

40 4. RECOMMENDED ALGORITHM FOR MATHIEU FUNCTION COMPUTATION

When a value of $q = 10,000.0$ is used, the convergence illustrated in Figure 4.3 is observed. Note that the upper limit of m now approaches 90 to produce an error of approximately -16.0 . In accordance, the value of N must increase significantly, to $N = 140$.

An inspection of Figure 4.3 suggests that a significant number of the terms with small values of m do not contribute to the reduction of the error. We observe that the region of convergence, once it begins, is relatively narrow, and that the error drops abruptly until it reaches a plateau (at an error level that depends on N). In fact, the magnitude of terms with small m is less than the smallest number that can be represented in double precision, and so they are effectively not included in the calculation. (This behavior was reported in [11].) To explore this aspect of the convergence in more detail, let us denote the position of the first value that is large enough to be included in the summation as m_1 . The minimum number of terms needed to reach the desired error level will be designated as m_2 . Figure 4.4 illustrates the critical values of m_1 , m_2 and N needed to obtain convergence to double precision accuracy as a function of q , for an argument of $u = v = 0$.

We see from these graphs that N must increase as q increases. As illustrated by Figures 4.3 and 4.4, it is not necessary to include terms associated with all values of m . However, it may be difficult, if not impossible, to know beforehand what the appropriate values of m_1 and m_2 should be!

4.3 ADAPTIVE ERROR ESTIMATION BASED ON THE PLANE WAVE

In many practical applications of Mathieu functions, including those considered in Chapters 5 and 6, summations similar to (4.1) are used to determine the fields in some boundary value problem. (Actually, the Mathieu functions actually used in the above example are only a subset of those that might be used in more complex target calculations.) Consequently, in the course of computing the various Mathieu functions required by a particular application, one can easily compute the plane wave of that same argument with minimal additional resources. Since the plane wave has a simple analytical expression, the accuracy of (4.1) can be used to estimate the accuracy of the desired summations for any value of q and any argument (u, v) . The authors recommend that this approach be used to provide an additional check on the accuracy of the resulting computations.

4.4 SUMMARY

The tuned algorithm for Mathieu function computation is summarized. Results from the convergence of a uniform plane wave are used to provide some insight into the necessary value of the parameter N (the order of the coefficient matrices). In addition, the plane wave provides a convenient means to estimate the convergence in summations of Mathieu functions arising in a variety of boundary value problems.

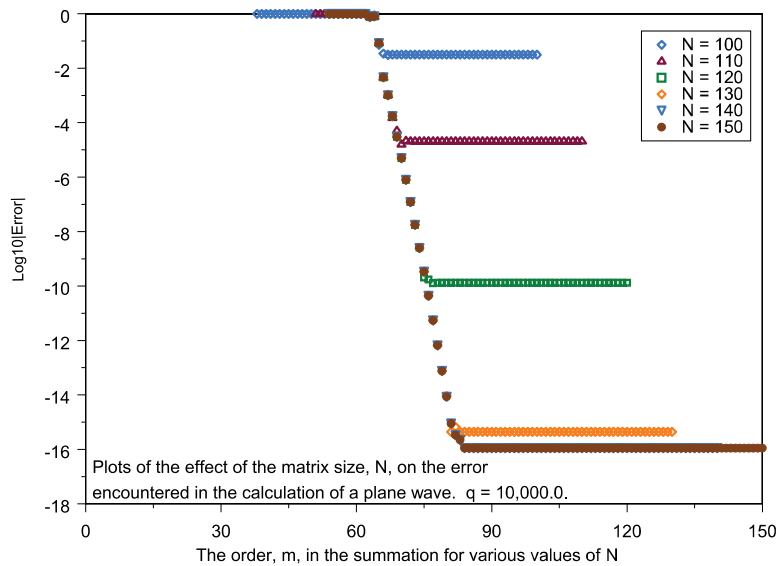


Figure 4.3: The error curves realized in the calculation of a plane wave for $q = 100,000$ and argument $(0, 0)$.

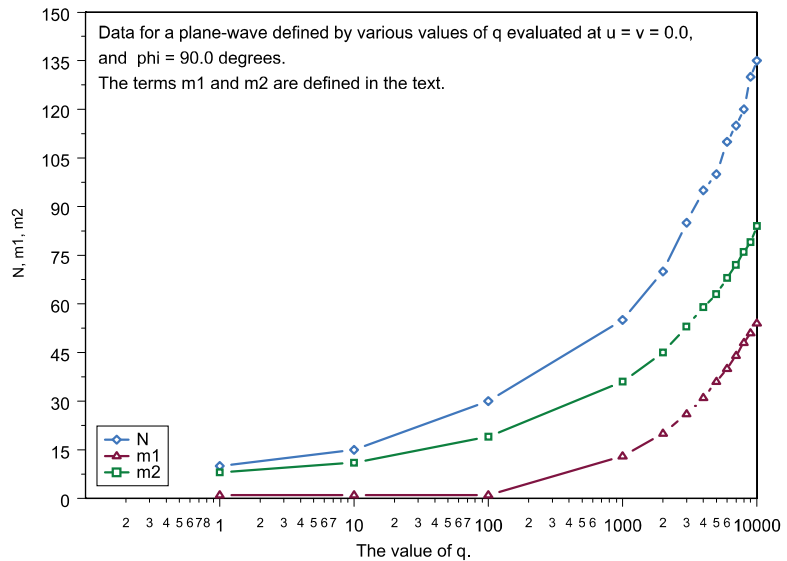


Figure 4.4: The parameters m_1 , m_2 , and N as a function of q , illustrating the index range necessary for double-precision convergence of the summation in (4.1) for an argument $(0, 0)$.

CHAPTER 5

Electromagnetic Scattering from Conducting Elliptic Cylinders

In this chapter we employ Mathieu functions to analyze the scattering of an electromagnetic plane wave by a perfectly conducting elliptic cylinder. This subject is discussed at length in a chapter in [9] and in references [14–17]. However, the validity of some of the results reported in [9] and [14] were questioned by subsequent computations [15, 16]. To provide reliable data for comparison purposes, we recompute some of these cases in the following sections. Numerical values for current density and scattering cross section are presented in tabular format to facilitate comparisons with other computations. We explore both the TM_z case and the TE_z case.

5.1 THE TM_z CASE

The specific cylinder surface is defined by the values of F (hence q) and the coordinate $u = u_0$. For this case, the excitation is a uniform plane wave of the form $\bar{E}^{inc} = \hat{z}E_z^{inc}$, where

$$E_z^{inc}(q, u, v) = 2E_0 \sum_{m=0}^{\infty} j^m \begin{bmatrix} Mc_m^{(1)}(q, u) ce_m(q, v) ce_m(q, \phi^{inc}) \\ + Ms_m^{(1)}(q, u) se_m(q, v) se_m(q, \phi^{inc}) \end{bmatrix}. \quad (5.1)$$

The scattered field $\bar{E}^s = \hat{z}E_z^s$ is expressed in terms of outgoing elliptical waves

$$E_z^s(q, u, v) = 2E_0 \sum_{m=0}^{\infty} j^m \begin{bmatrix} C_m Mc_m^{(4)}(q, u) ce_m(q, v) ce_m(q, \phi^{inc}) \\ + S_m Ms_m^{(4)}(q, u) se_m(q, v) se_m(q, \phi^{inc}) \end{bmatrix}, \quad (5.2)$$

where C_m and S_m are constants to be determined. These constants are determined by enforcing the boundary condition

$$(E_z^{inc} + E_z^s)|_{u=u_0} = 0 \quad (5.3)$$

44 5. ELECTROMAGNETIC SCATTERING FROM CONDUCTING ELLIPTIC CYLINDERS

on the cylindrical surface at u_0 . By exploiting the orthogonality of the various terms, we obtain

$$C_m = -\frac{Mc_m^{(1)}(q, u_0)}{Mc_m^{(4)}(q, u_0)} \quad (5.4)$$

$$S_m = -\frac{Ms_m^{(1)}(q, u_0)}{Ms_m^{(4)}(q, u_0)}. \quad (5.5)$$

Thus,

$$E_z^s(q, u, v) = -2E_0 \sum_{m=0}^{\infty} j^m \left[\begin{array}{l} \frac{Mc_m^{(1)}(q, u_0)}{Mc_m^{(4)}(q, u_0)} ce_m(q, v) ce_m(q, \phi^{inc}) Mc_m^{(4)}(q, u) \\ + \frac{Ms_m^{(1)}(q, u_0)}{Ms_m^{(4)}(q, u_0)} se_m(q, v) se_m(q, \phi^{inc}) Ms_m^{(4)}(q, u) \end{array} \right]. \quad (5.6)$$

The total electric field $E_z^{tot} = E_z^i + E_z^s$ at any location outside the cylinder is given by

$$E_z^{tot} = 2E_0 \sum_{m=0}^{\infty} j^m \left[\begin{array}{l} ce_m(q, v) ce_m(q, \phi_0) \left\{ Mc_m^{(1)}(q, u) - \frac{Mc_m^{(1)}(q, u_0)}{Mc_m^{(4)}(q, u_0)} Mc_m^{(4)}(q, u) \right\} \\ + se_m(q, v) se_m(q, \phi_0) \left\{ Ms_m^{(1)}(q, u) - \frac{Ms_m^{(1)}(q, u_0)}{Ms_m^{(4)}(q, u_0)} Ms_m^{(4)}(q, u) \right\} \end{array} \right]. \quad (5.7)$$

The magnetic field may be obtained as the curl of the electric field. For a general vector \bar{E} the curl operation is defined

$$\nabla \times \bar{E} = \frac{1}{(\cosh^2 u - \cos^2 v)} \begin{vmatrix} \hat{u} (\cosh^2 u - \cos^2 v)^{1/2} & \hat{v} (\cosh^2 u - \cos^2 v)^{1/2} & \hat{z}/F \\ \frac{\partial}{\partial u} & \frac{\partial}{\partial v} & \frac{\partial}{\partial z} \\ E_u (\cosh^2 u - \cos^2 v)^{1/2} & E_v (\cosh^2 u - \cos^2 v)^{1/2} & E_z/F \end{vmatrix}. \quad (5.8)$$

For the TM polarization, this simplifies to

$$\begin{aligned} \nabla \times \bar{E} &= \frac{1}{(\cosh^2 u - \cos^2 v)^{1/2}} \left\{ \hat{u} \frac{\partial}{\partial v} \left(\frac{E_z}{F} \right) - \hat{v} \frac{\partial}{\partial u} \left(\frac{E_z}{F} \right) \right\} \\ &= -j\omega\mu_0 \bar{H}, \end{aligned} \quad (5.9)$$

where we observe that $\omega\mu_0 = k\eta$. Therefore,

$$\bar{H} = \frac{j}{k\eta F} \frac{\hat{u} \frac{\partial E_z}{\partial v} - \hat{v} \frac{\partial E_z}{\partial u}}{\left(\cosh^2 u - \cos^2 v\right)^{1/2}}. \quad (5.10)$$

The current density is obtained from

$$\bar{J} = \hat{n} \times \bar{H}|_{u=u_0} = \hat{u} \times \bar{H}|_{u=u_0} = -\hat{z} \frac{j}{k\eta F} \frac{1}{\left(\cosh^2 u - \cos^2 v\right)^{1/2}} \frac{\partial E_z^{tot}}{\partial u} \Big|_{u=u_0}. \quad (5.11)$$

For shorthand, let us define

$$\bar{K} = -\hat{z} \frac{j}{k\eta F} \frac{1}{\left(\cosh^2 u - \cos^2 v\right)^{1/2}}. \quad (5.12)$$

Then

$$\begin{aligned} \bar{J} = & \left\{ 2\bar{K}E_0 \sum_{m=0}^{\infty} j^m \right. \\ & \left. \left[\begin{array}{l} ce_m(q, v) ce_m(q, \phi_0) \left\{ \frac{\partial}{\partial u} Mc_m^{(1)}(q, u) - \frac{Mc_m^{(1)}(q, u_0)}{Mc_m^{(4)}(q, u_0)} \frac{\partial}{\partial u} Mc_m^{(4)}(q, u) \right\} \\ + se_m(q, v) se_m(q, \phi_0) \left\{ \frac{\partial}{\partial u} Ms_m^{(1)}(q, u) - \frac{Ms_m^{(1)}(q, u_0)}{Ms_m^{(4)}(q, u_0)} \frac{\partial}{\partial u} Ms_m^{(4)}(q, u) \right\} \end{array} \right] \right\}_{u=u_0} \end{aligned} \quad (5.13)$$

Using the definition $M_m^{(4)} = M_m^{(1)} - jM_m^{(2)}$, we obtain the Wronskian relations

$$Mc_m^{(4)}(u, q) \frac{d}{du} Mc_m^{(1)}(u, q) - Mc_m^{(1)}(u, q) \frac{d}{du} Mc_m^{(4)}(u, q) = j \frac{2}{\pi}, \quad (5.14)$$

$$Ms_m^{(4)}(u, q) \frac{d}{du} Ms_m^{(1)}(u, q) - Ms_m^{(1)}(u, q) \frac{d}{du} Ms_m^{(4)}(u, q) = j \frac{2}{\pi}, \quad (5.15)$$

and use them to simplify (5.13), to obtain

$$\bar{J} = j \frac{4}{\pi} \bar{K} E_0 \sum_{m=0}^{\infty} j^m \left[\frac{ce_m(q, v) ce_m(q, \phi_0)}{Mc_m^{(4)}(q, u_0)} + \frac{se_m(q, v) se_m(q, \phi_0)}{Ms_m^{(4)}(q, u_0)} \right], \quad (5.16)$$

46 5. ELECTROMAGNETIC SCATTERING FROM CONDUCTING ELLIPTIC CYLINDERS

or, equivalently,

$$J_z = \frac{4E_0}{\pi k \eta F} \frac{1}{(\cosh^2 u - \cos^2 v)^{1/2}} \sum_{m=0}^{\infty} j^m \left[\frac{ce_m(q, v) ce_m(q, \phi_0)}{Mc_m^{(4)}(q, u_0)} + \frac{se_m(q, v) se_m(q, \phi_0)}{Ms_m^{(4)}(q, u_0)} \right]. \quad (5.17)$$

After substituting $kF = 2\sqrt{q}$, we obtain

$$\eta J_z = \frac{2}{\pi} \frac{E_0}{\sqrt{q (\cosh^2 u_0 - \cos^2 v)}} \left\{ \sum_{m=0}^{\infty} j^m \left[\frac{ce_m(q, v) ce_m(q, \phi_0)}{Mc_m^{(4)}(q, u_0)} + \frac{se_m(q, v) se_m(q, \phi_0)}{Ms_m^{(4)}(q, u_0)} \right] \right\}. \quad (5.18)$$

Using the above equations, we compute the surface current on elliptic cylinders with $q = 0.25$, or $c = 1$ in the nomenclature used in [9], for $E_0 = \eta$ and several values of u_0 . A value of $N = 20$ was used to calculate these results. Figure 5.1 shows the surface current magnitude obtained for an incident wave angle of $\phi_0 = 0$, while Figure 5.2 shows analogous results for $\phi_0 = \pi/2$. The results do not agree with the corresponding data shown in [9], but do agree with later results shown by van den Berg and van Schaik [15] and by Wall [16].

5.2 THE TE_z CASE

The uniform plane wave excitation can be expressed as

$$H_z^{inc} = 2H_0 \sum_{m=0}^{\infty} j^m \left[\begin{array}{l} Mc_m^{(1)}(q, u) ce_m(q, v) ce_m(q, \phi^{inc}) \\ + Ms_m^{(1)}(q, u) se_m(q, v) se_m(q, \phi^{inc}) \end{array} \right]. \quad (5.19)$$

The scattered field can be written in terms of outgoing elliptic-cylinder waves as

$$H_z^s = 2H_0 \sum_{m=0}^{\infty} j^m \left[\begin{array}{l} C_m Mc_m^{(4)}(q, u) ce_m(q, v) ce_m(q, \phi^{inc}) \\ + S_m Ms_m^{(4)}(q, u) se_m(q, v) se_m(q, \phi^{inc}) \end{array} \right], \quad (5.20)$$

where, again, C_m and S_m are constants to be determined. As in the TM_z case, these constants are determined by applying the boundary condition on the cylindrical surface at u_0 , which in this case is

$$(E_v^{inc} + E_v^s)|_{u=u_0} = 0, \quad (5.21)$$

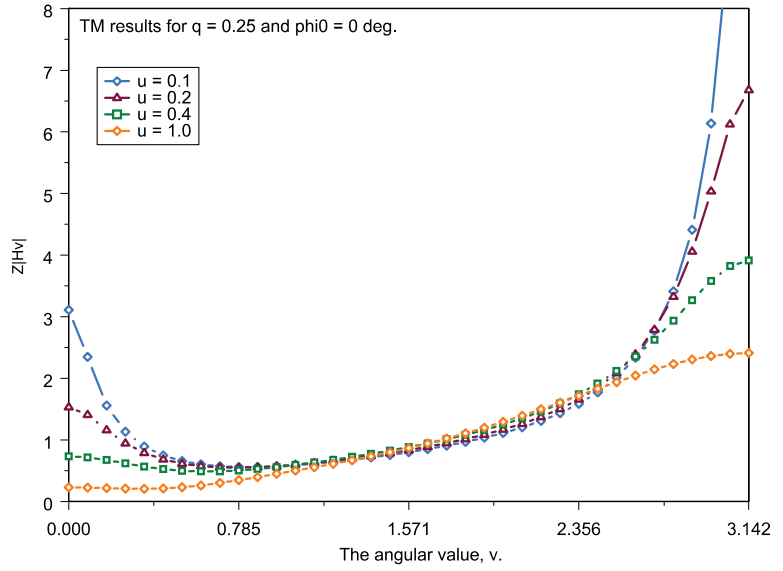


Figure 5.1: The surface current on elliptic cylinders with $q = 0.25$ illuminated by a TM_z plane wave incident at $\phi_0 = 0$.

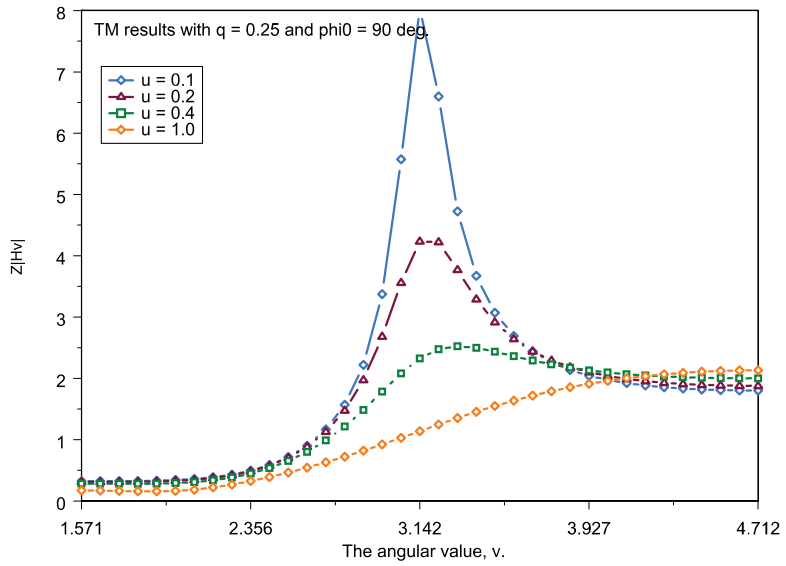


Figure 5.2: The surface current on elliptic cylinders with $q = 0.25$ illuminated by a TM_z wave incident at $\phi_0 = 90$ degrees.

48 5. ELECTROMAGNETIC SCATTERING FROM CONDUCTING ELLIPTIC CYLINDERS

or, equivalently,

$$\left(\frac{\partial H_z^{inc}}{\partial u} + \frac{\partial H_z^s}{\partial u} \right) \Big|_{u=u_0} = 0 . \quad (5.22)$$

Enforcing (5.22) at $u = u_0$, and imposing the orthogonality of the functions, one obtains the coefficients in (5.20) in the form

$$C_m = - \frac{\frac{\partial}{\partial u} M c_m^{(1)}(q, u) \Big|_{u=u_0}}{\frac{\partial}{\partial u} M c_m^{(4)}(q, u) \Big|_{u=u_0}} , \quad (5.23)$$

$$S_m = - \frac{\frac{\partial}{\partial u} M s_m^{(1)}(q, u) \Big|_{u=u_0}}{\frac{\partial}{\partial u} M s_m^{(4)}(q, u) \Big|_{u=u_0}} . \quad (5.24)$$

The scattered magnetic field is

$$H_z^s = -2H_0 \sum_{m=0}^{\infty} j^m \left[\begin{array}{l} \frac{\partial}{\partial u} M c_m^{(1)}(q, u) \Big|_{u=u_0} c e_m(q, v) c e_m(q, \phi^{inc}) M c_m^{(4)}(q, u) \\ \frac{\partial}{\partial u} M c_m^{(4)}(q, u) \Big|_{u=u_0} \\ + \frac{\partial}{\partial u} M s_m^{(1)(1)}(q, u) \Big|_{u=u_0} s e_m(q, v) s e_m(q, \phi^{inc}) M s_m^{(4)}(q, u) \\ \frac{\partial}{\partial u} M s_m^{(4)}(q, u) \Big|_{u=u_0} \end{array} \right] . \quad (5.25)$$

The surface current density in the *TE* case has only a v component, and is obtained from

$$\bar{J} = \hat{n} \times \bar{H}^{tot} \Big|_{u=u_0} = \hat{u} \times (\bar{H}^i + \bar{H}^s) \Big|_{u=u_0} . \quad (5.26)$$

We obtain

$$J_v = -2H_0 \sum_{m=0}^{\infty} j^m \left\{ \begin{array}{l} \left[M_{c_m}^{(1)}(q, u) - M_{c_m}^{(4)}(q, u) \frac{\frac{\partial}{\partial u} M_{c_m}^{(1)}(q, u) \Big|_{u=u_0}}{\frac{\partial}{\partial u} M_{c_m}^{(4)}(q, u) \Big|_{u=u_0}} \right] c_{e_m}(q, v) c_{e_m}(q, \phi^{inc}) \\ + \left[M_{s_m}^{(1)}(q, u) - M_{s_m}^{(4)}(q, u) \frac{\frac{\partial}{\partial u} M_{s_m}^{(1)}(q, u) \Big|_{u=u_0}}{\frac{\partial}{\partial u} M_{s_m}^{(4)}(q, u) \Big|_{u=u_0}} \right] s_{e_m}(q, v) s_{e_m}(q, \phi^{inc}) \end{array} \right\}_{u=u_0}. \quad (5.27)$$

Using the Wronskian relations from (5.14) and (5.15), we simplify this expression to

$$J_v = \frac{4}{\pi} H_0 \sum_{m=0}^{\infty} j^{m+1} \left\{ \frac{c_{e_m}(q, v) c_{e_m}(q, \phi^{inc})}{\frac{\partial}{\partial u} M_{c_m}^{(4)}(q, u) \Big|_{u=u_0}} + \frac{s_{e_m}(q, v) s_{e_m}(q, \phi^{inc})}{\frac{\partial}{\partial u} M_{s_m}^{(4)}(q, u) \Big|_{u=u_0}} \right\}. \quad (5.28)$$

If the electric field components are desired, they may be obtained from (5.8), which simplifies to

$$\bar{E} = \frac{1}{j\omega\epsilon_0} \nabla \times \bar{H} = \frac{1}{j\omega\epsilon_0} \frac{1}{(\cosh^2 u - \cos^2 v)^{1/2}} \left\{ \hat{u} \frac{\partial}{\partial v} \left(\frac{H_z}{F} \right) - \hat{v} \frac{\partial}{\partial u} \left(\frac{H_z}{F} \right) \right\}. \quad (5.29)$$

Using the preceding equations, the surface current on elliptic cylinders with $q = 0.25$, or $c = 1$ in the nomenclature used in [9], were computed for $H_0 = 1.0$ and several values of u_0 . A value of $N = 20$ was used to calculate these results. Figure 5.3 shows surface current magnitudes for an incident wave angle of $\phi_0 = 0$; Figure 5.4 shows similar results for $\phi_0 = \pi/2$. As in the TM case, the results do not agree with the corresponding data shown in [9] but do agree well with the results of van den Berg and van Schaik [15] and Wall [16].

5.3 EXAMPLES

The remainder of this chapter presents numerical values for the current density and scattering cross section associated with electromagnetic scattering from elliptic cylinders. Table 5.1 shows the range of cylinder sizes considered, as a function of the parameters q and u . As q increases in size, so does the dimension of the major axis. As the magnitude of u increases, so does the

50 5. ELECTROMAGNETIC SCATTERING FROM CONDUCTING ELLIPTIC CYLINDERS

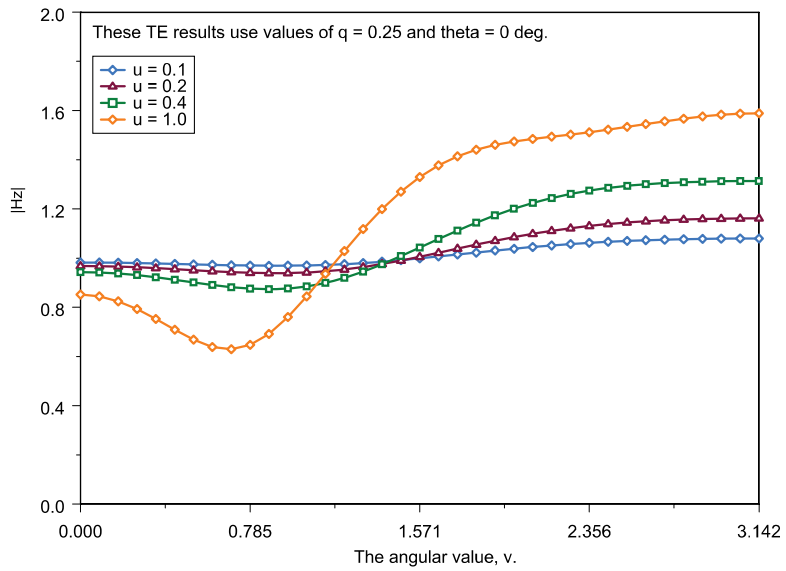


Figure 5.3: The surface current magnitude for elliptic cylinders illuminated by a TE_z incident wave with $H_0 = 1.0$ and $\phi_0 = 0$.

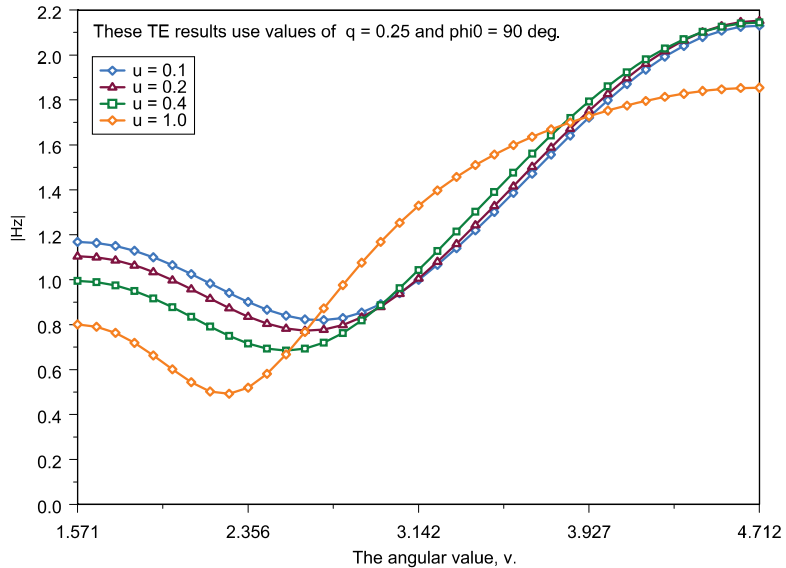


Figure 5.4: The surface current magnitude for elliptic cylinders illuminated by a TE_z incident wave with $H_0 = 1.0$ and $\phi_0 = 90$ degrees.

dimension of the minor axis. Consequently, the upper left-hand corner of each of the tables is associated with a small ellipse, whereas the lower right-hand corner is associated with a large ellipse that is approaching the shape of a circle. Table 5.1 also shows the eccentricity of the ellipse, $\xi = 1.0/\cosh(u)$. The limiting cases of a strip and a circle have eccentricities of $\xi = 1.0$ and $\xi = \infty$, respectively.

Table 5.1: The major radius a and minor radius b , in wavelengths, of an ellipse as a function of q and u

u	ξ	$q = 1.0$		$q = 10.0$		$q = 100.0$		$q = 1000.0$	
		a	b	a	b	a	b	a	b
0.1	1.00500	0.31990	0.03188	1.01162	0.10082	3.19902	0.31884	10.1162	1.00826
0.2	1.02007	0.32469	0.06408	1.02678	0.20266	3.24697	0.64087	10.2678	2.02661
0.4	1.08107	0.34411	0.13074	1.08819	0.41345	3.44116	1.30746	10.8819	4.13456
0.8	1.33743	0.42571	0.28269	1.34624	0.89395	4.25718	2.82692	13.4624	8.93953
1.6	2.57746	0.82043	0.75616	2.59443	2.39120	8.20432	7.56166	25.9443	23.9120
3.2	12.2866	3.91096	3.89798	12.3675	12.3265	39.1096	38.9798	123.675	123.265

5.4 THE SIZE, N , OF THE EIGENMATRIX FOR THE COMPUTATIONS TO FOLLOW

Table 5.2 reports the necessary size N of the eigenmatrices generated in the course of computing the Mathieu functions for the results depicted in the tables to follow, to ensure double precision accuracy at all of the seven angles where the current density was sampled. As observed from previous chapters, N must increase as the cylinder dimensions increase.

Table 5.2: Values of N as a function of u and q to obtain convergence in seven current values

u	$q = 1.0$	$q = 10.0$	$q = 100.0$	$q = 1000.0$
0.1	20	20	40	80
0.2	20	20	40	80
0.4	20	20	30	80
0.8	20	20	40	80
1.6	20	30	50	120
3.2	30	70	160	440

52 5. ELECTROMAGNETIC SCATTERING FROM CONDUCTING ELLIPTIC CYLINDERS

5.5 CURRENT DENSITY AND SCATTERING CROSS SECTION FOR TM_z EXCITATION

Tables 5.3–5.4 and 5.5–5.6 report numerical results for a TM_z incident wave of magnitude $E_0 = \eta$, propagating in either the $\phi_0 = 0$ direction or the $\phi_0 = 90$ degrees direction. Magnitudes are reported in Tables 5.3 and 5.5, while phases are reported in Tables 5.4 and 5.6. Tables 5.7 and 5.8 report the scattering cross section

$$\sigma_{TM}(v) = \frac{16}{k} \left| \begin{array}{l} \sum_{m=0}^{\infty} \frac{Mc_m^{(1)}(q, u)}{Mc_m^{(4)}(q, u)} \Big|_{u=u_0} ce_m(q, \phi_0) ce(q, v) \\ + \sum_{m=0}^{\infty} \frac{Ms_m^{(1)}(q, u)}{Ms_m^{(4)}(q, u)} \Big|_{u=u_0} se_m(q, \phi_0) se(q, v) \end{array} \right|^2 \quad (5.30)$$

for the same cylinders. The units of scattering cross section are wavelengths. In both cases, the numerical results were calculated at seven discrete values of v . These results were obtained in quad precision and are reported in double precision, in an attempt to provide reference data that others may use for comparison. The values of N needed for these calculations are shown in Table 5.2.

The current magnitudes reported in Table 5.3, where the plane wave is exiting at $\phi_0 = 0$ degrees, exhibit the behavior expected. That is, the largest magnitude is located at the specular point, particularly as the value of u increases. When the incident plane wave in the $\phi_0 = 90$ degrees direction, the current magnitude is largest at the tip(s) of the major axis for small values of q and u . However, as the dimensions increase, i.e., the ellipse becomes more like a circle, the largest current magnitude moves to the specular point.

Table 5.3: The magnitude of the surface current density observed on an elliptic cylinder when excited by TM_z plane wave, $E_0 = \eta$ and $\phi_0 = 0$ degrees (*Continues*)

u	v	$q = 1.0$	$q = 10.0$	$q = 100.0$	$q = 1000.0$
0.1	0	1.522581833258720	0.427967248734391	0.100961198036516	0.0169008306262872
30	0	0.359992357851115	0.185500885763228	0.093122549961756	0.0399930845747226
60	0	0.442322056083648	0.250990755548063	0.138493307725597	0.0741549452308864
90	0	0.599589711595543	0.341549003802596	0.203293423045178	0.125283509020296
120	0	0.862711345719612	0.516864805089817	0.324224150435347	0.219128686795425
150	0	1.684806118602860	1.026891085222910	0.664477031494575	0.473506582579585
180	0	8.961283002325530	5.486222335812350	3.586937524816790	2.600640189501290
0.2	0	0.729903586223655	0.184820346169846	0.0343901725254376	0.0036019253544745
30	0	0.329095142941342	0.159471479352722	0.0662571659984019	0.021597789270023
60	0	0.443524991839788	0.243788845127741	0.129602651548991	0.0644878037814721
90	0	0.679979002776933	0.365602094503850	0.226882582793526	0.147134670410835
120	0	0.925054700792177	0.587606627656470	0.40415149597196	0.308632606088883
150	0	1.783604986721930	1.170712701067570	0.85325846023808	0.710921954104755
180	0	5.020806985608950	3.332325747573060	2.477214801066650	2.117580729827010
0.4	0	0.3322587119605409	0.0705325886538393	0.0090874450485166	0.0005060575356978
30	0	0.259059658311478	0.113386424210514	0.0337157985479121	0.006649140453163
60	0	0.432924457254125	0.223911864316966	0.108268858163135	0.0450116877836537
90	0	0.649890898896317	0.403967185626592	0.262887530003020	0.175750246794528
120	0	1.032067150203290	0.721357942391210	0.561640657107068	0.481640586653717
150	0	1.860156569010550	1.386624737405610	1.183171407740300	1.116807187979570
180	0	3.121241303226880	2.377252489531290	2.084777603448240	2.011854042361440

Table 5.3: (Continued) The magnitude of the surface current density observed on an elliptic cylinder when excited by TM_z plane wave, $E_0 = \eta$ and $\phi_0 = 0$ degrees

0.8	0	0.130384050213996	0.0205715085132336	0.0016012896271609	0.0000434484567715
30		0.157634955649697	0.0501609797997018	0.0097284361921648	0.00009651474944334
60		0.365284338217342	0.170009713849646	0.0678950421231911	0.0202655583354658
90		0.669191553262465	0.434468411990929	0.289964218348239	0.195761951324142
120		1.152521797207560	0.910450084426204	0.791029594398580	0.737881566311035
150		1.83733110616590	1.600081922587170	1.527701607158110	1.511680062168370
180		2.302860750162230	2.062883694699150	2.008399822713860	2.000891315601210
1.6	0	0.0296799407451495	0.002715515515608	0.0000970885474288	0.000000875794957
30		0.0644786776644844	0.0117751354310323	0.0011546588775912	0.00046130580089
60		0.213725576658299	0.0821937577629918	0.0233589157351858	0.0040965611046718
90		0.574958243186249	0.382504896118470	0.257868682039384	0.17484771184529
120		1.164355748496650	1.02354468072640	0.962884644743885	0.943775812957517
150		1.776054769395470	1.710135448789370	1.696885851680140	1.695123124044540
180		2.047128301177700	2.006132541143640	2.000647142600110	2.000065138983410
3.2	0	0.0007867361836839	0.000017363724806	0.000000773103669	0.0000000000326031
30		0.0046242384586964	0.000320168568666	0.00007605044135	0.000000037289414
60		0.0503807819515376	0.0116083696071624	0.0014994943632385	0.000086539259085
90		0.3406437367742590	0.230302047841661	0.156353893264146	0.106350810851465
120		1.0471371872102300	1.008846480028430	0.999182661693196	0.997693394727073
150		1.7365003790727800	1.731281657810040	1.730677538322700	1.730615748256280
180		2.0020487460653200	2.000209241293650	2.000020972213910	2.000002097707650

Table 5.4: The phase (degrees) of the surface current density observed on an elliptic cylinder when excited by TM_z plane wave, $E_0 = \eta$ and $\phi_0 = 0$ degrees (*Continues*)

u	v	$q = 1.0$	$q = 10.0$	$q = 100.0$	$q = 1000.0$
0.1	0	145.2309286118371	-121.218961357110	134.620770309452	81.401144823795020
30	-168.176932100773	-11.7996191978909	14.29305922822292	-1.906681629802270	
60	-102.3666149981692	130.258218025408	94.8585609905671	-74.74141999850340	
90	-43.1186261647920	-41.4543839154721	-39.1102826946753	-36.20306309999680	
120	16.45566514946999	144.417764496829	-177.073027314108	-5.435667123752940	
150	60.2548355377670	-80.1735972993831	-112.134810258768	-107.3896060227270	
180	76.0964986541635	-30.6754801578444	43.2436381529669	22.07280690371910	
0.2	0	132.078063186170	-155.247508192115	47.0490310455911	-151.2432236170890
30	-175.590053284332	-30.6216708509533	-26.8928528921376	-105.2881042284710	
60	-105.520445507541	124.713598916324	79.9451305047837	-115.2958206043330	
90	-41.8103474219557	-38.8127542061528	-35.7675323305726	-33.09487589214210	
120	21.1139513084515	152.931622470874	-160.51457453562	30.73372490850430	
150	66.4835560735379	-68.0202637860315	-87.2561645986175	-49.68781681598420	
180	82.8860486405196	-17.3068516087094	70.9878035543154	87.32562035739630	
0.4	0	101.734009672831	122.662988850002	-178.897934940148	-78.65597430060500
30	167.540408539028	-80.2161524210684	-149.833591121954	-78.57817547053060	
60	-113.894114454633	106.084635977829	29.689477539419	102.6263643764310	
90	-39.5539934661048	-35.7345566905964	-32.9663186520943	-31.41878360782730	
120	30.7144529872372	172.071267870539	-116.808797651239	148.9274383158400	
150	80.2263176051988	-38.7161443027320	-16.6447040042211	148.6856450248000	
180	98.1405973133637	15.5069118126473	151.081661475917	-45.33549797505040	

Table 5.4: (Continued) The phase (degrees) of the surface current density observed on an elliptic cylinder when excited by TM_z plane wave, $E_0 = \eta$ and $\phi_0 = 0$ degrees

0.8	0	21.6473317790246	103.819935713192	-120.975625371155	75.06879439964780
30	122.448125520947	135.473379151967	172.081453176794	-177.6194679385040	
60	-138.555493188283	42.9027864777034	-151.358079691014	-74.89344102839220	
90	-36.3467300661611	-33.3009757125464	-31.5802307143995	-30.74317235398320	
120	53.4035994186177	-133.002369815687	37.2910771809549	-101.2207849855990	
150	115.882100353499	51.2701152086620	-116.133046212962	-123.9991763031290	
180	138.274145252080	117.927691429403	90.2103390213574	165.7011626321610	
1.6	0	101.660947974431	151.145340091936	-115.546152982117	178.3123085690280
30	-65.0782739095131	-41.1370725867955	-13.6265389542945	-165.1250334261660	
60	133.701286253628	141.90477713427	138.962116863573	8.412088465404640	
90	-33.7851480721533	-31.8144299778548	-30.8553834730576	-30.39982493735730	
120	133.102894775844	98.6974713755862	32.8046854409074	-11.56187037595610	
150	-111.775002440611	85.9223121677899	36.8607962306569	168.3301512164200	
180	-70.5193181802126	-148.037145826980	72.9037535890570	-20.24040433668160	
3.2	0	39.1199554100292	-168.033667311344	48.2991711540310	-57.83239612552980
30	135.655306511241	114.667509935282	12.1623569084243	39.74518032627530	
60	-123.264273414898	43.5502893105666	-13.3161756862537	168.9336329235650	
90	-31.3504072940919	-30.6339437130296	-30.2957712440289	-30.13761171233500	
120	-21.9562185031786	63.5999470601710	-161.182912251573	-58.71586140454410	
150	137.571836783460	-104.750016758925	-47.011058717532	38.13051020429360	
180	-33.2205097686555	131.945119117540	39.3420819537050	-116.8770789198870	

Table 5.5: The magnitude of the surface current density observed on an elliptic cylinder when excited by TM_z plane wave, $E_0 = \eta$ and $\phi_0 = 90$ degrees (*Continues*)

u	v	$q = 1.0$	$q = 10.0$	$q = 100.0$	$q = 1000.0$
0.1	90	0.1478626565342940	0.02984990289899277	0.0043545481418199	0.0004536309005825
	120	0.1399399171205400	0.0482384097652091	0.0071966229301348	0.000091583322741973
150	0.5815873239224780	0.2105094532043730	0.0543065037742213	0.0096642896636940	
	180	6.015870128136510	3.426867422062840	2.039706164553210	1.257008425741180
	210	2.145901627627100	1.910363391288860	1.978815754294500	1.971738299103560
	240	1.907812418976570	2.013776760026340	1.997381498837650	1.996684449372510
270	1.924481614618970	1.987741950610130	2.000729638028310	1.999977030585340	
0.2	90	0.1391185931482770	0.0260145482547914	0.0032234225081154	0.0002328659834646
	120	0.1355688348876980	0.0442320173987020	0.0059833636507535	0.0005984978831751
150	0.5771804543231340	0.208016752850450	0.0551092076643189	0.0094572468782496	
	180	3.141117147120940	1.852319196175360	1.149498237849590	0.7454562720566060
	210	2.132781560404660	1.905150457593400	1.905159774725130	1.894197442574840
	240	1.944629477566260	1.998118402513550	1.987334095686620	1.987182907219460
	270	1.957955449101800	1.995625035851890	2.000135863063940	2.000011793227250
0.4	90	0.1206306159192800	0.0202431327375136	0.0019630058907581	0.0000889233862612
	120	0.1266317624211860	0.0364513472086266	0.0051951458568549	0.0004115747542951
150	0.5265276963155710	0.1909788786196910	0.0538242240544690	0.0097080940773579	
	180	1.710468940456700	1.063214341286270	0.6919022187680820	0.4625627761985320
	210	1.989804092805940	1.766592313515780	1.697520769947620	1.675355910229910
	240	1.982264149704450	1.963906877686570	1.954871884823600	1.953691066746950

Table 5.5: (Continued) The magnitude of the surface current density observed on an elliptic cylinder when excited by TM_z plane wave, $E_0 = \eta$ and $\phi_0 = 90$ degrees

0.8	90	0.0823387918409447	0.0114486390720118	0.0007932598704553	0.0000201824651098
120	0.109571065666119	0.0239528546780693	0.0034951990802429	0.0002172332018333	
150	0.385041106279814	0.148813434519303	0.0440430494169818	0.0084008966658953	
180	1.007762797521790	0.654283665369435	0.4366689185469020	0.2948058904105250	
210	1.641937758878170	1.435499554985270	1.347715971772940	1.319018302774530	
240	1.956339320649320	1.885623871584690	1.869963965445290	1.867731788662220	
270	2.047207309564600	2.006919758826830	2.000759538912230	2.00007692185820	
1.6	90	0.02666136021343459	0.0023730966110844	0.0000835330259657	0.0000007479784978
120	0.0576342314423743	0.0098325622091762	0.0008813825554070	0.0000313956132818	
150	0.210837801051144	0.0769382057561087	0.0201611818161997	0.0031498967529827	
180	0.623823217616995	0.4150135038129760	0.2797846154200680	0.1897077971778320	
210	1.270304391069400	1.135788082317600	1.080741727210080	1.064889458087410	
240	1.825670185015760	1.776049604371870	1.766872771805950	1.765723658883080	
270	2.030783695578300	2.003818656721860	2.000397513018910	2.000039937762270	
3.2	90	0.0007821905957315	0.0000172552042151	0.000000768110698	0.0000000000323897
120	0.0045837263959111	0.00031612088538888	0.0000074706235756	0.0000000368012712	
150	0.0501882481640897	0.0115197051545350	0.0014802049479201	0.0000848262776629	
180	0.341777618941217	0.2310686416664430	0.1568743399131450	0.1067048149761490	
210	1.051811453616770	1.013719539417580	1.004145270144990	1.002675369868650	
240	1.739282719878460	1.734147621171580	1.733554204012410	1.733493530216230	
270	2.002008913738030	2.000205117815730	2.000020558269810	2.000002056297030	

Table 5.6: The phase (degrees) of the surface current density observed on an elliptic cylinder when excited by TM_z plane wave, $E_0 = \eta$ and $\phi_0 = 90$ degrees (*Continues*)

	<i>u</i>	<i>v</i>	$q = 1.0$	$q = 10.0$	$q = 100.0$	$q = 1000.0$
0.1	90	128.6215064985610	-150.25537321711500	100.5675626615240	48.99559443742110	
	120	-170.1693362448900	42.638733314644100	-36.12206686766050	84.90002035335740	
	150	-90.78282343976210	-149.48695156191700	66.91823558880720	23.975033327912460	
	180	-43.11862616479210	-41.454383915472100	-39.11028269467530	-36.20306309999680	
	210	-10.14784090569320	13.211673386489100	56.72988210953230	-178.8789821475390	
	240	7.104981900707450	31.277672863252100	99.1378821535150	-45.72534210881600	
	270	12.18212372614250	35.640067904225000	114.6654074873030	2.929935931814400	
0.2	90	117.3195620783120	179.74863148237300	19.42577780908860	-174.3332866491430	
	120	-174.5562933887730	20.14167559697800	-94.37123014699110	-88.57060964643690	
	150	-94.21876973885150	-160.87187320240400	29.93861521745540	-92.84575643511410	
	180	-41.81034742195570	-38.812754206152800	-35.76753233057250	-33.09487589214210	
	210	-4.522607576234830	30.564897155873700	113.4405764204740	4.106749840264810	
	240	15.63671698121330	62.042450027445400	-160.6207904579890	-88.29834209725130	
	270	21.75901402719040	72.089070942607700	-129.5659740360480	9.494307358431360	
0.4	90	90.23132818770170	104.70302311584700	163.7526567384130	-90.62048791295060	
	120	173.3753960339650	-33.195990203390700	110.6625368972600	139.6499533460870	
	150	-103.3602057277810	171.54823771853900	-62.91190531295140	-35.29672923256140	
	180	-39.55399346610480	-35.734556690596400	-32.96631865209430	-31.41878360782730	
	210	7.285133798444290	66.831636557702500	-127.9209621418550	23.01035734441210	
	240	34.24018296501200	126.6145495651270	46.86129322425390	-151.2139798780870	
	270	42.91127969456550	147.2956757769580	110.1853130034040	48.28539099679400	

60 5. ELECTROMAGNETIC SCATTERING FROM CONDUCTING ELLIPTIC CYLINDERS

Table 5.6: (Continued) The phase (degrees) of the surface current density observed on an elliptic cylinder when excited by TM_z plane wave, $E_0 = \eta$ and $\phi_0 = 90$ degrees

0.8	90	15.06626370083140	-112.1905618072260	-127.5075799441690	71.24492342761910
120	131.3236549673030	-176.6456293680600	0.2127876624485420	119.6692298056220	
150	-129.1814832344160	92.71985114895690	39.97148692429150	-137.1347680918380	
180	-36.34673006616110	-33.30097571254640	-31.58023071439950	-30.74317235398320	
210	34.74385671314840	152.04635585200620	144.6153628635440	167.4526012345800	
240	79.97297251871260	-84.45334625114600	160.2721115920620	-93.27443881961490	
270	95.51150126454670	-40.37302561146910	-63.01466448687790	-21.99227700392100	
16	90	99.98683612173140	149.6849574366090	-116.4427523253440	177.8428250117550
120	-60.51441442706250	-16.67660639910910	78.14029519938750	140.617499345470	
150	140.0926067164040	168.0618066942490	-128.9049819817700	-45.99254719701020	
180	-33.78514807215330	-31.81442997785480	-30.85538347305760	-30.39982493735730	
210	122.8913343652420	63.17909110796280	-82.20696975714820	-17.05864372069710	
240	-130.5437049275350	23.14948782623350	-163.2872924857730	-105.1964478723490	
270	-92.52138835930170	139.2341056507560	-158.3112114511900	-31.80858953530840	
3.2	90	39.06932479309550	-168.0623640037470	48.28463514805030	-57.83923585133930
120	137.4119360637210	120.6972500467510	31.87850282299930	102.9831384854520	
150	-121.5035094470290	49.57266598111440	6.39640979628883	-127.825937785660	
180	-31.35040729409190	-30.63394371302960	-30.29577124402890	-30.13761171233500	
210	-24.25449035579740	56.23533916543930	175.4706983402210	-132.5680113143440	
240	133.5430397030930	-117.5364927053060	-87.46135438640120	-89.78964970710490	
270	-37.88006007694200	117.1777810178510	-7.366799102730810	95.41315730843170	

Table 5.7: The bistatic scattering cross section for an elliptic cylinder when excited by a TM_z plane wave, $E_0 = \eta$ and $\phi_0 = 0$ degrees (*Continues*)

u	v	$q = 1.0$	$q = 10.0$	$q = 100.0$	$q = 1000.0$
0.1	0	2.6647	8.0123	13.6914	19.9382
	30	2.3571	6.2583	5.4985	8.333
	60	0.4354	-0.7817	1.1961	3.1468
	90	-4.1416	-3.4201	-1.9681	0.2071
	120	-6.3434	-5.0503	-3.7787	-1.512
	150	-6.5318	-6.0719	-4.6391	-2.4321
	180	-6.843	-6.2326	-4.9437	-2.7326
	0.2	3.2401	8.9634	15.3531	22.7735
0.2	30	2.8001	6.3609	7.7978	10.7429
	60	0.6179	1.0213	3.207	6.9032
	90	-3.6015	-1.6502	0.5964	4.2701
	120	-5.1734	-3.3406	-0.9706	2.6554
	150	-5.6674	-4.3464	-1.888	1.7663
	180	-6.0359	-4.6164	-2.1719	1.4811
	0.4	4.4721	10.9724	18.61	27.3602
	30	3.6456	5.6547	7.8648	12.2659
0.4	60	0.7338	2.8408	6.3066	10.7471
	90	-2.4348	0.6808	4.4947	9.1408
	120	-3.2311	-0.6625	3.2555	7.9331
	150	-4.0748	-1.3867	2.5141	7.2164
	180	-4.4029	-1.6303	2.2729	6.9805

62 5. ELECTROMAGNETIC SCATTERING FROM CONDUCTING ELLIPTIC CYLINDERS

Table 5.7: (Continued) The bistatic scattering cross section for an elliptic cylinder when excited by a TM_z plane wave, $E_0 = \eta$ and $\phi_0 = 0$ degrees

0.8	0	7.234	15.0373	23.9315	33.4336
	30	4.9234	4.7641	8.7374	12.2344
	60	0.3251	4.5525	8.548	13.2966
	90	0.1512	3.8114	8.4447	13.3508
	120	-0.7469	3.369	8.1124	13.0682
	150	-1.1077	3.0435	7.8368	12.8081
	180	-1.2295	2.924	7.7345	12.7095
1.6	0	13.361	22.3755	31.9355	41.7393
	30	2.1597	6.6862	9.8261	13.9986
	60	2.5891	6.8382	11.3193	16.1929
	90	3.0222	7.543	12.4296	17.4103
	120	3.3209	8.0757	13.034	18.0292
	150	3.476	8.3394	13.321	18.3191
	180	3.5257	8.4183	13.405	18.4036
3.2	0	26.358	36.0637	45.9313	55.8709
	30	7.644	10.9462	15.2895	20.0838
	60	8.3086	12.9581	17.8971	22.8886
	90	9.4554	14.3909	19.3829	24.382
	120	10.269	15.2535	20.2518	25.2516
	150	10.7242	15.7185	20.7179	25.7178
	180	10.8698	15.8659	20.8655	25.8655

Table 5.8: The bistatic scattering cross section for an elliptic cylinder when excited by a TM_z plane wave, $E_0 = \eta$ and $\phi_0 = 90$ degrees (*Continues*)

u	v	$q = 1.0$	$q = 10.0$	$q = 100.0$	$q = 1000.0$
0.1	90	4.7084	14.3186	24.2013	34.1522
	120	2.6544	-5.2819	1.327	0.7318
	150	-1.959	-3.4301	-1.2671	-0.392
	180	-4.1416	-3.4201	-1.9681	0.2071
	210	-1.8062	-1.4932	0.5968	3.6228
	240	2.2322	1.6908	6.4291	11.3217
	270	4.0606	13.2913	20.6876	25.0526
0.2	90	5.1807	14.6083	24.4076	34.3171
	120	3.0089	-3.08	3.2581	4.6475
	150	-1.787	-2.9578	-0.6875	2.0473
	180	-3.6015	-1.6502	0.5964	4.2701
	210	-1.3594	0.3986	3.9214	8.6375
	240	2.1957	4.977	10.4202	15.624
	270	3.8505	12.0633	17.0639	22.1361
0.4	90	6.1935	15.3568	25.0221	34.8702
	120	3.6589	0.8423	4.9508	4.7147
	150	-1.6615	-0.7059	2.8417	6.2086
	180	-2.4348	0.6808	4.4947	9.1408
	210	-0.3871	3.1961	7.987	12.9944
	240	2.1772	7.0219	12.2062	17.2119
	270	3.4146	9.6435	14.5417	19.5414

Table 5.8: (Continued) The bistatic scattering cross section for an elliptic cylinder when excited by a TM_z plane wave, $E_0 = \eta$ and $\phi_0 = 90$ degrees

0.8	90	8.4553	17.414	26.9608	36.7574
	120	4.4469	5.2366	6.7077	8.4366
	150	-1.2306	2.4857	6.4478	10.8334
	180	0.1512	3.8114	8.4447	13.3508
	210	1.107	5.705	10.6331	15.6236
	240	2.3644	7.3658	12.36	17.3593
	270	2.9765	8.0412	13.0409	18.0408
1.6	90	13.7823	22.9549	32.5873	42.4224
	120	1.4481	5.2719	9.1051	13.1582
	150	2.1495	6.4013	10.795	15.6677
	180	3.0222	7.543	12.4296	17.4103
	210	3.7917	8.5934	13.563	18.5595
	240	4.3251	9.2497	14.2399	19.2389
	270	4.5241	9.4729	14.4669	19.4662
3.2	90	26.383	36.0908	45.9594	55.8994
	120	7.6602	10.9558	15.2735	20.0508
	150	8.2904	12.9368	17.8755	22.867
	180	9.4554	14.3909	19.3829	24.382
	210	10.2905	15.2751	20.2734	25.2732
	240	10.7615	15.7559	20.7554	25.7553
	270	10.9129	15.9092	20.9088	25.9088

5.6 CURRENT DENSITY AND SCATTERING CROSS SECTION FOR TE_z EXCITATION

Tables 5.9–5.10 and 5.11–5.12 report numerical results for a TE_z incident wave of magnitude $H_0 = 1.0$ propagating in the $\phi_0 = 0$ direction and the $\phi_0 = 90$ degrees direction, respectively. Magnitudes are reported in Tables 5.9 and 5.11, while phases are reported in Tables 5.10 and 5.12. Tables 5.13 and 5.14 report the scattering cross section

$$\sigma_{TE}(v) = \frac{16}{k} \left| \begin{array}{l} \sum_{m=0}^{\infty} \frac{\frac{\partial Mc_m^{(1)}(q, u)}{\partial u}}{\frac{\partial Mc_m^{(4)}(q, u)}{\partial u}} \\ + \sum_{m=0}^{\infty} \frac{\frac{\partial Ms_m^{(1)}(q, u)}{\partial u}}{\frac{\partial Ms_m^{(4)}(q, u)}{\partial u}} \end{array} \right|_{u=u_0}^2 ce_m(q, \phi_0) ce(q, v) se_m(q, \phi_0) se(q, v) \quad (5.31)$$

for the same cylinders. In both cases, the numerical results were calculated at seven discrete values of v . These results were obtained in quad precision and are reported in double precision, in an attempt to provide reference data that others may use for comparison. The values of N needed for these calculations are those shown in Table 5.2.

The current magnitudes reported in these tables exhibit the behavior expected. That is, the largest values generally occur at the specular point, particularly as u and q increase.

Table 5.9: The magnitude of the surface current density observed on an elliptic cylinder when excited by TE_z plane wave, $H_0 = 1$ and $\phi_0 = 0$ degrees (*Continues*)

u	v	$q = 1.0$	$q = 10.0$	$q = 100.0$	$q = 1000.0$
0.1	0	0.962592781799015	0.895625776260597	0.761234081534698	0.537378928533178
30	0.941449563433780	0.855556238942251	0.909275443521785	0.7947744711257671	
60	0.967714995403532	1.00885196916427	1.01430367035937	1.04984609453086	
90	1.06915476342882	1.07014198402713	1.15778151371981	1.25536906766170	
120	1.07063976472624	1.11514212365251	1.24652438664746	1.40771476452517	
150	1.06219427119444	1.16792240689682	1.27728696748800	1.49895159958748	
180	1.07042013352759	1.15146244788105	1.29884747947719	1.53325689560369	
0.2	0	0.933247918307937	0.818352408140855	0.603515643021227	0.312401255092848
30	0.885721309998379	0.748309322600748	0.724647976152659	0.601630246352694	
60	0.947200699117891	0.991631522658586	1.05912004604466	0.975649050135323	
90	1.13655040591712	1.12775940978103	1.27518596775874	1.35245371516160	
120	1.13373308225902	1.23241171861752	1.43210302951344	1.63691745919852	
150	1.13965497428732	1.31772958812346	1.56663715626852	1.80602427215730	
180	1.16370303147559	1.32770715351022	1.59806126771166	1.85592752857996	
0.4	0	0.883692881065272	0.685105036162773	0.384042510109355	0.135719722117305
30	0.768226487395196	0.676231001101423	0.578970182912916	0.312407784149575	
60	0.949576102867207	0.977559399425473	0.944517407487421	0.781226988235958	
90	1.25689647878181	1.28715307163399	1.35259652402091	1.37902147712344	
120	1.23924615382723	1.50083942595403	1.67050396845971	1.80770464663501	
150	1.34640054997784	1.60629842144388	1.83962554583679	1.95822175948903	
180	1.40383448051258	1.64896805536892	1.89450739783910	1.98377822919823	

Table 5.9: (Continued) The magnitude of the surface current density observed on an elliptic cylinder when excited by TE_z plane wave, $H_0 = 1$ and $\phi_0 = 0$ degrees

0.8	0	0.766008064684886	0.463201022591861	0.190576412914646	0.0481420300815151
30	0	0.503896753581062	0.57734909116682	0.289744213738769	0.133769054392571
60	0	1.07516568133833	0.869284785313310	0.741933083816104	0.521541238316319
90	0	1.22827422086689	1.37038302247658	1.37851348649407	1.38922187078370
120	0	1.53606851462881	1.68754246141392	1.82883358066551	1.92860098328782
150	0	1.65299331645508	1.86504900089443	1.96791030041848	1.99508638952082
180	0	1.66919619112823	1.92213592248804	1.98886187840921	1.998761776075219
1.6	0	0.498280161379489	0.2220465940569455	0.0631697310778727	0.0097790141737645
30	0	0.596623671907651	0.278132047951664	0.129020487382989	0.0372293647530153
60	0	0.912969100167108	0.6933638636326304	0.489403257931602	0.270540881545266
90	0	1.35530760039208	1.37141952921204	1.38730276983414	1.393999518921504
120	0	1.71079105077017	1.84852006801398	1.93974912670112	1.98586509904703
150	0	1.88646862673733	1.97466790379771	1.99635669769184	1.99960315962834
180	0	1.9541676526573	1.99233262730645	1.99908027046836	1.99990889737254
3.2	0	0.13886018057365160	0.0319628916796476	0.0036248713636953	0.0001463163080788
30	0	0.2041089497413520	0.0788220841249432	0.0182321781138755	0.0021496186516903
60	0	0.5968569357785050	0.3775189295464050	0.1832456464421380	0.0628638869110851
90	0	1.38239989639449	1.39074687584714	1.39541021599510	1.39753342032653
120	0	1.89887338664228	1.96828466417311	1.99438794518739	1.99934499098112
150	0	1.9859624099513	1.99874977255151	1.99987125881180	1.99998707694698
180	0	1.99726237956415	1.99970870030626	1.99997064682103	1.99999706325298

Table 5.10: The phase (degrees) of the surface current density observed on an elliptic cylinder when excited by TE_z plane wave, $H_0 = 1$ and $\phi_0 = 0$ degrees (*Continues*)

u	v	$q = 1.0$	$q = 10.0$	$q = 100.0$	$q = 1000.0$
0.1	0	-122.5536818705450	-22.157993302522400	-114.936967556177880	-148.3741271789560
30		-104.5373925508180	41.080214326677200	69.32731701396500	60.32477445035120
60		-55.38004991500310	176.6671310825180	144.8224475360330	-23.87566760272380
90		3.697444121472600	2.634109077423430	5.907617724750620	5.4835689085639990
120		60.10488965766030	-172.9615455466660	-136.2497340557650	30.268942855980400
150		104.1116305837520	-38.33548655650610	-73.28856911318640	-74.89139394236160
180		120.3821084541280	10.94550685088190	81.39599568729670	53.38813915947160
0.2	0	-132.6005706640490	-49.51124090720260	169.7594013947660	1.229847945099250
30		-111.5188013676820	32.24300975215030	36.49405434394070	-24.71214931560330
60		-54.34274660669710	172.7535907019900	132.1841838326180	-62.00047735117990
90		5.832130086781680	4.951965772824860	4.677051421054780	3.185622138847610
120		63.08092433705960	-166.4225110485130	-126.0889699518340	56.04861525908030
150		109.5105993397170	-30.40356165420440	-56.42008973706350	-30.60457003281890
180		126.3674928094920	21.04130929613170	100.4355308261070	104.3759670304580
0.4	0	-158.8625100056070	-123.7496168271820	-40.46702454627280	104.9723624227600
30		-129.8319998172240	2.104503946859790	-62.27508041193800	29.25238626690990
60		-55.24762871932270	161.8873653531460	85.54488671137500	164.8720545627690
90		5.965095347978950	7.278172313883970	2.659770563700670	1.379966186895070
120		70.23005170928810	-153.8148323954480	-92.84087577645460	164.2060435992110
150		120.3806868672710	-9.02192239525873	0.26870470463735	156.2180647702020
180		137.1891672005710	42.633346511460	165.9033523369140	-39.73655505064230

Table 5.10: (Continued) The phase (degrees) of the surface current density observed on an elliptic cylinder when excited by TE_z plane wave, $H_0 = 1$ and $\phi_0 = 0$ degrees

0.8	0	125.9367418826050	21.07626481378870	41.58567752987130	-63.02108177284470
30		-173.016055257150	-143.0517119014770	-83.70346991211300	-33.69427472469560
60		-76.36329537223100	99.57047622358620	-86.75543849152610	6.291887666934480
90		4.25771743422480	3.788648558065960	1.6833855595767390	0.706952771787069
120		88.78763360334100	-110.4891344032950	51.51769925192190	-93.44139041843920
150		143.4380881321870	66.58323472502300	-109.6082013167640	-121.6940424413130
180		164.7175777407410	130.7371839291290	94.93886082366630	167.2324611294720
1.6	0	-140.4790834310310	-56.82972486881630	89.56079122972710	103.2118194666880
30		30.50450801135130	76.1907211904360	127.8227678041000	32.61643107694480
60		-162.7604329676230	-150.4006115908020	-136.5112394731250	119.5070381718700
90		5.117528669645290	1.538032345042270	0.822571724157821	0.381110599943544
120		155.7980702664400	112.0524266863320	39.85042470812240	-8.592316590093140
150		-98.00239876492750	91.58261478893490	38.83428048914040	168.9657181616360
180		-59.15617416979310	-144.004475910080	74.20866055511110	-19.82675346064460
3.2	0	-150.3665741686760	64.76787391482080	14.20899545967290	45.62579279486660
30		-107.1753587187220	-82.03432471761190	-121.0152927921120	-1.308536316608350
60		-48.06062686702720	139.4744636769290	114.9476685473980	-16.54290013049360
90		1.398559360108390	0.611239516469710	0.281667110573200	0.130724917677668
120		-11.93727538754370	68.34357437969940	-159.3903264337010	-58.12552040303870
150		141.0022307879210	-103.6154035274120	-46.6499641493560	38.24477708033900
180		-30.89810505544840	132.6867644054720	39.57677863279280	-116.8023553518620

Table 5.11: The magnitude of the surface current density observed on an elliptic cylinder when excited by TE_z plane wave, $H_0 = 1$ and $\phi_0 = 90$ degrees (*Continues*)

u	v	$q = 1.0$	$q = 10.0$	$q = 100.0$	$q = 1000.0$
0.1	90	0.7057184785342980	0.4113047469518730	0.2181805594034920	0.0975632096086113
120	0.3772394496061410	0.4548091218249950	0.1949441498342720	0.1022154434846830	
150	0.5203544979380220	0.5983740609234640	0.3175126203667780	0.189305240922080	
180	1.0691547634288200	1.0701419840271300	1.1577815137198100	1.2553690676617000	
210	1.6286472898490000	1.885858072524473400	2.0811992101650200	2.9710550241660700	
240	2.23339357920814800	2.1574512594221400	1.92226802032861100	1.99222929635772500	
270	2.5411797135126300	1.9276535582880500	2.0552918642252200	2.0081104788761000	
0.2	90	0.693505397555230	0.4091042182374130	0.1982676989364160	0.0779486705438200
120	0.3581375534340130	0.4521968354103360	0.1567143348224100	0.0622222261146476	
150	0.5910610053255350	0.66663017449496180	0.4074719097479350	0.2256323775761520	
180	1.1385504059171200	1.1277594097810300	1.2751859877587400	1.3524537151616000	
210	1.64798832329523700	1.9873429680674100	1.9714762455745100	1.9978674001295600	
240	2.1537427908597400	1.9708014767923000	2.0119372932735500	2.0000345923802300	
270	2.3940733574509000	2.0759185465232800	1.9782051695910200	2.000068149774900	
0.4	90	0.6783435930605430	0.3903165445557330	0.1749887612347090	0.0559280815366375
120	0.3234884579735320	0.4083348038095720	0.1291158325100350	0.0809049910789646	
150	0.7421105264380430	0.69991788644917540	0.4299977829117310	0.2629090528641760	
180	1.250896478781100	1.2871530716339900	1.3525965240209100	1.3790214771234400	
210	1.6633514459295000	1.92889523777127300	1.9627650639892800	1.9911526536321200	
240	2.0244122391373800	1.9697034838377800	1.9978476769737800	1.9997771636094200	
270	2.1717874668082200	2.0091730733329000	1.9992161652869000	1.99993354437341900	

Table 5.11: (Continued) The magnitude of the surface current density observed on an elliptic cylinder when excited by TE_z plane wave, $H_0 = 1$ and $\phi_0 = 90$ degrees

0.8	90	0.6403564291494360	0.3422979917488500	0.1327336725882680	0.0326579314235654
120		0.3036586801772130	0.2415800212885320	0.1404147953709730	0.06573608890549912
150		0.9554444241638900	0.7199122149418740	0.4957974547229800	0.2944748932303620
180		1.2282742208668900	1.3703830224765800	1.3785134864940700	1.3892218707837000
210		1.6980861753833300	1.8551414853726300	1.9375800371639400	1.9843354414323200
240		1.9326454220591500	1.9777834218437700	1.9960922655870700	1.9995321539395200
270		1.9430648915765400	1.9918500717167400	1.9986915824366400	1.99983855924744300
1.6	90	0.4713287313938500	0.2055818701497890	0.0585252261572250	0.0090341917459068
120		0.5714658831914910	0.2877586260706830	0.1120626021320030	0.0308504180973022
150		0.8870259346515300	0.66517447257984960	0.4411632114625410	0.232708511835890
180		1.35553706003920800	1.3714195292120400	1.3873027698341400	1.3939951892150400
210		1.7383008487311100	1.8725116374413100	1.95337028105943400	1.9903969288674300
240		1.9163972504101400	1.98339702540186100	1.9976761244515200	1.9997558014186100
270		1.9708552654397400	1.9953250871269200	1.9994525500968100	1.9999441617769200
3.2	90	0.1381897842552250	0.0318617865888352	0.0036130993015638	0.0001458355851531
120		0.2015354110257370	0.0776270202991839	0.0179391231735118	0.0021269668035500
150		0.5950822670770460	0.3756071243836580	0.1819669452533940	0.0622374059091838
180		1.3823998963944900	1.3907468758471400	1.3954102159951000	1.3975334203265300
210		1.8996993341283600	1.9686904682760900	1.9944846106372400	1.9993576385534300
240		1.9897671312627000	1.9987730447132500	1.9998737968218600	1.9999873319733200
270		1.9973311359007600	1.9997138759811900	1.9999712249847500	1.9999971212268800

Table 5.12: The phase (degrees) of the surface current density observed on an elliptic cylinder when excited by TE_z plane wave, $H_0 = 1$ and $\phi_0 = 90$ degrees (*Continues*)

u	v	$q = 1.0$	$q = 10.0$	$q = 100.0$	$q = 1000.0$
0.1	90	-161.6633057123880	-54.88563346795690	-150.5340301829440	-177.1769470700720
120	-135.5639367318960	128.5882018379150	47.73895342590970	-163.1223576160400	
150	-23.69975407402730	-67.08287954785790	158.2532723580410	134.8820992921340	
180	3.697444121472600	2.634109077423430	5.907617724750620	5.483569085639990	
210	14.75508429315580	31.85909822047160	55.41883969684990	-178.3055242053140	
240	16.54563826126010	24.51875719265950	100.5231154752720	-45.19654984857180	
270	15.86359937417650	44.779097577735110	112.8096837897670	3.376625266424000	
0.2	90	-165.6949256926700	-78.24027497052750	144.3369565069380	-14.81869469147520
120	-134.0702123862430	107.6395796699670	-2.6535244137760420	37.29493951792640	
150	-23.4972780650930	-83.16344833000400	122.3166130448060	14.41510123057050	
180	5.832130086781680	4.951965772824860	4.677051421054780	3.185622138847610	
210	21.491183663888380	47.93500270778800	115.7709086563580	5.427418557681660	
240	26.6328468358990	59.00957243564870	-159.4129627595720	-88.01988574991980	
270	26.95862836805240	78.02154558749900	-128.81189630713890	9.657841939425890	
0.4	90	178.1338869920380	-143.2816088642440	-52.85585236045430	98.40979720533160
120	-135.83471716840	51.173374470584440	-123.2419573958880	-68.32830440663340	
150	-29.71522178833860	-121.6596517985370	20.73189561169120	75.04055517185150	
180	5.965095347978950	7.278172313883970	2.659770563700670	1.379966186895070	
210	33.49284479369090	80.29528035585080	-121.9239247953580	25.35774315210940	
240	47.81474707253540	131.0719478440140	48.40316074914100	-150.726232499570	
270	51.34113033202620	150.0504690723590	111.2171827649940	48.60276691182020	

Table 5.12: (Continued) The phase (degrees) of the surface current density observed on an elliptic cylinder when excited by TE_z plane wave, $H_0 = 1$ and $\phi_0 = 90$ degrees

0.8	90	115.7641507847240	14.23443118580660	37.84611899363990	-64.89809074814060
120	-149.3165892844830	-81.63074902512710	128.1677162812720	-68.50174784458340	
150	-63.96651725259470	165.2854653975700	122.3148946276310	-30.71378340570880	
180	4.257717434222480	3.788648558065960	1.683385595767590	0.7069527717870690	
210	62.401173656922300	166.6383964097190	152.1147594873880	170.6359307177240	
240	94.9463403359090	-78.34723580327970	162.4113219888930	-92.58432955691720	
270	106.3297253348380	-35.90555701008870	-61.59788458913230	-21.54269861803200	
1.6	90	-142.0443248732470	-57.71290371549250	89.111558939003000	102.9942043584750
120	34.73036827975110	103.4578706164600	-128.0808268173600	-16.93048509062190	
150	-155.1179141766930	-119.7811078999990	-40.21498853270650	71.63546756557250	
180	5.117528669645290	1.538032345042270	0.8225717241578210	0.3811105999435440	
210	143.7614433344560	75.15717219491200	-76.22251396415340	-14.655854991776680	
240	-119.0656410142390	27.71532664548260	-161.7314824265090	-104.6984403481030	
270	-83.20805942787350	142.4362605563410	-157.2881849681270	-31.48470044840170	
3.2	90	-150.4144214150490	64.75404080769570	14.20236983179520	45.62267294882850
120	-105.27449240712200	-75.95081247241100	-100.8771127961100	62.23784511181090	
150	-46.10186937706320	145.7346215499910	134.9615915279960	47.10832964226420	
180	1.398559360108390	0.6112395164697100	0.2816671105732000	0.1307249176776680	
210	-14.28749722290110	60.94341110768390	177.2468120738260	-131.9834626285910	
240	136.9410660374540	-116.4130471173910	-87.10383636581960	-89.6765167969680	
270	-35.58019847819310	117.9120869186180	-7.134430167704170	95.48664460231830	

Table 5.13: The bistatic scattering cross section for an elliptic cylinder when excited by TE_z plane wave, $H_0 = 1$ and $\phi_0 = 0$ degrees (*Continues*)

u	v	$q = 1.0$	$q = 10.0$	$q = 100.0$	$q = 1000.0$
0.1	0	-37.1795	-21.8367	-6.8216	7.7797
	30	-31.0073	-10.3669	0.2874	5.6319
	60	-19.0616	-13.6452	-16.2128	-3.9121
	90	-16.6137	-16.8072	-10.2066	-4.4091
	120	-21.6662	-19.2218	-9.1784	-4.8651
	150	-39.7358	-15.4129	-13.7943	-7.2374
	180	-31.0791	-22.8601	-12.9075	-6.9793
0.2	0	-24.9099	-9.8223	4.6765	17.7598
	30	-24.8962	-3.913	1.2497	8.915
	60	-12.8438	-9.6902	-0.505	5.0157
	90	-10.469	-12.967	-0.9507	2.2209
	120	-16.1376	-15.4316	-4.1641	1.6179
	150	-26.6817	-10.401	-6.6215	0.3935
	180	-21.1461	-17.0754	-6.3282	0.1988
0.4	0	-12.51	1.6287	14.3381	25.4772
	30	-14.8898	3.0943	7.8058	9.3239
	60	-6.2385	-5.9867	2.9044	10.407
	90	-4.675	-4.4244	4.2894	8.7259
	120	-12.024	-4.0688	2.3704	7.9364
	150	-12.5486	-6.1209	1.9113	7.1446
	180	-9.9281	-3.351	1.5608	6.8661

Table 5.13: (Continued) The bistatic scattering cross section for an elliptic cylinder when excited by TE_z plane wave, $H_0 = 1$ and $\phi_0 = 0$ degrees

0.8	0	-1.0201	11.3283	22.2816	32.6883
	30	-2.9547	3.892	5.5194	12.895
	60	0.6521	1.1863	8.9482	12.8145
	90	-3.8995	1.9323	8.6236	13.2518
	120	-3.8707	3.3179	8.1836	13.069
	150	-2.6306	2.9355	7.7596	12.8032
	180	-3.9132	2.1852	7.6371	12.7011
1.6	0	10.113	20.9132	31.2706	41.4341
	30	4.4411	3.1547	9.8503	12.6559
	60	1.688	5.8546	11.3968	16.0105
	90	0.2482	7.2512	12.5141	17.422
	120	2.289	8.1729	13.0461	18.0255
	150	3.5852	8.3702	13.3177	18.3182
	180	2.7871	8.321	13.4052	18.4031
3.2	0	25.3695	35.6114	45.7229	55.7746
	30	4.7455	11.5734	15.4632	19.9617
	60	7.6891	12.4739	17.8379	22.8867
	90	9.6459	14.3394	19.3818	24.3816
	120	10.1512	15.2583	20.2509	25.2516
	150	10.6938	15.7193	20.7177	25.7178
	180	10.8531	15.8639	20.8654	25.8655

Table 5.14: The bistatic scattering cross section for an elliptic cylinder when excited by TE_z plane wave, $H_0 = 1$ and $\phi_0 = 90$ degrees (*Continues*)

u	v	$q = 1.0$	$q = 10.0$	$q = 100.0$	$q = 1000.0$
0.1	90	5.234	13.8629	24.0515	34.0643
	120	2.9545	-7.9067	-1.097	-4.4175
	150	-3.9685	-2.0397	-3.3407	-2.6197
	180	-16.6137	-16.8072	-10.2066	-4.4091
	210	-3.1837	-4.5592	-1.3667	2.5423
	240	3.3736	-5.4951	6.3645	11.7653
	270	5.5759	14.0635	20.9019	24.9069
0.2	90	4.8367	13.9217	24.0973	34.1589
	120	2.5191	-6.1374	-1.0297	-2.3227
	150	-4.1678	-1.7429	-1.0385	1.5022
	180	-10.469	-12.967	-0.9507	2.2209
	210	-2.6364	-6.4814	2.6326	8.6171
	240	3.2001	3.2923	10.8692	15.619
	270	5.2851	13.4172	16.9736	22.1355
0.4	90	4.4021	14.2854	24.4979	34.6212
	120	1.9604	-5.1998	1.8883	4.6642
	150	-3.3851	-1.5022	-3.1126	3.6552
	180	-4.675	-4.4244	4.2894	8.7259
	210	-1.3707	2.6715	7.943	13.0081
	240	2.6056	7.4475	12.1952	17.2102
	270	4.3078	9.7591	14.5822	19.5425

Table 5.14: (Continued) The bistatic scattering cross section for an elliptic cylinder when excited by TE_z plane wave, $H_0 = 1$ and $\phi_0 = 90$ degrees

0.8	90	5.2455	15.9181	26.2685	36.4371
	120	2.2861	-0.78	-8.3779	9.2126
	150	-0.4325	0.1929	5.3156	10.0416
	180	-3.8995	1.9323	8.6236	13.2518
	210	-1.8262	5.2555	10.6212	15.6307
	240	2.4261	7.4696	12.3557	17.3575
	270	4.0595	8.0708	13.0232	18.0407
1.6	90	11.0792	21.7271	32.0259	42.164
	120	3.544	6.1434	6.0381	13.5027
	150	2.101	3.0294	10.4489	15.4723
	180	0.2482	7.2512	12.5141	17.422
	210	3.3139	8.5621	13.5451	18.56
	240	4.3716	9.1554	14.2411	19.2385
	270	4.1346	9.4855	14.4636	19.4661
3.2	90	25.4015	35.6417	45.7525	55.8037
	120	4.3788	11.3798	15.7259	20.1834
	150	7.5723	12.5133	17.7818	22.8594
	180	9.6459	14.3394	19.3818	24.3816
	210	10.1818	15.2767	20.2731	25.2732
	240	10.7371	15.7563	20.7552	25.7553
	270	10.8932	15.9076	20.9087	25.9088

5.7 SUMMARY

This chapter reviewed the use of Mathieu functions for the boundary value problem of electromagnetic scattering from elliptic, perfectly conducting cylinders. Surface currents and scattering cross section have been computed for targets encompassing a range of parameters q , u , and v . The results are presented in tabular format to facilitate their comparison with the work of others.

CHAPTER 6

Electromagnetic Scattering from an Infinite Conducting Strip

In this final chapter we consider the scattering of electromagnetic waves from an infinitesimally thin 2D perfectly conducting strip. This target has dimensions $-F \leq x \leq F$, $y = 0$ and $-\infty < z < \infty$. The strip can be considered as the limiting case of an ellipse with $u = 0$. However, for clarity we will specialize the derivations of the preceding chapter for the strip. Results obtained for the current density on the strip will be compared with results obtained from a high-order Method of Moments (MoM) solution. We will consider both TM, E-polarized, and TE, H-polarized, cases.

6.1 THE TM_z CASE

For this case, as in the previous chapter, the uniform plane wave excitation is given by

$$E_z^{inc} = 2E_0 \sum_{m=0}^{\infty} j^m \begin{bmatrix} Mc_m^{(1)}(kF, u) ce_m(kF, v) ce_m(kF, \phi^{inc}) \\ + Ms_m^{(1)}(kF, u) se_m(kF, v) se_m(kF, \phi^{inc}) \end{bmatrix}. \quad (6.1)$$

Following the procedure used in Chapter 5, we express the scattered field in terms of outgoing cylindrical waves, and apply the boundary condition

$$(E_z^{inc} + E_z^s)|_{u=0} = 0 \quad (6.2)$$

in order to obtain

$$E_z^s = -2E_0 \sum_{m=0}^{\infty} j^m \begin{bmatrix} \frac{Mc_m^{(1)}(kF, 0)}{Mc_m^{(4)}(kF, 0)} ce_m(kF, v) ce_m(kF, \phi^{inc}) Mc_m^{(4)}(kF, u) \\ + \frac{Ms_m^{(1)}(kF, 0)}{Ms_m^{(4)}(kF, 0)} se_m(kF, v) se_m(kF, \phi^{inc}) Ms_m^{(4)}(kF, u) \end{bmatrix}. \quad (6.3)$$

80 6. ELECTROMAGNETIC SCATTERING FROM AN INFINITE CONDUCTING STRIP

The total electric field, $E_z^{tot} = E_z^{inc} + E_z^s$, is then

$$E_z^{tot} = 2E_0 \sum_{m=0}^{\infty} j^m \left[\begin{array}{l} ce_m(q, v) ce_m(q, \phi_0) \left\{ Mc_m^{(1)}(q, u) - \frac{Mc_m^{(1)}(q, 0)}{Mc_m^{(4)}(q, 0)} Mc_m^{(4)}(q, u) \right\} \\ + se_m(q, v) se_m(q, \phi_0) \left\{ Ms_m^{(1)}(q, u) - \frac{Ms_m^{(1)}(q, 0)}{Ms_m^{(4)}(q, 0)} Ms_m^{(4)}(q, u) \right\} \end{array} \right]. \quad (6.4)$$

To obtain the total magnetic field, we use Equation (5.10),

$$\bar{H} = \frac{j}{k\eta} \nabla \times \bar{E} = \frac{j}{k\eta F} \frac{1}{(\cosh^2 u - \cos^2 v)^{1/2}} \left(\hat{u} \frac{\partial E_z}{\partial v} - \hat{v} \frac{\partial E_z}{\partial u} \right). \quad (6.5)$$

The current density is given by $\bar{J} = \hat{n} \times \bar{H} = \hat{u} \times \bar{H}$, or

$$\bar{J} = -\hat{z} \left\{ \frac{j}{k\eta F} \frac{1}{(\cosh^2 u - \cos^2 v)^{1/2}} \frac{\partial E_z^{tot}}{\partial u} \right\}_{u=0}, \quad (6.6)$$

where

$$\frac{\partial E_z^{tot}}{\partial u} = 2E_0 \sum_{m=0}^{\infty} j^m \left[\begin{array}{l} ce_m(q, v) ce_m(q, \phi_0) \left\{ \frac{\partial}{\partial u} Mc_m^{(1)}(q, u) - \frac{Mc_m^{(1)}(q, 0)}{Mc_m^{(4)}(q, 0)} \frac{\partial}{\partial u} Mc_m^{(4)}(q, u) \right\} \\ + se_m(q, v) se_m(q, \phi_0) \left\{ \frac{\partial}{\partial u} Ms_m^{(1)}(q, u) - \frac{Ms_m^{(1)}(q, 0)}{Ms_m^{(4)}(q, 0)} \frac{\partial}{\partial u} Ms_m^{(4)}(q, u) \right\} \end{array} \right]. \quad (6.7)$$

The current density on the strip ($u = 0$) is therefore

$$J_z = 2E_0 \frac{-j}{k\eta F} \frac{1}{(1 - \cos^2 v)^{1/2}} \sum_{m=0}^{\infty} j^m \left[\begin{array}{l} \frac{ce_m(q, v) ce_m(q, \phi_0)}{Mc_m^{(4)}(q, 0)} \left\{ \begin{array}{l} Mc_m^{(4)}(q, 0) \frac{\partial}{\partial u} Mc_m^{(1)}(q, u) \Big|_{u=0} \\ -Mc_m^{(1)}(q, 0) \frac{\partial}{\partial u} Mc_m^{(1)}(q, u) \Big|_{u=0} \end{array} \right\} \\ + \frac{se_m(q, v) se_m(q, \phi_0)}{Ms_m^{(4)}(q, 0)} \left\{ \begin{array}{l} Ms_m^{(4)}(q, 0) \frac{\partial}{\partial u} Ms_m^{(1)}(q, u) \Big|_{u=0} \\ -Ms_m^{(1)}(q, 0) \frac{\partial}{\partial u} Ms_m^{(1)}(q, u) \Big|_{u=0} \end{array} \right\} \end{array} \right]. \quad (6.8)$$

Using the Wronskian relations from Equations (5.14) and (5.15) to simplify the expression in brackets, we obtain

$$J_z = \frac{4E_0}{\pi k \eta F} \frac{1}{(1 - \cos^2 v)^{1/2}} \left\{ \sum_{m=0}^{\infty} j^m \left[\frac{ce_m(q, v) ce_m(q, \phi_0)}{Mc_m^{(4)}(q, 0)} + \frac{se_m(q, v) se_m(q, \phi_0)}{Ms_m^{(4)}(q, 0)} \right] \right\}. \quad (6.9)$$

Therefore,

$$\begin{aligned} \eta J_z &= \frac{4E_0}{\pi k F} \frac{1}{(1 - \cos^2 v)^{1/2}} \left\{ \sum_{m=0}^{\infty} j^m \left[\frac{ce_m(q, v) ce_m(q, \phi_0)}{Mc_m^{(4)}(q, 0)} + \frac{se_m(q, v) se_m(q, \phi_0)}{Ms_m^{(4)}(q, 0)} \right] \right\} \\ &= \frac{2}{\pi} \frac{E_0}{\sqrt{q}} \frac{1}{(1 - \cos^2 v)^{1/2}} \left\{ \sum_{m=0}^{\infty} j^m \left[\frac{ce_m(q, v) ce_m(q, \phi_0)}{Mc_m^{(4)}(q, 0)} + \frac{se_m(q, v) se_m(q, \phi_0)}{Ms_m^{(4)}(q, 0)} \right] \right\}. \end{aligned} \quad (6.10)$$

This expression gives the current density as a function of v , where v ranges from 0 to π on one side of the strip and from π to 2π on the other. For comparison with MoM results (below), current on both sides of the strip is superimposed. We note that, as expected, (6.10) is the limiting case of the current density in equation (5.18) as $u \rightarrow 0$.

82 6. ELECTROMAGNETIC SCATTERING FROM AN INFINITE CONDUCTING STRIP

6.2 THE TE_z CASE

For the TE polarization, the incident plane wave has a magnetic field

$$H_z^{inc} = 2H_0 \sum_{m=0}^{\infty} j^m \begin{bmatrix} Mc_m^{(1)}(kF, u) ce_m(kF, v) ce_m(kF, \phi^{inc}) \\ + Ms_m^{(1)}(kF, u) se_m(kF, v) se_m(kF, \phi^{inc}) \end{bmatrix}. \quad (6.11)$$

Following a similar process used in the TM case, we express the scattered magnetic field in terms of outward propagating elliptic-cylinder waves, and impose the boundary condition

$$(E_v^{inc} + E_v^s)|_{u=0} = 0 \quad (6.12)$$

which is equivalent to

$$\left(\frac{\partial H_z^{inc}}{\partial u} + \frac{\partial H_z^s}{\partial u} \right) \Big|_{u=0} = 0 \quad (6.13)$$

in order to obtain the scattered magnetic field

$$H_z^s = -2H_0 \sum_{m=0}^{\infty} j^m \left[\begin{array}{l} \frac{\partial}{\partial u} Mc_m^{(1)}(q, u) \Big|_{u=0} ce_m(q, v) ce_m(q, \phi^{inc}) Mc_m^{(4)}(q, u) \\ \frac{\partial}{\partial u} Mc_m^{(4)}(q, u) \Big|_{u=0} \\ + \frac{\partial}{\partial u} Ms_m^{(1)}(q, u) \Big|_{u=0} se_m(q, v) se_m(q, \phi^{inc}) Ms_m^{(4)}(q, u) \\ \frac{\partial}{\partial u} Ms_m^{(4)}(q, u) \Big|_{u=0} \end{array} \right]. \quad (6.14)$$

The surface current density is $\bar{J} = \hat{n} \times \bar{H}^{tot} = \hat{u} \times (\bar{H}^i + \bar{H}^s)$, or

$$J_v = -2H_0 \sum_{m=0}^{\infty} j^m \left\{ \begin{array}{l} \left[Mc_m^{(1)}(q, u) - Mc_m^{(4)}(q, u) \frac{\frac{\partial}{\partial u} Mc^{(1)}(q, u) \Big|_{u=u_0}}{\frac{\partial}{\partial u} Mc^{(4)}(q, u) \Big|_{u=u_0}} \right] ce_m(q, v) ce_m(q, \phi^{inc}) \\ + \left[Ms_m^{(1)}(q, u) - Ms_m^{(4)}(q, u) \frac{\frac{\partial}{\partial u} Ms^{(1)}(q, u) \Big|_{u=u_0}}{\frac{\partial}{\partial u} Ms^{(4)}(q, u) \Big|_{u=u_0}} \right] se_m(q, v) se_m(q, \phi^{inc}) \end{array} \right\}_{u=0}. \quad (6.15)$$

Using the Wronskian relations from Equations (5.14) and (5.15), we obtain

$$J_v = \frac{4}{\pi} H_0 \sum_{m=0}^{\infty} j^{m+1} \left\{ \frac{ce_m(kF, v) ce_m(kF, \phi^{inc})}{\frac{\partial}{\partial u} Mc_m^{(4)}(c, u) \Big|_{u=0}} + \frac{se_m(kF, v) se_m(kF, \phi^{inc})}{\frac{\partial}{\partial u} Ms_m^{(4)}(c, u) \Big|_{u=0}} \right\}. \quad (6.16)$$

Note that v ranges from 0 to π on one side of the strip and from π to 2π on the other. For comparison with MoM results (below), we use the difference of current on both sides of the strip (since the direction \hat{v} changes). As expected, (6.16) is the limiting case of the current density in equation (5.28) as $u \rightarrow 0$.

6.3 RESULTS

The preceding expressions for current density were implemented in quad precision arithmetic, although the results in the tables below are reported in double precision. Since one application of the boundary value analysis of strip scattering is to validate computational techniques, we illustrate that by comparing the results obtained from (6.10) and (6.16) to numerical results for currents calculated using high-order MoM techniques [45, 46]. A similar comparison was carried out for the Locally Corrected Nystrom method [47] as reported in [48]. The use of high-order basis function is expected to provide high accuracy and expressions developed in Sections 6.1 and 6.2 were used to obtain reference values to verify that, in fact, accuracy improves as the order of the basis function increases.

Figures 6.1 and 6.2 show the error in the MoM results obtained when high-order basis functions are used to model the current density on the strip, including special terms to correctly model the currents in the end regions. The current density was sampled at 48 points located at the nodes of a 48 point Gauss-Legendre integration rule. This sampling scheme has the advantage of clustering the sampling points towards the ends of the strip. The sampling points closest to the ends are within approximately 0.002 wavelengths of those ends. As can be seen in the figures, the MoM results approach those of the Mathieu function summations. As the basis order increases, the MoM results approach double precision accuracy. In these figures, it should be noted that the parameter q is the order of the basis function as defined in [45, 46], and not the elliptic-cylinder parameter.

The following tables provide numerical values for the magnitude and phase of the current density for four strips of different width. The independent variable is v spanning the strip from the center to a point close to one end. The sampling points are taken from the Chebyshev rule [49, p. 328] and are given by

$$v_j = \frac{(2j - 1)}{2N_c} \pi \quad j = 1, 2, \dots, N_c. \quad (6.17)$$

With $N_c = 39$, due to symmetry, only the 20 largest values are used and the equivalent positions in the Cartesian system are derived from $x_j = |F * \cos(v_j)|$ using Eq. (2.1). The sampling points

84 6. ELECTROMAGNETIC SCATTERING FROM AN INFINITE CONDUCTING STRIP

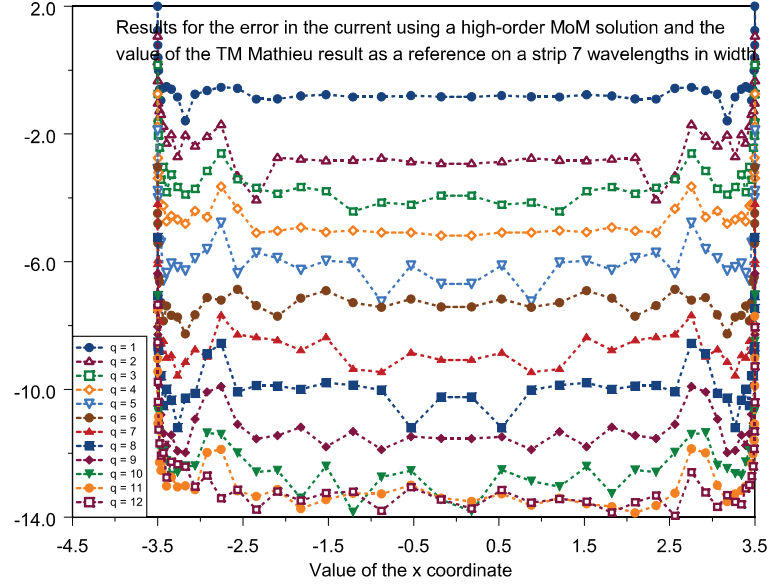


Figure 6.1: Error in the MoM current density induced on an infinite strip of width 7 wavelengths by a TM plane wave.

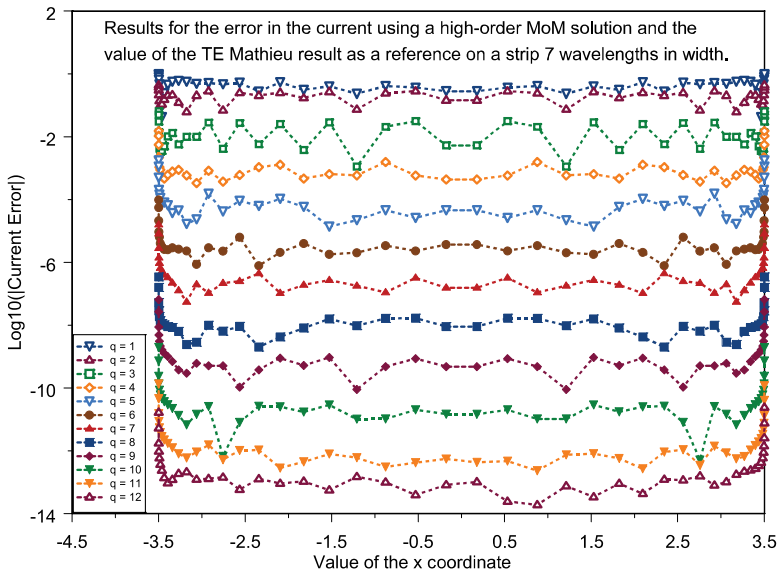


Figure 6.2: Error in the MoM current density induced on an infinite strip of width 7 wavelengths by a TE plane wave.

for a strip width of one wavelength, centered on the origin, are shown in Table 6.1. This particular set of sampling points was selected to emphasize the values closest to an edge.

Table 6.1: Locations of the sampling points used in Tables 6.2 and 6.3

Node ID	ν	x
1	1.5707963267948900	0.0000000000000000
2	1.6971929173649100	0.0630301526267871
3	1.8227697775427300	0.1246577885992210
4	1.9467124932022700	0.1835624375371920
5	2.0682172482717500	0.2385802961460580
6	2.1864960377893500	0.2887649431807000
7	2.3007817784177200	0.3334293969274290
8	2.4103332832738400	0.3721669879078250
9	2.5144400688103600	0.4048508850732060
10	2.6124269625740000	0.4316142705932680
11	2.7036584819580500	0.4528148249222940
12	2.7875429555508700	0.4689881905967020
13	2.8635363603521100	0.4807953884421220
14	2.9311458499705600	0.4889688382328380
15	2.9899329509221300	0.4942608466711500
16	3.0395164062987100	0.4973973709667340
17	3.0795746483654200	0.4990387499155710
18	3.1098478840508600	0.4997480885576970
19	3.1301397798048100	0.4999672082789540
20	3.1403187348966700	0.4999995942828450

Tables 6.2, 6.3, 6.4, and 6.5 report values of the current density produced at 20 sample points on a 1.0, 2.0, 4.0, and 8.0 wavelength strip, respectively, by a normally incident TM_z plane wave with $E_0 = \eta$. The sample locations are defined in Table 6.1 for the 1.0 wavelength strip; they must be scaled by 2.0, 4.0, etc., for the larger strips. To facilitate comparisons with numerical techniques such as the MoM, we report the superposition of the currents on the two sides of the strip.

86 6. ELECTROMAGNETIC SCATTERING FROM AN INFINITE CONDUCTING STRIP

Table 6.2: Current density on a 1.0 wavelength strip excited by a normally incident TM_z plane wave. These values are the superposition of the current on the two sides of the strip

Node ID	$ J_z $	Phase (deg.)
1	1.7235009252399800	50.0859314635982000
2	1.6804492306020400	49.5735731631666000
3	1.5594090690369000	48.0476752052331000
4	1.3817892572130500	45.5460610698130000
5	1.1750550548533700	42.1447471425348000
6	0.9647895231529680	37.9715020939194000
7	0.7693366392789140	33.2098538393032000
8	0.5983032378753800	28.0760170671334000
9	0.4541328168996400	22.7514587476012000
10	0.3349959140665740	17.2576597153108000
11	0.2374813154708870	11.2349264938137000
12	0.1584687057519590	3.4325712890034600
13	0.0966737788061317	-9.9414992570227100
14	0.0565179261975804	-40.1296149832822000
15	0.0523367844697975	-88.6923222345034000
16	0.0729913309117108	-115.8412738388580000
17	0.0956119156097400	-126.4241112660660000
18	0.1137415368934450	-130.9567936413030000
19	0.1260418512135940	-132.9845914790510000
20	0.1322201358821980	-133.7749697707440000

Table 6.3: Current density on a 2.0 wavelength strip excited by a normally incident TM_z plane wave. These values are the superposition of the current on the two sides of the strip

Node ID	$ J_z $	Phase (deg.)
1	1.8517443832068500	63.7501785788727000
2	1.7646559336821000	60.3545981809933000
3	1.5534060169993700	50.3093747599976000
4	1.3197694407472100	34.7596394272032000
5	1.1239450849029100	16.7312848029917000
6	0.9566050478872120	-0.4672279632709250
7	0.7936335256372850	-15.4772203392813000
8	0.6332054292852300	-28.4737631624107000
9	0.4865634723970500	-39.8986552891100000
10	0.3623040986271330	-49.9566024159030000
11	0.2619567632609190	-58.6832970785044000
12	0.1825786030774880	-66.2336625915359000
13	0.1201266334877130	-73.2933473536014000
14	0.0713665126216949	-82.0507712768213000
15	0.0352423428344407	-101.0335586010890000
16	0.0200643378213044	-161.4156445488160000
17	0.0322236989851532	152.9208370722770000
18	0.0467182389596011	140.9132890988260000
19	0.0568656973954944	137.0130297920910000
20	0.0619715038630708	135.7340051016180000

Table 6.4: Current density on a 4.0 wavelength strip excited by a normally incident TM_z plane wave. These values are the superposition of the current on the two sides of the strip

Node ID	$ J_z $	Phase (deg.)
1	1.6050166269532200	65.1404703955063000
2	1.6597616783619900	60.2109130948130000
3	1.6445770810768900	44.2189346342876000
4	1.4537174356759800	15.1938504855435000
5	1.2498602382072300	-21.8166038601597000
6	1.0201140006489300	-58.4197964508406000
7	0.7627174767246380	-95.7605758227045000
8	0.5765128955722690	-133.8969610043950000
9	0.4562692238070680	-166.4719973378250000
10	0.3538409601857540	168.7123996936480000
11	0.2612668513538560	149.7038510747290000
12	0.1847816337918960	134.9512322166810000
13	0.1254963217487430	123.7495246824500000
14	0.0804815339262072	115.3909318174860000
15	0.0464326888397868	108.2345609447810000
16	0.0211594875432111	96.5139097164368000
17	0.0069747109979247	32.1924421229422000
18	0.0146294312136675	-34.7120625898713000
19	0.0227135538601500	-44.1427099367547000
20	0.0268174037994018	-46.2667122185920000

Table 6.5: Current density on an 8.0 wavelength strip excited by a normally incident TM_z plane wave. These values are the superposition of the current on the two sides of the strip

Node ID	$ J_z $	Phase (deg.)
1	1.6438512163213300	66.2049500115483000
2	1.6896734589131700	55.5681949979413000
3	1.5411115941124000	20.3722070089665000
4	1.4170696689987100	-29.0071117578070000
5	1.3064026749627000	-97.9183300446460000
6	1.0698260773653200	-176.9969883167740000
7	0.8358150113004000	102.5213439693800000
8	0.6042347254573040	24.1450468224097000
9	0.4450193211907230	-43.5739968736859000
10	0.3081991397742730	-103.6168012331960000
11	0.2316584724539150	-153.3938199546470000
12	0.1721265494050860	172.1466011074750000
13	0.1193907809643640	148.3113541714390000
14	0.0783203955467514	131.8961741985620000
15	0.0482524672369906	121.4067550424880000
16	0.0264793849446619	115.0733349051070000
17	0.0109125883163450	108.7384681926920000
18	0.0016406677419598	26.8375293165615000
19	0.0070569226495696	-47.2071679391186000
20	0.0103013110545637	-50.5915192675772000

Table 6.6: Current density on a 1.0 wavelength strip excited by a normally incident TE_z plane wave. Shown are the superposition of the currents on the two sides, or the difference of the J_v values

Node ID	$ J_v $	Phase (deg.)
1	2.9818074723771900	168.9482962593600000
2	2.9108191062471200	170.0142694195530000
3	2.7159540635712900	173.2154135271640000
4	2.4436636237862700	178.5105754747000000
5	2.1491974072900300	-174.3272735480970000
6	1.8752652318784100	-165.8669708959130000
7	1.6398864225569700	-157.0090115684510000
8	1.4390338595666100	-148.7014982572100000
9	1.2591825827675100	-141.5924548645980000
10	1.0887708269785200	-135.9155444723980000
11	0.9226044867147780	-131.6061401663680000
12	0.7609165169425950	-128.4642146381400000
13	0.6068330789627420	-126.2602685420010000
14	0.4643158269083950	-124.7815805034890000
15	0.3370127489822420	-123.8452446122090000
16	0.2277993517725910	-123.2982011526010000
17	0.1387130644236080	-123.0142890692170000
18	0.0710709702543328	-122.8920971769360000
19	0.0256486489968100	-122.8544127541580000
20	0.0028530602271006	-122.8488454416780000

Table 6.7: Current density on a 2.0 wavelength strip excited by a normally incident TE_z plane wave. Shown are the superposition of the currents on the two sides, or the difference of the J_v values

Node ID	$ J_v $	Phase (deg.)
1	1.4273050253085100	-160.0091005291950000
2	1.5493502706937900	-168.3756924768260000
3	1.9518808006162500	177.4027160168320000
4	2.4558889483070800	169.6667492197620000
5	2.7614750041273200	168.8513409730140000
6	2.7598967385222600	172.8877712790550000
7	2.5336701360623000	-179.6084501005340000
8	2.2214437417282900	-169.9018267529440000
9	1.9145944519682100	-159.5525601223960000
10	1.6382189141253100	-150.0690471845880000
11	1.3844392913717700	-142.3368555352400000
12	1.1438095104809600	-136.5352735748940000
13	0.9149324951344790	-132.4384283089360000
14	0.7019346230998110	-129.6957742225420000
15	0.5104530579350610	-127.9666545676800000
16	0.3454363668650080	-126.9602772229360000
17	0.2104750631148560	-126.4392771942060000
18	0.1078677441862950	-126.2153406802860000
19	0.0389313742084080	-126.1463147892460000
20	0.0043306340316296	-126.1361187348680000

Table 6.8: Current density on a 4.0 wavelength strip excited by a normally incident TE_z plane wave. Shown are the superposition of the currents on the two sides, or the difference of the J_v values

Node ID	$ J_v $	Phase (deg.)
1	1.5859345059219600	-166.0219294150960000
2	1.9847873624601800	178.9600946884530000
3	2.5036068917634000	171.0190390788080000
4	2.1158852865711400	-178.4298349884870000
5	1.5942007211031700	-164.2009340299340000
6	1.5988303615333700	-176.7756359702850000
7	2.2122836788062000	168.8204346898930000
8	2.6768365958165400	169.4516983101170000
9	2.6641419284200200	177.8244315694770000
10	2.3746614324675700	-170.4135829265470000
11	2.0196417617871400	-158.3303545051730000
12	1.6733630263913600	-148.0906882003600000
13	1.3444326070141500	-140.4846272024620000
14	1.0358322116626200	-135.3210054267940000
15	0.7555393308933030	-132.0662510240480000
16	0.5122073471035450	-130.1788294765010000
17	0.3123749973626900	-129.2047943293380000
18	0.1601534445820930	-128.7868968662800000
19	0.0578091035704827	-128.6581836133670000
20	0.0064306611527084	-128.6391749761460000

Table 6.9: Current density on an 8.0 wavelength strip excited by a normally incident TE_z plane wave. Shown are the superposition of the currents on the two sides, or the difference of the J_v values

Node ID	$ J_v $	Phase (deg.)
1	1.7016719628186400	-170.2777971979860000
2	2.3429812286758200	172.9330484187320000
3	1.6952567632947900	-170.0007821863310000
4	2.3451704593830100	172.4274822254820000
5	1.7680504708972100	-169.7614660362610000
6	2.0630293163197400	173.3777490902450000
7	2.3118590649988500	179.2221673472150000
8	1.6242640934144000	-165.7786717749020000
9	1.7948307018335900	172.3586753598650000
10	2.5401574129353600	168.3004306415300000
11	2.6603594481565900	179.3549033993200000
12	2.3467261172932500	-165.9936397149870000
13	1.9237557146704100	-152.8337100616950000
14	1.4977636398369700	-143.1972717848840000
15	1.0992191818571400	-136.9963635742160000
16	0.7475989243607660	-133.3963063719090000
17	0.4566034377645470	-131.5439064029460000
18	0.2342349421815560	-130.7510004082880000
19	0.0845641683672032	-130.5070442960360000
20	0.0094071200601172	-130.4710273003890000

94 6. ELECTROMAGNETIC SCATTERING FROM AN INFINITE CONDUCTING STRIP

Shown in Tables 6.6, 6.7, 6.8, and 6.9 are the values of current density calculated at 20 nodes on a 1.0, 2.0, 4.0, and 8.0 wavelength strip, respectively, for a normally incident TE_z plane wave with $H_0 = 1.0$. The sample locations are defined in Table 6.1 for the 1.0 wavelength strip; they must be scaled by 2.0, 4.0, etc., for the larger strips. To facilitate comparison with numerical techniques such as the MoM, we report the superposition of the current on the two sides. This is actually the difference of the J_v components since the vector \hat{v} changes direction on the opposite side.

6.4 SUMMARY

Expressions for the total current density induced by an electromagnetic plane wave on an infinite flat perfectly conducting strip have been derived in terms of the Mathieu functions. These results are accurate and therefore provide an excellent reference solution with which to compare other methods. The comparison between the MoM results and the Mathieu summations in Figures 6.1 and 6.2 is excellent, confirming the quality of both solutions. Tables of reference values for the current density are provided for strips of four different widths.

APPENDIX A

Converting Between Two Common Mathieu Function Conventions

There are several sets of nomenclatures used to denote Mathieu functions. Chief among these are the Goldstein-Ince convention and the Stratton convention. Chapters 2–6 follow the Goldstein-Ince convention, which uses ce and se for the angular functions and uses Mc and Ms for the radial functions. The Stratton convention employs Se and So for the angular functions and employs Re and Ro for the radial functions.

It is sometimes necessary to be able to convert from one convention to the other. First, under the Goldstein-Ince convention, the angular functions are normalized so that

$$\int_0^{2\pi} ce_m^2(c, v) dv = \int_0^{2\pi} se_m^2(c, v) dv = \pi. \quad (\text{A.1})$$

Under the Stratton convention, normalization factors are defined as:

$$Ne_m(c) = \int_0^{2\pi} Se_m(c, v) Se_m(c, v) dv \quad (\text{A.2})$$

$$No_m(c) = \int_0^{2\pi} So_m(c, v) So_m(c, v) dv. \quad (\text{A.3})$$

The two sets of functions are related by the conversions, as indicated by Erricolo [37]

$$Se_m(c, v) = \frac{ce_m(c, v)}{ce_m(c, 0)}; \quad So_m(c, v) = \frac{se_m(c, v)}{\left. \frac{d}{dv} se_m(c, v) \right|_{v=0}} \quad (\text{A.4})$$

$$Re_m^{(1,2)}(c, u) = \sqrt{\frac{\pi}{2}} Mc_m^{(1,2)}(c, u) \quad Ro_m^{(1,2)}(c, u) = \sqrt{\frac{\pi}{2}} Ms_m^{(1,2)}(c, u). \quad (\text{A.5})$$

96 A. CONVERTING BETWEEN TWO COMMON MATHIEU FUNCTION CONVENTIONS

Furthermore, the normalization factors are related by

$$\begin{aligned} Ne_m(c) &= \int_0^{2\pi} [Se_m(c, v)]^2 dv = \int_0^{2\pi} \left[\frac{ce_m(c, v)}{ce_m(c, 0)} \right]^2 dv \\ &= \frac{1}{[ce_m(c, 0)]^2} \int_0^{2\pi} [ce_m(c, v)]^2 dv = \frac{\pi}{[ce_m(c, 0)]^2} \end{aligned} \quad (\text{A.6})$$

$$\begin{aligned} No_m(c) &= \int_0^{2\pi} [So_m(c, v)]^2 dv = \int_0^{2\pi} \left[\frac{se_m(c, v)}{\left. \frac{d}{dv} se_m(c, v) \right|_{v=0}} \right]^2 dv \\ &= \frac{1}{\left[\left. \frac{d}{dv} se_m(c, v) \right|_{v=0} \right]^2} \int_0^{2\pi} [se_m(c, v)]^2 dv = \frac{\pi}{\left[\left. \frac{d}{dv} se_m(c, v) \right|_{v=0} \right]^2}. \end{aligned} \quad (\text{A.7})$$

APPENDIX B

Tables of Select Eigenvalues and Eigenvectors

This appendix provides a sampling of solutions to the basic eigenvalue equations identified in Chapter 2. Some of the eigenvalues and eigenvectors are documented for the matrices shown in Equations (2.16a)–(2.16d) for values of $q = 10.0$ and $q = 100.0$. The size of the underlying matrices is 20×20 . The values shown here are largely independent of the choice of matrix size. These tables are included to assist others in developing software for computing Mathieu functions.

Table B.1: The first five eigenvalues and a portion of their corresponding eigenvectors for ce_{2r} from Equation (2.16a) with $N = 20$ and $q = 10$

Eigenvalues						
Eigenvectors						
1	-1.39369799566589E+01	2	7.71736984977962E+00	3	2.110463370865778E+01	4
1	4.87775355587567E-01	1	4.09509568956169E-01	1	3.04235058341570E-01	1
2	-6.79811535417610E-01	2	3.160333680065859E-01	2	6.42076946763998E-01	2
3	2.43825877333986E-01	3	-7.01537730533166E-01	3	4.89778982032475E-01	3
4	-5.01295048486223E-02	4	2.65024075777259E-01	4	-3.92062716615591E-01	4
5	6.50573055230306E-03	5	-4.80200610780535E-02	5	9.42127952843176E-02	5
6	-5.74194317204345E-04	6	5.24545796744910E-03	6	-1.206665196896136E-02	6
7	3.64660857508352E-05	7	-3.86404679809705E-04	7	9.86453793058514E-04	7
8	-1.74007560949628E-06	8	2.056663923293380E-05	8	-5.65403331273514E-05	8
9	6.45330845540242E-08	9	-8.29413003123892E-07	9	2.41043419575046E-06	9
10	-1.91098568381275E-09	10	2.62449956701197E-08	10	-7.964492058467981E-08	10

Table B.2: The first five eigenvalues and a portion of their corresponding eigenvectors for ce_{2r} from Equation (2.16a) with $N = 20$ and $q = 100$

Eigenvalues						
Eigenvectors						
1	-1.80253249152251E+02	2	-1.03370507064967E+02	3	-3.09501040006232E+01	4
1	3.58103803200266E-01	1	2.62396602675935E-01	1	2.37328698351105E-01	1
2	-6.4549374066265E-01	2	-2.712404698707361E-01	2	-7.34534792724934E-02	2
3	4.73135583740915E-01	3	-2.33560691783216E-01	3	-4.438985331304397E-01	3
4	-2.83050215380752E-01	4	5.50043280793431E-01	4	2.84452559267450E-01	4
5	1.38969703752407E-01	5	-5.33037417735370E-01	5	2.588677947250466E-01	5
6	-5.63878013771594E-02	6	3.42104448116265E-01	6	-5.29867539208388E-01	6
7	1.90589417174669E-02	7	-1.62701322978964E-01	7	4.35184146408521E-01	7
8	-5.41143640116097E-03	8	6.03714342792225E-02	8	-2.31487577527544E-01	8
9	1.30176356770894E-03	9	-1.80327459451381E-02	9	9.01771515387642E-02	9
10	-2.67549459249577E-04	10	4.43293626155777E-03	10	-2.72158525977394E-02	10

Table B.3: The first five eigenvalues and a portion of their corresponding eigenvectors for ce_{2r+1} from Equation (2.16b) with $N = 20$ and $q = 10$

Eigenvalues									
Eigenvectors									
1	-1.399142400036260E+00	2	1.550278436973260E+01	3	2.77037687339380E+01	4	5.006267154731230E+01	5	8.162833115873910E+01
1	5.693674529505960E-01	1	7.552688374953210E-01	1	3.2361960500538310E-01	1	2.566715956421520E-02	1	1.076291220284650E-03
2	-7.629035580030990E-01	2	3.400812941555240E-01	2	5.405667040755000E-01	2	1.002627823609400E-01	2	7.6016656272950810E-03
3	3.002771765685680E-01	3	-5.341213550877640E-01	3	6.874435567657630E-01	3	3.860386104864770E-01	3	5.41333505989110E-02
4	-5.983015401972550E-02	4	1.671852740439890E-01	4	3.546977834493100E-01	4	8.672531075594040E-01	4	2.989463771768990E-01
5	7.244684061029380E-03	5	-2.590276239791990E-02	5	6.792874582379960E-02	5	-2.938780903143180E-01	5	9.21278842634270E-01
6	-5.898897451807500E-04	6	2.470607375625800E-03	6	-7.336831254558720E-03	6	4.192719295086330E-02	6	2.410595593164420E-01
7	3.450480555866660E-05	7	-1.614575064926070E-04	7	5.2112477247377100E-04	7	-3.542215431142100E-03	7	2.781290977929880E-02
8	1.519662962795560E-06	8	7.720393962889800E-06	8	9.2.646470794145520E-05	8	2.029710675294170E-04	8	1.946474958434960E-03
9	5.219988901436690E-08	9	-2.825834217227580E-07	9	1.0139891028899130E-06	9	-8.506199536526050E-06	9	9.40265355566300E-05
10	-1.437326420801750E-09	10	8.1846061549999170E-09	10	-3.0445171784439000E-08	10	2.737917248851320E-07	10	-3.369000919031160E-06

Table B.4: The first five eigenvalues and a portion of their corresponding eigenvectors for ce_{2r+1} from Equation (2.16b) with $N = 20$ and $q = 100$

Eigenvalues									
Eigenvectors									
1	-1.4128000568086200E+02	2	6.657438996748530E+01	3	3.432562047992840E+00	4	6.810880736142380E+01	5	1.263959061006850E+02
1	2.281492422096010E-01	1	2.865733718537960E-01	1	3.313464494439670E-01	1	3.756361874284940E-01	1	1.4323412148902340E-01
2	-5.527601136338580E-01	2	-4.802235796932520E-01	2	-3.232862414674200E-01	2	-1.235512220273090E-01	2	1.097969689680830E-01
3	6.025389705747520E-01	3	7.635266897940030E-02	3	-3.133473885428920E-01	3	4.486658412493010E-01	3	-3.034440682990650E-01
4	-4.491420288319150E-01	4	4.103040888514730E-01	4	3.908673097679580E-01	4	-6.986327117336380E-02	4	-4.174768315287010E-01
5	5.25038737282830E-01	5	-5.505591166811380E-01	5	1.352394696896990E-01	5	4.353158033443940E-01	5	-1.986590422300240E-02
6	-1.12009593872450E-01	6	4.021801690010930E-01	6	-4.957691015061380E-01	6	1.374387237807250E-02	6	4.085493142979400E-01
7	3.956920222431430E-02	7	-2.038278818928630E-01	7	4.476235611087530E-01	7	-4.425661591837330E-01	7	4.171084559751040E-02
8	-1.1574383753077380E-02	8	7.798612035166650E-02	8	-2.453497602911630E-01	8	4.32784582076630E-01	8	-4.263198421225010E-01
9	2.825457161692540E-03	9	-2.355967278181730E-02	9	9.599161678976630E-02	9	2.364147331906530E-01	9	3.786579718403730E-01
10	-5.829949273605470E-04	10	5.786042420615820E-03	10	2.877104042408190E-02	10	8.943474164247760E-02	10	-1.893935219660620E-01

Table B.5: The first five eigenvalues and a portion of their corresponding eigenvectors for se_{2r+2} from Equation (2.16c) with $N = 20$ and $q = 10$

Eigenvalues					
Eigenvectors					
1 -2.382158235956960E+00	2	1.7381380677862300E+01	3	3.741985877672420E+01	4
1	8.339073559756880E-01	1	5.354554494777520E-01	1	1.332191982284660E-01
2	-5.322128699965330E-01	2	7.165133205905010E-01	2	4.452166791143760E-01
3	1.444147631732170E-01	3	-4.364776637737770E-01	3	8.204286409387400E-01
4	-2.208215917573390E-02	4	9.614786305552880E-02	4	3.287273984630990E-01
5	2.171375286298970E-03	5	-1.1750373886118130E-02	5	5.333342657218290E-02
6	-1.488496394168720E-04	6	9.321447458610760E-04	6	-5.033938217742600E-03
7	7.517860749603220E-06	7	-5.230921167914540E-05	7	3.183580434422170E-04
8	-2.913046654945440E-07	8	2.195170330793340E-06	8	-1.458813112065450E-05
9	8.932067365169500E-09	9	-7.165398364872000E-08	9	5.09532611416110E-07
10	-2.220932398614110E-10	10	1.83776650678470E-09	10	-1.406165309626140E-08

Table B.6: The first five eigenvalues and a portion of their corresponding eigenvectors for se_{2r+2} from Equation (2.16c) with $N = 20$ and $q = 100$

Eigenvalues					
Eigenvectors					
1 -1.412800568086190E+02	2	-6.657438996584240E-01	3	3.43253359324830E+00	4
1	4.211137875976560E-01	1	4.672263714304420E-01	1	4.633282356611140E-01
2	-6.117943498508040E-01	2	-3.297421613965750E-01	2	-2.629094175735050E-03
3	5.41116713396120E-01	3	-1.949437931970370E-01	3	-4.629978559163550E-01
4	-3.474976670649630E-01	4	5.297045680447090E-01	4	1.534-156177787480E-01
5	1.722266949599710E-01	5	-4.967147151485420E-01	5	3.700779188213120E-01
6	-6.805100037406370E-02	6	2.976949385845470E-01	6	-5.107903775576470E-01
7	2.190923756599170E-02	7	-1.301545857350560E-01	7	3.47927021518700E-01
8	-5.844488534848500E-03	8	4.405767092184660E-02	8	-1.592037991611630E-01
9	1.309749805427750E-03	9	-1.196417747424880E-02	9	5.416985728698730E-02
10	-2.495161038963310E-04	10	2.671342262631670E-03	10	-1.444715377564410E-02

Table B.7: The first five eigenvalues and a portion of their corresponding eigenvectors for se_{2r+1} from Equation (2.16d) with $N = 20$ and $q = 10$

Eigenvalues									
Eigenvectors									
1	-1.393655247925010E+01	2	7.9886069144681660E-00	3	2.676642636048010E+01	4	5.005415721355730E+01	5	8.162831318438320E+01
1	8.902865333150730E-01	1	4.3223950133466190E-01	1	1.419460131170340E-01	1	1.658531110458350E-02	1	8.350135653358070E-04
2	-4.3946946193279490E-01	2	7.344691594521210E-01	2	5.078901625314140E-01	2	9.7943156940568350E-02	2	7.567587091246190E-03
3	1.177626067412810E-01	3	-5.068651076514420E-01	3	7.600379755384180E-01	3	3.8951206519984990E-01	3	5.412704965697650E-02
4	-1.903237241956970E-02	4	1.279076300033910E-01	4	-3.734350510357180E-01	4	8.67924831980500E-01	4	2.98945021458710E-01
5	2.020583817607050E-03	5	-1.773436163122750E-02	5	7.024159513963390E-02	5	-2.940191429527760E-01	5	9.212808353589570E-01
6	-1.503537443276210E-04	6	1.5777915387175780E-03	6	-7.510221220550860E-03	6	4.194218542207580E-02	6	-2.410597791564580E-01
7	8.237773584551160E-06	7	-9.8280414949842010E-05	7	5.290033039526250E-04	7	-3.54322654666460E-03	7	2.781293934790100E-02
8	-3.452456386208920E-07	8	4.536206518507600E-06	8	-2.678283980621580E-05	8	2.030190718179700E-04	8	-1.946476082510730E-03
9	1.140668050614720E-08	9	-1.615658288651950E-07	9	1.022502729805360E-06	9	-8.507907425169990E-06	9	9.402658168079570E-05
10	-3.044081555592710E-10	10	4.580319281943790E-09	10	-3.061458308668030E-08	10	2.738391876574280E-07	10	-3.369002354568330E-06

Table B.8: The first five eigenvalues and a portion of their corresponding eigenvectors for se_{2r+1} from Equation (2.16d) with $N = 20$ and $q = 100$

Eigenvalues									
Eigenvectors									
1	-1.802532491522510E+02	2	-1.033705070649310E+02	3	-3.0950103947238200E+01	4	3.6488219666573140E+01	5	9.8155153339732680E+01
1	6.978205207831220E-01	1	4.56530096252150E-01	1	3.598836008747810E-01	1	2.918301055879450E-01	1	2.316886980418840E-01
2	-5.670018463874480E-01	2	-1.995267632420080E-02	2	2.449684662022780E-01	2	3.953954145097320E-01	2	4.567862080287450E-01
3	3.752488962583810E-01	3	-4.341090360666360E-01	3	-4.5784875777605460E-01	3	-1.831429454992810E-01	3	1.755597464239760E-01
4	-2.032087055908400E-01	4	5.772207113229450E-01	4	1.119838968588550E-02	4	-4.164352783909800E-01	4	-3.283552062283280E-01
5	9.06136638685230E-02	5	-4.4540503368598880E-01	5	4.488956335662630E-01	5	2.352464127659600E-01	5	-3.369632517336190E-01
6	-3.352243544243630E-02	6	2.439748169470410E-01	6	-5.13737180779300E-01	6	3.117229118963490E-01	6	2.705486435008050E-01
7	1.037376209645310E-02	7	-1.020024952349270E-01	7	3.312190591691130E-01	7	-4.986889953193890E-01	7	2.751568291402470E-01
8	-2.708265738751090E-03	8	3.384989654321110E-02	8	-1.495550805339060E-01	8	3.490987541324510E-01	8	4.654830770219930E-01
9	6.015728055128600E-04	9	-9.156581684970180E-03	9	5.105732496698570E-02	9	-1.594032812204450E-01	9	3.15284465869730E-01
10	-1.146341971343470E-04	10	2.054287213497030E-03	10	-1.380288375064380E-02	10	5.341330918835520E-02	10	-1.362210782291000E-01

APPENDIX C

Tables of Select Angular Mathieu Functions

Tables C.1–C.8 give the first five angular functions evaluated at angles in the range $0 \leq \nu \leq 90$, in degrees. Results are provided for $q = 10.0$ and $q = 100.0$. The size of the underlying matrices is 20×20 . The values shown here are largely independent of the choice of matrix size.

Table C.1: Values of the first five angular function of Equation (2.11) for various angles, in degrees, for $q = 10$

v	0.0	7.626517570935790E-03	2.458883492913190E-01	1.127106792419860E+00	1.1864072003811060E+00	1.089103567783310E+00
10.0	1.189063543600590E-02	2.925157846414380E-01	1.104754243946530E+00	8.802168491596300E-01	4.244568493993130E-01	
20.0	2.882186972818320E-02	4.376637700156760E-01	9.9948159588912870E-01	9.732106774498060E-02	-7.582505628293220E-01	
30.0	7.258175729748430E-02	6.795282254440040E-01	7.202641568205240E-01	-7.291378970239940E-01	-9.149717253257810E-01	
40.0	1.701979278100970E-01	9.5851254333681200E-01	2.140081540501410E-01	-9.662496692333380E-01	2.396983764928230E-01	
50.0	3.570409418056640E-01	1.105781366215340E-00	-3.826646671627700E-01	-2.913364201752550E-01	9.741273714042450E-01	
60.0	6.527102135896200E-01	8.882767248018320E-01	-6.938153224035570E-01	6.799146702637770E-01	1.493492844148340E-02	
70.0	1.0191455338847900E+00	2.2834719796228240E-01	-3.989579184258410E-01	7.631761298710630E-01	-9.375287358564050E-01	
80.0	1.3394453821631240E-00	-5.646040344262210E-01	2.858295803682340E-01	-2.125026435513780E-01	-3.233639981512630E-02	
90.0	1.4686604712850E-00	-9.267592641263200E-01	6.513246115598880E-01	-8.624724253247980E-01	9.253453435714710E-01	

Table C.2: Values of the first five angular function of Equation (2.11) for various angles, in degrees, for $q = 100$

v	0.0	1.162686991129640E-08	1.275240859577300E-06	5.257616222476000E-05	1.246436324533910E-03	1.934714264799800E-02
10.0	1.728196071804070E-07	1.318051722076770E-05	3.693194150368170E-04	5.776453423540160E-03	5.686541091393100E-02	
20.0	4.675492035310920E-06	2.450833357019450E-04	4.5859075333223630E-03	4.591578390740500E-02	2.694451512071850E-01	
30.0	1.040894885103720E-04	3.6665367956109720E-03	4.441842011564180E-02	2.7247674448926830E-01	8.874443438599500E-01	
40.0	1.728100839780690E-03	3.911400616811200E-02	2.872018324498640E-01	9.610764822257860E-01	1.319663626326630E+00	
50.0	1.9569805675353870E-02	2.641143671960120E-01	1.025810322620770E+00	1.336470597798990E+00	-2.619884869823170E-01	
60.0	1.407689289956900E-01	9.8112204801639520E-01	1.394544783098200E+00	-4.698100822183850E-01	-6.118753726517540E-01	
70.0	6.023506246800700E-01	1.578916591556020E+00	-4.591014196359130E-01	-5.010412348894760E-01	8.782209078052860E-01	
80.0	1.467761430695800E+00	1.801527178482310E-01	-7.4112099956419210E-01	9.228771102896180E-01	-9.185865097143820E-01	
90.0	1.981236286456530E+00	-1.371746016885920E+00	1.158447684923180E+00	-1.024810582489000E+00	9.188562461379820E-01	

Table C.3: Values of the first five angular function of Equation (2.12) for various angles, in degrees, for $q = 10$

ν	0.0	5.359874774717620E-02	7.048279338844100E-01	1.258019941308280E+00	1.123923278972790E+00	1.067934097778210E+00
10.0	7.275579178734110E-02	7.514202081098640E-01	1.109610522454420E+00	6.44635485049610E-01	2.108508628400770E-01	-9.759282799692080E-01
20.0	1.404690814535520E-01	8.684809035755050E-01	6.643159927560830E-01	-3.946698509570610E-01	-9.759282799692080E-01	
30.0	2.843724271245800E-01	9.738580310953270E-01	-1.38071801397220E-02	-1.029904558700150E+00	-4.895994341016480E-01	
40.0	5.321655337748800E-01	9.141441055914690E-01	-6.637758881941630E-01	-5.260066226547580E-01	8.523927576457860E-01	
50.0	8.656455441389880E-01	5.358026265151050E-01	-8.371745466503970E-01	6.093923488907410E-01	5.151646189082970E-01	
60.0	1.16028964232490E+00	-1.188554109960830E-01	-2.836935082383870E-01	8.520801553255340E-01	-8.564340838849380E-01	
70.0	1.189187885137070E+00	-6.679194810078100E-01	5.4228281908323860E-01	-2.247198975249610E-01	-3.291203083525950E-01	
80.0	7.743952163122060E-01	-6.33550107448900E-01	7.210677582648800E-01	-9.00961188770310E-01	9.270324489936920E-01	
90.0	2.979926582738910E-16	-2.716624512856830E-16	3.379866034416660E-16	-5.321241408360430E-16	9.633102610874780E-16	

Table C.4: Values of the first five angular function of Equation (2.12) for various angles, in degrees, for $q = 100$

ν	0.0	1.462107963590140E-07	8.896415747194900E-06	2.713926151582940E-04	5.154452244047200E-03	6.626649110605150E-02
10.0	1.816819099499260E-06	7.604890740009470E-05	1.556047261738320E-03	1.913177409008430E-02	1.522832086361510E-01	
20.0	4.087345369807590E-05	1.16047718076250E-03	1.555052749220140E-02	1.188200908828480E-01	5.314384829709540E-01	
30.0	7.486654692020470E-04	1.404338522297420E-02	1.189292628592670E-01	5.343630183829120E-01	1.212916357348340E+00	
40.0	1.002284462818390E-02	1.17744682410950E-01	5.783204789244340E-01	1.2909347247982910E+00	8.4253589319336920E-01	
50.0	8.861835046392680E-02	5.903040145522360E-01	1.375989802380890E+00	7.183629379213490E-01	-9.559126221952110E-01	
60.0	4.68214855853150E-01	1.430963539406230E+00	6.399508485286520E-01	-1.076195342208600E+00	4.398246532199820E-01	
70.0	1.317692345052160E+00	8.569777531414850E-01	-1.154064113267570E+00	6.798388543415450E-01	-1.140715280522110E-01	
80.0	1.592631047865950E+00	-1.163122971637250E+00	6.854824363887480E-01	-2.91225632964670E-01	4.366328957510980E-03	
90.0	8.958912020388180E-16	-1.345540326458570E-15	1.342653123864340E-15	-6.831264038240980E-16	4.906790157752410E-16	

Table C.5: Values of the first five angular function of Equation (2.13) for various angles, in degrees, for $q = 10$

v	0.0	0.000000000000E+00	0.000000000000E+00	0.000000000000E+00	0.000000000000E+00
10.0	9.061572452010440E-03	1.5790718870388630E-01	5.733794689428830E-01	9.055328611530250E-01	1.041416540197590E+00
20.0	2.771100541263340E-02	3.660881579569180E-01	1.001001300142880E+00	1.004397028947790E+00	3.815145691285740E-01
30.0	7.210450945463630E-02	6.501810142564180E-01	1.079151892486420E+00	1.3650450129886650E-01	-9.0316546968622880E-01
40.0	1.699727312230680E-01	9.629172661925930E-01	6.315347845128380E-01	-8.511869472368780E-01	-5.3208725498922380E-01
50.0	3.569348140349350E-01	1.134640981952110E+00	-2.15738525129850E-01	-7.491777418273290E-01	8.377547539904320E-01
60.0	6.526801615759180E-01	9.227428982227230E-01	-8.5172556421173320E-01	3.927610948754240E-01	4.4556079373550750E-01
70.0	1.019177081904540E+00	2.440407119028690E-01	-6.145789090331430E-01	8.911932736532240E-01	-8.931004822356630E-01
80.0	1.339522355137550E+00	-5.791896413165240E-01	3.134487648644520E-01	-1.007262271722890E-01	-1.75291190779280E-01
90.0	1.468755664102930E+00	-9.56262143674240E-01	8.46038433535110E-01	-9.034869753227380E-01	9.406462596360390E-01

Table C.6: Values of the first five angular function of Equation (2.13) for various angles, in degrees, for $q = 100$

v	0.0	0.000000000000E+00	0.000000000000E+00	0.000000000000E+00	0.000000000000E+00
10.0	1.724216579512820E-07	1.311740181997310E-05	3.654535950354800E-04	5.634796468893640E-03	0.00000000000000E+00
20.0	4.675476593440910E-06	2.450797254957000E-04	4.585569254492710E-03	4.589562086216080E-02	5.3233052275873330E-02
30.0	1.040894877526340E-04	3.665367684518300E-03	4.441837847769820E-02	2.724724651910740E-01	2.6855505588786340E-01
40.0	1.728100839727180E-03	3.911400613713000E-02	2.8772018241622920E-01	9.610759406415650E-01	8.872717093226680E-01
50.0	1.959805675353210E-02	2.641143671900820E-01	1.025810322113730E+00	1.336472131973690E+00	1.3199118559571330E+00
60.0	1.407689289956890E-01	9.812204801636030E-01	1.334544786750730E+00	-4.698100842894090E-01	-2.619196986044650E-01
70.0	6.023506246800710E-01	1.578916591558790E+00	-4.591014198887650E-01	5.010420548484760E-01	-6.120538915218660E-01
80.0	1.467761430695800E+00	1.801527178489600E-01	-7.411210017149540E-01	9.228781733407150E-01	8.784077780490790E-01
90.0	1.981236286456530E+00	-1.377146016888510E+00	1.158447687777900E+00	-1.024811688862250E+00	-9.190326142157750E-01

Table C.7: Values of the first five angular function of Equation (2.14) for various angles, in degrees, for $q = 10$

Table C.8: Values of the first five angular function of Equation (2.14) for various angles, in degrees, for $q = 100$

APPENDIX D

Tables of Select Radial Mathieu Functions

Tables D.1–D.16 give the first three radial functions evaluated at arguments in the range $0 \leq u \leq 3.2$. Results are provided for $q = 10.0$ and $q = 100.0$.

Tables D.15 and D.16 use Equations (2.24) and (2.25) with an index starting at $k = 1$, whereas the indices for all other tables start at $k = 0$.

110 D. TABLES OF SELECT RADIAL MATHIEU FUNCTIONS

Table D.1: Values for the first three radial functions of the first kind using Equation (2.17). $q = 10.0$

u	$Mc_{even}^{(1)}$		
0.0	3.32122614664512E-01	4.41872646767900E-01	4.67102045496234E-01
0.1	2.77240067774540E-01	4.14869201952176E-01	4.69528005071557E-01
0.2	1.29816271646030E-01	3.35595266368613E-01	4.74932079338051E-01
0.4	-2.30408873740411E-01	5.21668423930048E-02	4.67346827752816E-01
0.8	1.39122672546336E-01	-2.78230676199580E-01	4.55382812542658E-02
1.6	-5.61006829866678E-02	1.68024720276129E-01	-2.03183617238508E-01
3.2	2.39032500194488E-02	-1.15359715304328E-02	3.74747896239079E-03
	The first derivatives of $Mc_{even}^{(1)}$		
0.0	0.00000000000000E+00	0.00000000000000E+00	0.00000000000000E+00
0.1	-1.06836764023176E+00	-5.37344590584760E-01	4.54289614769104E-02
0.2	-1.79807350268442E+00	-1.03827957382207E+00	5.30692632473068E-02
0.4	-1.32719112406621E+00	-1.67507544969818E+00	-2.09089210538488E-01
0.8	1.91937611884810E+00	1.05176071310538E+00	-1.90666346042614E+00
1.6	-3.04668746652493E+00	1.67426038667539E+00	-3.99582355585560E-01
3.2	-6.79421647893463E+00	6.97410403856692E+00	-7.01745834720549E+00

Table D.2: Values for the first three radial functions of the second kind using Equation (2.17). $q = 10.0$

u	$Mc_{even}^{(2)}$		
0.0	-1.84081602665671E-05	-1.90334588713659E-02	-6.32949374037955E-01
0.1	1.80970352681662E-01	1.23243073231191E-01	-4.99721588337982E-01
0.2	3.01253660907759E-01	2.49787992290978E-01	-3.69846012146994E-01
0.4	2.17317361435897E-01	3.78827510773018E-01	-1.00650087090452E-01
0.8	-2.43689096031902E-01	-1.35717179249812E-01	3.33677608934829E-01
1.6	1.90648022900157E-01	-1.14049409357950E-01	3.40052057275692E-02
3.2	8.73217574674891E-02	-8.98783777431259E-02	9.05887107634044E-02
	The first derivatives of $Mc_{even}^{(2)}$		
0.0	1.91682151187040E+00	1.44073134425533E+00	1.36291368985819E+00
0.1	1.59889191803850E+00	1.37488097683739E+00	1.30752145335448E+00
0.2	7.31368617345152E-01	1.12418153649236E+00	1.29911695551906E+00
0.4	-1.51121826825413E+00	3.93949356938109E-02	1.40723030640918E+00
0.8	1.2139555396633E+00	-1.77506586220161E+00	8.97855250386220E-03
1.6	-9.94191648133202E-01	2.65241545067552E+00	-3.06634905229311E+00
3.2	1.81301073189511E+00	-8.49396615062190E-01	2.44769314931483E-01

Table D.3: Values for the first three radial functions of the first kind using Equation (2.20). $q = 10.0$

u	$Mc_{odd}^{(1)}$		
0.0	3.71203149872778E-01	5.46737926590870E-01	1.92317583867312E-01
0.1	3.30282726222195E-01	5.34309374289145E-01	1.99707768116479E-01
0.2	2.15369357286012E-01	4.95488437114154E-01	2.21612294929594E-01
0.4	-1.27448228977260E-01	3.22398206717995E-01	3.01948461774735E-01
0.8	-7.59994299105893E-02	-2.76099345772840E-01	3.31399102245073E-01
1.6	1.59796027374925E-01	-6.95271375685943E-02	-9.92921031951410E-03
3.2	8.88984139693733E-02	-9.03732089957082E-02	9.06910746369133E-02
The first derivative of $Mc_{odd}^{(1)}$			
0.0	0.000000000000000E+00	0.000000000000000E+00	0.000000000000000E+00
0.1	-8.05345118632721E-01	-2.51229805928332E-01	1.47427953158623E-01
0.2	-1.45362340972924E+00	-5.32150326931007E-01	2.88856525345518E-01
0.4	-1.67557089094271E+00	-1.22077043241655E+00	4.80234525640862E-01
0.8	2.12306835880541E+00	-8.51466274229464E-01	-9.32700294039034E-01
1.6	-1.99998871316712E+00	2.96133459836046E+00	-3.05845537206560E+00
3.2	1.30264459691641E+00	-4.98200303861839E-01	-5.40630596110980E-02

Table D.4: Values for the first three radial functions of the second kind using Equation (2.20). $q = 10.0$

u	$Mc_{odd}^{(2)}$		
0.0	-9.02636245666229E-04	-1.81989273004755E-01	-1.28335884344980E+00
0.1	1.64333856970985E-01	-6.23066118232065E-02	-9.97449392025841E-01
0.2	2.92501272625763E-01	6.02941552347780E-02	-7.84464581541270E-01
0.4	3.20105996544388E-01	2.82210843564938E-01	-4.79254967748674E-01
0.8	-2.84378718336941E-01	1.69833196811106E-01	1.26395877887409E-01
1.6	1.21907429519758E-01	-1.92590816295632E-01	2.07297398893749E-01
3.2	-1.73601302778258E-02	7.01469216602888E-03	1.09947005227757E-04
The first derivatives of $Mc_{odd}^{(2)}$			
0.0	1.71501716131926E+00	1.16439658089417E+00	3.31025254979706E+00
0.1	1.52679587151846E+00	1.22077785221674E+00	2.45142116773523E+00
0.2	9.81723109394765E-01	1.22007734725015E+00	1.85017739750047E+00
0.4	-7.86668307171857E-01	9.06038286657340E-01	1.34614029122959E+00
0.8	-4.32428421995367E-01	1.78201267250792E+00	1.56527370286315E+00
1.6	2.45817305805240E+00	-9.53497110095100E-01	-2.62853643117815E-01
3.2	6.90682392456336E+00	-7.00567189806256E+00	7.01958633575356E+00

112 D. TABLES OF SELECT RADIAL MATHIEU FUNCTIONS

Table D.5: Values for the first three radial functions of the first kind using Equation (2.22). $q = 10.0$

u	$M_{S_{odd}^{(1)}}$		
0.0	0.00000000000000E+00	0.00000000000000E+00	0.00000000000000E+00
0.1	1.80985257086647E-01	1.40115111271998E-01	5.36454855264603E-02
0.2	3.01260816897224E-01	2.62742684497284E-01	1.10612449709691E-01
0.4	2.17308519654805E-01	3.81448653926757E-01	2.40376372620761E-01
0.8	-2.43685476056668E-01	-1.41265706798328E-01	3.36939816712385E-01
1.6	1.90647343978746E-01	-1.12631351261529E-01	-3.61728027083412E-03
3.2	8.73218248387692E-02	-8.98992277101727E-02	9.06865360894345E-02
The first derivatives of $M_{S_{odd}^{(1)}}$			
0.0	1.91681522274878E+00	1.42989357062745E+00	5.30558291961004E-01
0.1	1.59883132511372E+00	1.34344864780519E+00	5.48072754307270E-01
0.2	7.31279415180994E-01	1.07838064324829E+00	5.95102458042492E-01
0.4	-1.51126931673927E+00	-1.27277908255223E-02	6.84806274915656E-01
0.8	1.21400984497415E+00	-1.75121220921092E+00	-8.12115499875371E-01
1.6	-9.94232568552275E-01	2.66606952898987E+00	-3.06830012905936E+00
3.2	1.81299198515124E+00	-8.37303786543114E-01	-1.16169352187953E-02

Table D.6: Values for the first three radial functions of the second kind using Equation (2.22). $q = 10.0$

u	$M_{S_{odd}^{(2)}}$		
0.0	-3.32123704367626E-01	-4.45221788142054E-01	-1.19990542417980E+00
0.1	-2.77231614879613E-01	-4.12109403964354E-01	-9.53865096530265E-01
0.2	-1.29802230567952E-01	-3.28166169556567E-01	-7.68490767774699E-01
0.4	2.30418371076643E-01	-4.13432546114771E-02	-4.96096930675316E-01
0.8	-1.39129930263315E-01	2.75967234562966E-01	1.01525038406024E-01
1.6	5.61032782552456E-02	-1.69046941993207E-01	2.07283440946658E-01
3.2	-2.39030099749355E-02	1.13804115800845E-02	-4.38284887325814E-04
The first derivatives of $M_{S_{odd}^{(2)}}$			
0.0	1.06257634794377E-04	6.62343152652959E-02	2.83309615010565E+00
0.1	1.06844715033121E+00	5.92169895956455E-01	2.12193627399497E+00
0.2	1.79810331355989E+00	1.07607839925134E+00	1.62087566049255E+00
0.4	1.32712494937851E+00	1.67033222979117E+00	1.23510259364436E+00
0.8	-1.91933747905674E+00	-1.08549049400681E+00	1.64471424143276E+00
1.6	3.04667274036829E+00	-1.65077369016772E+00	-1.69177866591120E-01
3.2	6.79422135253666E+00	-6.97548718305838E+00	7.02005933126488E+00

Table D.7: Values for the first three radial functions of the first kind using Equation (2.24). $q = 10.0$

u	$M_{even}^{(1)}$		
0.0	0.00000000000000E+00	0.00000000000000E+00	0.00000000000000E+00
0.1	1.65106517560315E-01	1.00329336362959E-01	2.06578174591724E-02
0.2	2.92997874242073E-01	1.97435311336015E-01	4.48369434514625E-02
0.4	3.19932923231404E-01	3.55614795795681E-01	1.17666325512473E-01
0.8	-2.84490372601514E-01	1.31669931810166E-01	3.50824960411679E-01
1.6	1.21995786436554E-01	-1.96841139182126E-01	1.96110584096776E-01
3.2	-1.73504127396535E-02	5.92005770529567E-03	5.79212942818907E-03
The first derivatives of $M_{even}^{(1)}$			
0.0	1.71465142057638E+00	1.00788773988001E+00	2.00740033027155E-01
0.1	1.52465256537971E+00	9.93713927308865E-01	2.18273368888607E-01
0.2	9.78476614982303E-01	9.39562153972601E-01	2.71261949743771E-01
0.4	-7.89529733153195E-01	5.59229402750213E-01	4.75951711288672E-01
0.8	-4.29825748493109E-01	-1.86556527309438E+00	2.94805771772928E-01
1.6	2.45704468489645E+00	-7.69881372027876E-01	-1.19556307461855E+00
3.2	6.90696162091068E+00	7.01064509472624E+00	6.99957207312003E+00

Table D.8: Values for the first three radial functions of the second kind using Equation (2.24). $q = 10.0$

u	$M_{even}^{(2)}$		
0.0	-3.71282328715872E-01	-6.31637579442494E-01	-3.17136429025823E+00
0.1	-3.29980007407046E-01	-5.69396049982082E-01	-2.14358073017212E+00
0.2	-2.14807024282081E-01	-4.89712364157437E-01	-1.48540756314033E+00
0.4	1.28017697510466E-01	-2.64428165451730E-01	-7.93627007721404E-01
0.8	7.56688683201164E-02	3.00583078582268E-01	-1.69248359041327E-01
1.6	-1.59732881011342E-01	5.78736426049029E-02	7.47833589036347E-02
3.2	-8.89003761277587E-02	9.04586165607133E-02	-9.05428640276881E-02
The first derivatives of $M_{even}^{(2)}$			
0.0	4.19071367055000E-03	5.40262178444944E-01	1.27000279203849E+01
0.1	8.08659219050128E-01	7.05705727879914E-01	8.16800638507386E+00
0.2	1.45542394625466E+00	8.93986832843752E-01	5.21189007629307E+00
0.4	1.67393211178175E+00	1.37436285866036E+00	2.20021861641482E+00
0.8	-2.12342983307353E+00	5.76155985210609E-01	1.67241344108071E+00
1.6	2.00128998883448E+00	-3.00782618640944E+00	2.79032135051115E+00
3.2	-1.30188755204667E+00	4.13258792782611E-01	4.93509327529718E-01

114 D. TABLES OF SELECT RADIAL MATHIEU FUNCTIONS

Table D.9: Values for the first three radial functions of the first kind using Equation (2.17). $q = 100.0$

u	$Mc_{even}^{(1)}$		
0.0	1.80747650165816E-01	1.91286578889874E-01	2.04867861052005E-01
0.1	-6.70822417937632E-02	-3.28001943335418E-02	1.01026101568055E-02
0.2	-1.26754832919240E-01	-1.76096784894330E-01	-2.00851172238646E-01
0.4	-2.78999429287131E-02	1.09816942298532E-01	1.91633979661186E-01
0.8	1.76396904578231E-02	-1.57068528691139E-01	-3.37383035066196E-02
1.6	-1.09043424992933E-01	9.47112174594335E-02	-3.09988664246705E-02
3.2	3.27369026587395E-02	-3.84289306027518E-02	4.29361153314386E-02
The first derivatives of $Mc_{even}^{(1)}$			
0.0	0.000000000000000E+00	0.000000000000000E+00	0.000000000000000E+00
0.1	-3.27430347282033E+00	-3.28717065799194E+00	-3.11809795434845E+00
0.2	2.52437596673243E+00	1.23862746063165E+00	-1.95504157492175E-01
0.4	-3.61613049891765E+00	-2.81663312456586E+00	-2.72651058028105E-01
0.8	4.06506351557331E+00	8.15730532422949E-01	-3.76153010599674E+00
1.6	-1.10358860658966E+00	-3.08578102799314E+00	5.43433526776823E+00
3.2	9.56071218830694E+00	-8.18330846236344E+00	6.70246110502048E+00

Table D.10: Values for the first three radial functions of the second kind using Equation (2.17). $q = 100.0$

u	$Mc_{even}^{(2)}$		
0.0	-7.32000234470043E-16	6.38690153918854E-12	-2.07666429851472E-08
0.1	1.67326084713810E-01	1.87812357249488E-01	2.03725695186086E-01
0.2	-1.26196584762126E-01	-6.80765210348732E-02	1.46030146260443E-02
0.4	1.71234471295388E-01	1.44974406763796E-01	1.24719741014146E-02
0.8	-1.54359897442155E-01	-3.03672077492890E-02	1.61540693684738E-01
1.6	2.24735481432126E-02	6.00825884611069E-02	-1.08631692713966E-01
3.2	-3.89796299064516E-02	3.34063651366657E-02	-2.74010322188346E-02
The first derivatives of $Mc_{even}^{(2)}$			
0.0	3.52214688148674E+00	3.32809429714206E+00	3.10746601589933E+00
0.1	-1.32290438904166E+00	-5.86841108742815E-01	1.36904936824370E-01
0.2	-2.50919147921559E+00	-3.13633394454625E+00	-3.15539518684856E+00
0.4	-6.24143866343409E-01	2.07873258246269E+00	3.30431626245413E+00
0.8	5.17978761003945E-01	-3.89542271084232E+00	-8.58952191332183E-01
1.6	-5.61077589709544E+00	4.76414592574361E+00	-1.49291696092085E+00
3.2	8.06266714895861E+00	-9.45238850393326E+00	1.05497531899854E+01

Table D.11: Values for the first three radial functions of the first kind using Equation (2.20). $q = 100.0$

u	$Mc_{odd}^{(1)}$		
0.0	1.85716224610362E-01	1.97603350742071E-01	2.13371716710817E-01
0.1	-5.09257669343104E-02	-1.25329636755793E-02	3.54209104674113E-02
0.2	-1.53646562500005E-01	-1.92436860308495E-01	-1.99369975787470E-01
0.4	4.18691846241300E-02	1.63791638085786E-01	1.83427654640905E-01
0.8	-9.23419900469479E-02	-1.36020834523629E-01	9.46535760085063E-02
1.6	-2.06513683611392E-02	9.05395786518421E-02	-1.13094289509624E-01
3.2	-3.62662556219860E-02	3.04386017198412E-02	-2.43310895614096E-02
The first derivatives of $Mc_{odd}^{(1)}$			
0.0	0.000000000000000E+00	0.000000000000000E+00	0.000000000000000E+00
0.1	-3.30244176453631E+00	-3.22637179564383E+00	-2.96059769265711E+00
0.2	1.91538474457791E+00	5.23508212048118E-01	-8.79413352682981E-01
0.4	-3.49462887456514E+00	-1.68014805358656E+00	1.14897813250788E+00
0.8	3.30668291402966E+00	-2.08691295181260E+00	-3.17739759527639E+00
1.6	-5.58896375243783E+00	3.31656968074795E+00	4.41724440707374E-01
3.2	8.79414719792602E+00	-1.00372936024253E+01	1.09915772194587E+01

Table D.12: Values for the first three radial functions of the second kind using Equation (2.20). $q = 100.0$

u	$Mc_{odd}^{(2)}$		
0.0	7.45813820244792E-14	-4.41902915472879E-10	-9.47673305734555E-08
0.1	1.78031141810683E-01	1.96460502262234E-01	2.09299670229930E-01
0.2	-1.00440994660338E-01	-2.94904645978463E-02	6.30887062660893E-02
0.4	1.72484413095048E-01	8.95913525361708E-02	-7.45928147026560E-02
0.8	-1.27736454371798E-01	8.88070875441264E-02	1.38462819685023E-01
1.6	1.09825345074113E-01	-6.68882088352929E-02	-7.77749135435562E-03
3.2	-3.57311051370986E-02	4.08295363297181E-02	-4.47556210263698E-02
The first derivatives of $Mc_{odd}^{(2)}$			
0.0	3.42791683226764E+00	3.22170536583488E+00	2.98362127973283E+00
0.1	-9.55946217298987E-01	-2.20630087073344E-01	4.79029124833030E-01
0.2	-2.89128904829824E+00	-3.22797446900545E+00	-2.91487581752242E+00
0.4	8.08488683433614E-01	2.96775245346256E+00	3.00344165938854E+00
0.8	-2.32002603678676E+00	-3.31777931476070E+00	2.07776980393774E+00
1.6	-1.10452243408274E+00	4.58120496164328E+00	-5.59872887565280E+00
3.2	-8.88967357445957E+00	7.45112179142801E+00	-5.94650344310442E+00

116 D. TABLES OF SELECT RADIAL MATHIEU FUNCTIONS

Table D.13: Values for the first three radial functions of the first kind using Equation (2.22). $q = 100.0$

u	$Mc_{odd}^{(1)}$		
0.0	0.00000000000000E+00	0.00000000000000E+00	0.00000000000000E+00
0.1	1.67326084713810E-01	1.87812357249241E-01	2.03725695854038E-01
0.2	-1.26196584762126E-01	-6.80765210351121E-02	1.46030142358000E-02
0.4	1.71234471295388E-01	1.44974406763922E-01	1.24719744315014E-02
0.8	-1.54359897442155E-01	-3.03672077494121E-02	1.61540693648806E-01
1.6	2.24735481432126E-02	6.00825884611413E-02	-1.08631692731213E-01
3.2	-3.89796299064516E-02	3.34063651366629E-02	-2.74010322141695E-02
The first derivatives of $Mc_{odd}^{(1)}$			
0.0	3.52214688148671E+00	3.32809429737394E+00	3.10746531477136E+00
0.1	-1.32290438904166E+00	-5.86841108740263E-01	1.36904907902065E-01
0.2	-2.50919147921559E+00	-3.13633394454432E+00	3.15539518776345E+00
0.4	-6.24143866343409E-01	2.07873258245950E+00	3.30431626183560E+00
0.8	5.17978761003946E-01	-3.89542271084163E+00	-8.58952195766741E-01
1.6	-5.61077589709544E+00	4.76414592574248E+00	-1.49291695798971E+00
3.2	8.06266714895861E+00	-9.45238850393386E+00	1.05497531907123E+01

Table D.14: Values for the first three radial functions of the second kind using Equation (2.22). $q = 100.0$

u	$Mc_{odd}^{(2)}$		
0.0	-1.80747650165816E-01	-1.91286578883379E-01	-2.04867884969076E-01
0.1	6.70822417937632E-02	3.28001943339874E-02	-1.01026103743970E-02
0.2	1.26754832919240E-01	1.76096784894251E-01	2.00851172260733E-01
0.4	2.78999429287131E-02	-1.09816942298373E-01	-1.91633979648340E-01
0.8	-1.76396904578231E-02	1.57068528691118E-01	3.37383036983443E-02
1.6	1.09043424992933E-01	-9.47112174594122E-02	3.09988663664379E-02
3.2	-3.27369026587395E-02	3.84289306027543E-02	-4.29361153344292E-02
The first derivatives of $Mc_{odd}^{(2)}$			
0.0	-8.58814569833139E-16	-2.28074214008240E-10	8.60016032039994E-07
0.1	3.27430347282033E+00	3.28717065798457E+00	3.11809797843296E+00
0.2	-2.52437596673243E+00	-1.23862746063591E+00	1.95504151682745E-01
0.4	3.61613049891765E+00	2.81663312456811E+00	2.72651063713586E-01
0.8	-4.06506351557331E+00	-8.15730532425983E-01	3.76153010488781E+00
1.6	1.10358860658966E+00	3.08578102799485E+00	-5.43433526854216E+00
3.2	-9.56071218830694E+00	8.18330846236274E+00	-6.70246110387121E+00

Table D.15: Values for the first three radial functions of the first kind using Equation (2.24). $q = 100.0$

u	$M s_{even}^{(1)}$		
0.0	0.00000000000000E+00	0.00000000000000E+00	0.00000000000000E+00
0.1	1.78031141810680E-01	1.96460502273581E-01	2.09299674858380E-01
0.2	-1.00440994660341E-01	-2.94904646093442E-02	6.30886961075335E-02
0.4	1.72484413095049E-01	8.95913525447686E-02	-7.45928068747680E-02
0.8	-1.27736454371800E-01	8.88070875392954E-02	1.38462822551377E-01
1.6	1.09825345074113E-01	-6.68882088338094E-02	-7.77749285226979E-03
3.2	-3.57311051370987E-02	4.08295363298203E-02	-4.47556210916419E-02
The first derivatives of $M s_{even}^{(1)}$			
0.0	3.42791683227045E+00	3.22170535052092E+00	2.98361835911503E+00
0.1	-9.55946217298973E-01	-2.20630087712627E-01	4.79028875063503E-01
0.2	-2.89128904829820E+00	-3.22797446898047E+00	-2.91487586091984E+00
0.4	8.08488683433561E-01	2.96775245337166E+00	3.00344170545719E+00
0.8	-2.32002603678673E+00	-3.31777931483359E+00	2.07776970911337E+00
1.6	-1.10452243408277E+00	4.58120496169730E+00	-5.59872886905573E+00
3.2	-8.88967357445956E+00	7.45112179139436E+00	-5.94650341369477E+00

Table D.16: Values for the first three radial functions of the second kind using Equation (2.24). $q = 100.0$

u	$M s_{even}^{(2)}$		
0.0	-1.85716224610367E-01	-1.97603350709476E-01	-2.13371810398774E-01
0.1	5.09257669343137E-02	1.25329636894191E-02	-3.54209010689516E-02
0.2	1.53646562500003E-01	1.92436860306990E-01	1.99369979304139E-01
0.4	-4.18691846241274E-02	-1.63791638081346E-01	-1.83427658089888E-01
0.8	9.23419900469465E-02	1.36020834526920E-01	-9.46535720053168E-02
1.6	2.06513683611398E-02	-9.05395786529608E-02	1.13094289421782E-01
3.2	3.62662556219859E-02	-3.04386017197047E-02	2.43310894419265E-02
The first derivatives of $M s_{even}^{(2)}$			
0.0	2.52884501187347E-13	-9.86862778590098E-10	3.61248191747459E-06
0.1	3.30244176453630E+00	3.22637179559421E+00	2.96059780119580E+00
0.2	-1.91538474457796E+00	-5.23508212246056E-01	8.79413202213092E-01
0.4	3.49462887456516E+00	1.68014805373860E+00	-1.14897800092129E+00
0.8	-3.30668291402968E+00	2.08691295169153E+00	3.17739765439422E+00
1.6	5.58896375243783E+00	-3.31656968067175E+00	-4.41724514796376E-01
3.2	-8.79414719792603E+00	1.00372936024502E+01	-1.09915772352921E+01

References

- [1] E. Mathieu, “Memoire sur le movement vibratoire d’une membrane de forme elliptique,” *J. Math. Pures Appl.*, vol. 13, pp. 137–203, 1868. [1](#)
- [2] N. W. McLachlan, *Theory and Application of Mathieu Functions*. Oxford: Clarendon Press, 1947. [1](#)
- [3] S. Goldstein, “Mathieu Functions,” *Camb. Phil. Soc. Trans.*, Vol. 23, pp. 303–336, 1927. [1](#)
- [4] E. L. Ince, “Tables of elliptic cylinder functions,” *Roy. Soc. Edin. Proc.*, vol. 52, pp. 355–423, 1932.
- [5] J. A. Stratton, *Electromagnetic Theory*, N.Y., McGraw-Hill, 1941 [5](#), [38](#)
- [6] P. M. Morse and H. Feshbach, *Methods of Theoretical Physics. Parts I and II*, New York: McGraw-Hill, 1953. [33](#), [38](#)
- [7] G. Blanch, “*Mathieu Functions*,” in M. Abramowitz and I. Stegun, Eds., *Handbook of Mathematical Functions*. Washington DC: National Bureau of Standards, chap. 20, pp. 721–750, 1964. [1](#), [5](#), [9](#), [12](#), [14](#), [15](#), [26](#)
- [8] P. Moon and D. E. Spencer, *Field Theory Handbook*, 2nd Edition, Berlin: Springer-Verlag, 1988. [3](#)
- [9] J. J. Bowman, T. B. A. Senior and P. L. E. Uslenghi, *Electromagnetic and Acoustic Scattering by Simple Shapes*. Hemisphere Publishing Co., New York, 1987. [1](#), [43](#), [46](#), [49](#)
- [10] L. Ruby, “Applications of the Mathieu equation,” *Am. J. Phys.*, vol. 64, pp. 39–44, January 1996. DOI: [10.1119/1.18290](https://doi.org/10.1119/1.18290). [1](#)
- [11] J. C. Gutierrez-Vega, R. M. Rodriguez-Dagnino, M. A. Meneses-Nava, and S. Chavez-Cerda, “Mathieu functions, a visual approach,” *Am. J. Phys.*, vol. 71, pp. 233–242, March 2003. DOI: [10.1119/1.1522698](https://doi.org/10.1119/1.1522698). [1](#), [2](#), [40](#)
- [12] H. B. Wilson and R. W. Scharstein, “Computing elliptic membrane high frequencies by Mathieu and Galerkin methods,” *J. Eng. Math.*, vol. 57, pp. 41–55, 2007. DOI: [10.1007/s10665-006-9070-1](https://doi.org/10.1007/s10665-006-9070-1). [1](#), [7](#), [12](#)

120 D. TABLES OF SELECT RADIAL MATHIEU FUNCTIONS

- [13] G. Wolf, “Mathieu Functions and Hill’s Equation” in F. W. J. Olver, D. W. Lozier, R. F. Boisvert, and C. W. Clark, Eds., *NIST Handbook of Mathematical Functions*, Cambridge: Cambridge University Press, pp. 651–681, 2010. [1](#)
- [14] R. Barakat, “Diffraction of plane waves by an elliptic cylinder,” *J. Acoustic Soc. Am.*, vol. 35, pp. 1990–1996, December 1963. [DOI: 10.1121/1.1918878](#). [1](#), [43](#)
- [15] P. M. van den Berg and H. J. van Schaik, “Diffraction of a plane electromagnetic wave by a perfectly conducting elliptic cylinder,” *Applied Scientific Research*, vol. 28, pp. 145–157, July 1973. [DOI: 10.1007/BF00413063](#). [12](#), [21](#), [22](#), [26](#), [43](#), [46](#), [49](#)
- [16] D. J. N Wall, “Surface Currents on Perfectly Conducting Elliptic Cylinders,” *IEEE Trans. Antennas Propagat.*, vol. 23, pp. 301–302, March 1975. [DOI: 10.1109/TAP.1975.1141055](#). [43](#), [46](#), [49](#)
- [17] A. Sebak and L. Shafai, “Generalized solutions for electromagnetic scattering by elliptical structures,” *Computer Physics Communications*, vol. 68, pp. 315–330, 1991. [DOI: 10.1016/0010-4655\(91\)90206-Z](#). [1](#), [43](#)
- [18] R. Holland and V. P. Cable, “Mathieu functions and their applications to scattering by a coated strip,” *IEEE Trans. Electromagnetic Compat.*, vol. 34, pp. 9–16, February 1992. [DOI: 10.1109/15.121661](#). [1](#), [12](#)
- [19] S. Caorsi, M. Pastorino and M. Raffetto, “Electromagnetic scattering by a multilayer elliptic cylinder under transverse-magnetic illumination: Series solution in terms of Mathieu functions,” *IEEE Trans. Antennas Propagat.*, vol. 45, pp. 926–935, June 1997. [DOI: 10.1109/8.585739](#). [1](#)
- [20] J. G. Kretzschmar, “Wave propagation in hollow conducting elliptic waveguides,” *IEEE Trans. Microwave Theory Tech.*, vol. MTT-16, pp. 547–554, Sept. 1970. [DOI: 10.1109/TMTT.1970.1127288](#). [1](#)
- [21] A.-K. Hamid, M. I. Hussein, H. A. Ragheb, and M. Hamid, “Mathieu functions of complex argument and their applications to the scattering by lossy elliptic cylinders,” *ACES Journal*, vol. 17, pp. 209–217, November 2002. [1](#), [7](#)
- [22] H. A. Ragheb and E. Hassan, “Analysis of a suspended strip in a circular cylindrical waveguide,” *ACES Journal*, vol. 19, pp. 165–169, November 2004. [1](#)
- [23] A.-K. Hamid, “Scattering from a semi-elliptic channel in a ground plane loaded by a lossy or lossless dielectric elliptic shell,” *ACES Journal*, vol. 22, pp. 414–419, November 2007. [1](#)
- [24] P. L. E. Uslenghi, “Exact penetration, radiation and scattering for a slotted semielliptical channel filled with isorefractive material,” *IEEE Trans. Antennas Propagat.*, vol. 52, pp. 1473–1480, June 2004. [DOI: 10.1109/TAP.2004.829848](#). [1](#)

- [25] D. Erricolo, P. L. E. Uslenghi, and B. Elnour, “Scattering by a blade on a metallic plane,” *Electromagnetism*, vol. 26, pp. 57–71, 2006. DOI: [10.1080/02726340500214910](https://doi.org/10.1080/02726340500214910). 1
- [26] Delft University Numerical Analysis Group, “On the computation of Mathieu functions,” *J. Eng. Math.*, vol. 7, pp. 39–61, January 1973. DOI: [10.1007/BF01535268](https://doi.org/10.1007/BF01535268). 1, 7, 9, 12
- [27] J. J. Stammes and B. Spjelkavik, “New method for computing eigenfunctions (Mathieu functions) for scattering by elliptic cylinders,” *Pure Appl. Opt.*, vol. 4, pp. 251–262, 1995. DOI: [10.1088/0963-9659/4/3/011](https://doi.org/10.1088/0963-9659/4/3/011). 7, 9
- [28] S. J. Zhang and J. M. Jin, *Computation of Special Functions*. New York: Wiley, 1996. 1, 12, 26
- [29] F. A. Alhargan, “Algorithms for the computation of all Mathieu functions of integer orders,” *ACM Trans. Math. Software*, vol. 26, pp. 390–414, September 2000. DOI: [10.1145/358407.358420](https://doi.org/10.1145/358407.358420). 1
- [30] D. Frenkel and R. Portugal, “Algebraic methods to compute Mathieu functions,” *J. Phys. A: Mathematical and General*, vol. 34, pp. 3541–3551, 2001. DOI: [10.1088/0305-4470/34/17/302](https://doi.org/10.1088/0305-4470/34/17/302).
- [31] L. Chaos-Cador and E. Ley-Koo, “Mathieu functions revisited: matrix evaluation and generating functions,” *Revista Mexicana de Fisica*, vol. 48, pp. 67–75, February 2002. 7, 9
- [32] D. Erricolo, “Algorithm 861: Fortran 90 subroutines for computing the expansion coefficients of Mathieu functions using Blanch’s algorithm,” *ACM Trans. on Math. Software*, vol. 32, pp. 622–634, December 2006. DOI: [10.1145/1186785.1186793](https://doi.org/10.1145/1186785.1186793). 1
- [33] A. L. van Buren and J. E. Boisvert, “Accurate calculations of the modified Mathieu functions of integer order,” *Quarterly of Applied Mathematics*, vol. 65, pp. 1–23, March 2007. DOI: [10.1090/S0033-569X-07-01039-5](https://doi.org/10.1090/S0033-569X-07-01039-5). 12, 17, 21, 26
- [34] E. Cojucaru, “Mathieu functions computational toolbox implemented in Matlab,” arXiv:0811.1970v2, November 2008. 1, 7, 12
- [35] A. L. VanBuren and J. E. Boisvert, *MATFCN*. Code available at <http://mathieuandspheroidalfunctions.com> 1
- [36] E. Cojucaru, *Matlab Mathieu Functions Toolbox v 1.0* available at <http://www.mathworks.com/matlabcentral/fileexchange> 1, 12
- [37] D. Erricolo, “Acceleration of the convergence of series containing Mathieu functions using Shanks transformation,” *IEEE Antennas Wireless Propagat. Letters*, vol. 2, pp. 58–61, 2003. DOI: [10.1109/LAWP.2003.813380](https://doi.org/10.1109/LAWP.2003.813380). 1, 33, 95

122 D. TABLES OF SELECT RADIAL MATHIEU FUNCTIONS

- [38] P. Moon and D. E. Spencer, *Field Theory for Engineers*, Princeton: Van Nostrand, 1961. [3](#)
- [39] B. T. Smith, J. M. Boyle, J. J. Dongarra, B. S. Garbow, Y. Ikebe, V. C. Klema, and C. B. Moler, *Matrix Eigensystem Routines – EISPACK Guide*. Berlin: Springer-Verlag, 1976. [DOI: 10.1007/3-540-07546-1. 9](#)
- [40] V. A. Barker, L. S. Blackford, J. Dongarra, J. Du Croz, S. Hammarling, M. Marinova, J. Wasniewski, and P. Yalamov, *LAPACK95 User’s Guide*. Philadelphia: SIAM, 2001. [DOI: 10.1137/1.9780898718201.](#)
- [41] W. H. Press, S. A. Teukolsky, W. T. Vetterling, and B. P. Flannery, *Numerical Recipes in Fortran 90*. Cambridge: Cambridge University Press, 1996. [9](#)
- [42] D. H. Bailey, *A Fortran-90 Based Multiprecision System*, code available at crd-legacy.lbl.gov/~dhbailey/mpdist [15, 17, 29](#)
- [43] A. L. van Buren, private communication, 2011. [17](#)
- [44] Y. Hida, X. S. Li and D. H. Bailey, *Quad Double Computation Package*, code available at crd-legacy.lbl.gov/~dhbailey/mpdist [17, 34](#)
- [45] M. M. Bibby, A. F. Peterson, and C. M. Coldwell, “High order representations for singular currents at corners,” *IEEE Trans. Antennas Propagat.*, vol. 56, pp. 2277–2287, August 2008. [DOI: 10.1109/TAP.2008.926771. 83](#)
- [46] M. M. Bibby, A. F. Peterson, and C. M. Coldwell, “Optimum cell size for high order singular basis functions at geometric corners,” *ACES Journal*, vol. 24, pp. 368–374, August 2009. [83](#)
- [47] A. F. Peterson and M. M. Bibby, *An Introduction to the Locally-Corrected Nyström Method*. San Rafael: Morgan & Claypool Synthesis Lectures, 2010. [DOI: 10.2200/S00217ED1V01Y200910CEM025. 83](#)
- [48] M. M. Bibby and A. F. Peterson, “High-order Treatment of Junctions and Edge Singularities with the Locally-corrected Nyström Method,” *ACES J.*, to appear in 2013. [83](#)
- [49] R. W. Hamming, *Numerical Methods for Scientists and Engineers*. New York: McGraw-Hill, 1973. [83](#)

Authors' Biographies

MALCOLM M. BIBBY

Malcolm M. Bibby received the B.Eng. and Ph.D. degrees in Electrical Engineering from the University of Liverpool, England in 1962 and 1965, respectively. He also holds an MBA from the University of Chicago, U.S.A. His career includes both engineering and management. He was president of LXE Inc., a manufacturer of wireless data communications products from 1983 to 1994. Thereafter he was president of NDI, a manufacturer of hardened hand-held computers, for five years. He is currently an Adjunct Professor in ECE at Georgia Tech. His interests lie in the field of high accuracy computational electromagnetics.

ANDREW F. PETERSON

Andrew F. Peterson received the B.S., M.S., and Ph.D. degrees in Electrical Engineering from the University of Illinois, Urbana-Champaign in 1982, 1983, and 1986 respectively. Since 1989, he has been a member of the faculty of the School of Electrical and Computer Engineering at the Georgia Institute of Technology, where he is now Professor and Associate Chair for Faculty Development. He teaches electromagnetic field theory and computational electromagnetics, and conducts research in the development of computational techniques for electromagnetic scattering, microwave devices, and electronic packaging applications.